Variation in Urban Heat Island effect across major Canadian cities

by

Yuwei Duan

A thesis submitted in partial fulfillment of the requirements for the degree of

Master of Science

Department of Earth and Atmospheric Science
University of Alberta

Abstract

The escalating global climate change poses a more severe challenge, and Canada, as a high-latitude country, is experiencing heightened Urban Heat Island (UHI) effects. Given the substantial influence of UHIs on urban, regional, and national climates, ecosystems, and human life, researching this issue has become a focal point. This study, based on land use cover data, land surface temperature (LST) data, vegetation cover data, water body index, nighttime light value data, and census data in 2021, employed statistical analysis, correlation analysis, regression analysis, local and global spatial autocorrelation Moran's I analysis, ordinary least squares (OLS), and geographically weighted regression (GWR) models. It quantitatively investigated the spatiotemporal distribution patterns of monthly, seasonal, and annual average UHI intensity, as well as the influencing factors of UHI at the scale of cities and census tracts for five cities: Toronto, Montreal, Vancouver, Edmonton and Calgary.

The research reveals distinct seasonal variations in the UHI for each city. Moreover, the high Urban Heat Island Intensity (UHI) areas showed in the annual average UHI distribution maps are consistent with built-up areas in each city, indicating that as urbanization intensifies, the UHI effect becomes stronger. In addition, the UHI data of all cities have significant spatial autocorrelation, indicating that the UHI phenomenon exists with interdependencies among residential areas in each city. The results showed that Vancouver had the highest GWR model fit. Among all cities, the Enhanced Vegetation Index (EVI) and Normalized Difference Water Index (NDWI) are closely correlated with the UHI, but significant spatial differences exist both within cities and among different urban areas. However, in most urban areas, there is a notable negative

correlation between EVI, NDWI, and UHI. The results of this study can help in developing more environmentally friendly cities and urban planning policies with the aim of reducing the urban heat island effect.

Keywords： Urban Heat Island, Land Surface Temperature, Spatiotemporal Variation, Spatial Differences

Acknowledgements

I extend my heartfelt gratitude to my supervisor, Dr. Sandeep Agrawal, whose unwavering guidance and support have illuminated my path throughout this academic journey. His wisdom and patience have been the bedrock upon which I have built my research.

I am indebted to Dr. Arturo Sanchez-Azofeifa for his invaluable advice and insight, which have significantly shaped my perspective and understanding.

My sincere thanks go to Dr. Josh Evans and Dr. Bob Summers for their steadfast support and encouragement of my research pursuits.

I am equally grateful to Dr. Nilusha Welegedara, whose mentorship and astute advice on data collection have been instrumental to my work's success.

The resources provided by Google Earth Engine and the Earth Observation Group have been indispensable to my research, and I thank them for their data support.

Finally, I would like to express my gratitude to ChatGPT for its assistance in grammar and syntax, which enhanced the articulation of my research narrative.

To all, your collective wisdom and support have been the pillars of my academic venture, and I am profoundly thankful.

Table of Content

List of Tables

List of Figure

Chapter 1. Introduction

In recent years, with the process of large-scale urbanization, the research on ecological and environmental problems in cities and their surrounding areas has become a major issue (Dalby, 2002). According to the 2018 revision of the world urbanization prospects of the United Nations (United Nations, 2018), about 55% of the global population now live in urban areas, and this proportion is expected to increase to 68% within the next 30 years. Cities are the centers of demographic, intellectual, political and economic activities of human societies. However, urbanization also brings several negative consequences. Rapid urbanization is a key contributor to greenhouse gas (GHG) emissions (Hoornweg et al., 2011; Chien et al., 2022). Large-scale urbanization is also increasing the land surface temperature inside urban areas leading to the Urban Heat Island (UHI) effect (Li et al., 2017; Parker, 2010).

The massive emissions of GHG have been recognized as the major driver of global warming and climate change. In turn, climate change can trigger a series of adverse reactions, such as melting glaciers, rising sea levels, frequent extreme weather events, such as heavy rainfall and heat waves, and desertification (IPCC, 2014). These phenomena have significant impacts on the ecosystems, human activities, and overall life safety (IPCC, 2014). Particularly during the summer, higher temperatures within urban areas not only increase the energy consumption for cooling but also raise the probability of extreme weather events (Kornhuber et al., 2019). This has significant negative impacts not only on humans but also on the growth of vegetation and wildlife (Huang et al., 2012; Hondula, 2017).

As extreme high temperatures become more prevalent worldwide, countries located at high latitudes, such as Canada, are not exempted from this trend (Welegedara et al., 2023). In fact, Canada is experiencing even greater warming compared to some other regions, and the warming rate in Canada is about twice the global average (Wang et al., 2016; Hayes et al., 2022). Health Canada (2020) also indicates that the rise in outdoor temperatures has led to an increase in heat-related illnesses and deaths. Across Canada, the impact on public health due to the rising urban temperatures has significantly increased. For instance, in July 2009, 156 people died due to extreme heat weather in British Columbia, and in July 2010, 280 people died from heat-related

causes in Quebec. In July 2018 heat waves in Quebec resulted in 86 deaths (Health Canada, 2020).

The UHI refers to the phenomenon of higher temperatures in urban areas than in the surrounding rural areas (Maimaitiyiming et al., 2014). The UHIs occur primarily due to the reduced natural land cover and the increased absorption and retention of heat by urban built-up materials (Bokaie et al., 2016). Urbanization often involves the replacement of natural landscapes with impervious surfaces, such as buildings and roads, which can reduce green spaces and limit evaporative cooling, contributing to higher UHI intensity (He et al., 2007; Chen et al., 2006). The UHI has far-reaching impacts that can affect every aspect of urban life. In addition to the ecological impact of high temperatures, the UHI phenomenon is closely related to increased air pollution. UHI can lead to increased energy consumption and exacerbate the emission of air pollutants, which can lead to the degradation of air quality and adversely affect the health of urban residents who are chronically exposed to high concentrations of pollutants (Crutzen, 2004; Singh et al., 2020). Therefore, understanding the characteristics and the influencing factors of UHI is critical to developing effective mitigation strategies and urban planning efforts and is worthy of an in-depth study.

Furthermore, studying the spatiotemporal changes and the influencing factors of UHI is crucial not only for addressing local environmental problems but also for broader implications for regional, national, and even global climate change considerations. Despite the importance of research on UHI, there is a lack of comprehensive and systematic research on the similarities and differences in the spatial variation of UHI across major Canadian cities.

To bridge this research gap, this study aims to conduct a detailed analysis of the spatial variation patterns of the daytime and nighttime UHI in five major Canadian cities (Edmonton, Calgary, Vancouver, Toronto and Montreal) throughout the four seasons of 2021. These five cities were chosen because of their large populations, large size, high population density, and high degree of urbanization (Newbold, 2011). In addition, the year 2021 was exceptionally warm, indicating that the UHI in this year would also be more pronounced. Therefore, selecting the year 2021 as the focus of this study would be more conducive to find the spatial and temporal distribution

patterns of UHI in Canadian cities which are situated at higher latitudes, as well as identifying the influencing factors of the UHI phenomenon. This study is guided by three fundamental research questions:

1. What are the spatial variation patterns of UHI in 2021 in five major Canadian cities (Toronto, Montreal, Vancouver, Edmonton and Calgary)?
2. What are the similarities or differences in the UHI distribution patterns among these five cities?
3. What are the factors that influence the daytime and nighttime UHI in the five cities? And what are their spatial characteristics?

Through comparing the spatial and temporal distribution patterns of UHI in these cities and investigating potential spatial variations in the effects of each influencing factor on the daytime and nighttime UHI, this study aimed to identify the main influencing factors of UHI in each major city, as well as the similarities and differences among the cities. This provides a better reference for planners when formulating unified plans or seeking inspiration from each other. On the other hand, due to the larger size, substantial population, and diverse geographical characteristics of the five cities chosen for this analysis—Edmonton is positioned significantly northward, Calgary is located near Rocky Mountains, Vancouver is close to the Pacific Ocean, and Toronto is adjacent to Lake Ontario—studying these five cities could provide valuable insights for better improving urban ecosystems and promoting sustainable urban development.

This study primarily uses the land surface temperature (LST) product of MODIS satellite imagery data to calculate the urban heat island intensity (UHII) and create the distribution maps of UHII. Additionally, due to the spatial heterogeneity commonly present in UHI (Buyantuyev & Wu, 2010; Zhao et al., 2018), both Ordinary Least Squares (OLS) and Geographically Weighted Regression (GWR) spatial regression models used to analyze the main factors influencing the spatial distribution of daytime and nighttime UHI in each city.

The findings of this study can be used as a basis for urban planning decisions in these five cities, enabling policymakers to design more efficient and sustainable cities that consider the potential

impacts of UHI. Moreover, the results can offer guidance to researchers and environmental practitioners in related fields to develop effective strategies to mitigate the UHI effect, ultimately leading to improved living conditions and well-being for urban residents. As global urbanization continues, understanding and addressing the challenges posed by UHI is critical in achieving a more resilient and sustainable urban future.

Chapter 2. Literature review

Due to the increasing severity of the UHI problem and the lack of research on the spatial variation patterns of UHI and the main factors affecting UHI in Canadian cities, this study examined the current status of UHI research around the world, as well as the factors affecting the UHI in different regions and the methods of spatial analysis.

2.1 The current status of global urban heat island research

The UHI phenomenon mainly results from the absorption, storage and re-radiation of solar radiation by the urban structures (Rizwan et al., 2008). Urbanization disrupts the equilibrium of urban surface energy, leading to a decrease in evaporative cooling and subsequently creating the temperature difference between urban areas and rural areas (Gunawardena et al., 2017; Zhao et al., 2014). The concept of UHI was first observed by Luke Howard in 1833, who noticed that urban areas tend to have higher temperatures than their surrounding regions (Oke, 1982). Subsequently, Manley (1958) introduced the term “urban heat island” in 1958. Initially, the researchers calculated the UHI intensity using air temperatures from observation stations (Oke, 1973). In recent years, satellite-obtained surface temperature data, such as Landsat TM/ETM+ data and MODIS data, have become increasingly prevalent in the study of UHI (Zhou et al., 2014; Li & Zhou, 2019).

Urbanization leads to urban warming, and this trend has been continuing (Cai et al., 2017; McCarthy et al., 2010). The UHI effect is the most evident urban environmental change resulting from urbanization (Oke & Maxwell, 1975). This is mainly because urbanization alters the energy balance in cities, reducing latent heat flux and increasing sensible heat flux (Oke, 1982). Urban land covers replace natural environment land covers, fundamentally changing the aerodynamic, radiative, thermal, and humidity properties within the urban areas (Oke & Maxwell, 1975). In addition, Imhoff et al. (2010) found that the ecological environment is one of the main factors influencing the daytime UHI. They studied the UHI in different ecological environments across the United States and observed that areas with forest ecosystems have higher UHI intensity compared to arid or desert regions (Imhoff et al., 2010).

The UHII is generally calculated by subtracting the rural temperature from the urban temperature (Hardin et al., 2018). UHI research can be classified into two types based on the different methods of obtaining temperature data: UHI based on air temperature and UHI based on land surface temperature (Imhoff et al., 2010; Zhou et al., 2014). Specifically, when the land surface temperature is used to calculate UHI intensity, it is referred to as surface urban heat island intensity (SUHII) (Peng et al., 2012). The UHI based on air temperature is determined using observed data from ground-based meteorological stations. However, this UHI value is sensitive to various factors such as the selection of indicators, environmental influences, and experimental conditions (Schwarz et al., 2012). Moreover, Stewart (2011) suggested that the UHI research based on meteorological data often lacks comparability due to uncontrollable factors such as weather, topography, or time. In contrast, SUHII is not affected by these factors and offers more comparable results.

Furthermore, according to the different scales of the study area, research on UHI can be conducted at various spatial scales, including the global scale, national scale, regional scale, and city scale (Wang, 2018). On a global scale, by investigating SUHI in 419 large cities around the world, Peng et al. (2012) found that SUHII was higher during the day than at night, and there was no correlation between these. At the regional level, Santamouris (2015) found that there are obvious seasonal variations in the UHI effect in Asia and Oceania. Zhao et al. (2014) studied 65 major cities in North America and found that local climate has a strong influence on UHI. On a national scale, Kalnay and Cai (2003) found that changes in land use due to urbanization led to a reduction in the temperature difference between day and night in cities across the USA. At the city scale, Huang and Wang (2019) found that both the two-dimensional and three-dimensional urban forms have a combined influence on the local LST within the city of Wuhan.

Research on strategies to mitigate UHI in Canada has primarily focused on individual cities. Rinner and Hussain (2011) conducted that in Toronto, the average temperature of commercial and industrial lands is significantly higher, while the average temperature of non-built-up areas such as parks and water bodies is lower. Wang et al. (2016) found that increasing vegetation and shading within the urban area significantly contributed to UHI reduction in the case of Toronto. Additionally, Welegedara et al. (2021) conducted an analysis of neighborhood-level UHI in

Edmonton and discovered that increasing natural land cover played a crucial role in mitigating UHI in high-latitude cities, with a 20% increase in vegetation coverage there is a 30% reduction in surrounding UHI intensity.

Gaur et al. (2018) utilized the statistical-dynamical Physical Scaling (SP) downscaling model to study the future evolution of the UHI phenomenon in Canada. Their research predicted an increase in UHI intensity for more than half of the 16 Canadian cities previously affected by UHI, with the larger cities experiencing a more significant rise in UHI intensity. Therefore, for most major cities in Canada, it is imperative to urgently develop and implement effective strategies to reduce UHI intensity.

2.2 Factors contributing to urban heat island formation

It is evident that the UHI is not the result of a single factor but a complex interaction of many features within the urban environmental system (Oke & Maxwell, 1975). In addition, Oke and Maxwell (1975) illustrated that the features include possible "causes" such as, "the release of anthropogenic heat; the high heat capacity of building materials; the reduction of the area of evapotranspiration and transpiration surfaces; the trapping of long-wave radiation beneath roof-level; increased counter-radiation from the urban pollution dome; trapping of heat due to stagnation between the large roughness elements; and redistribution of potential energy in an initially stable rural atmosphere due to increased mechanical turbulence over the rough city."

UHI is influenced firstly by climatic conditions determined by environmental natural factors, such as geographical latitude, topography, proximity to bodies of water, and vegetation cover. Kalnay and Cai (2003) illustrated that land use cover change is one of the most important factors affecting climate. Water bodies had the strongest impact in reducing UHI, while vegetation exhibited a smaller effect on UHI, and built-up areas significantly enhanced the UHI phenomenon (Tran et al., 2017; Zhang et al., 2013). Schwaab et al. (2021) found that there is a negative correlation between vegetation cover and the land surface temperature. Huang and Wang (2019) indicated that the distribution of high-rise buildings and scattered vegetation, including grasslands and shrubs, played a significant role in alleviating the UHI effect in the city. Besides, the climate of the area is also an important influencing factor on UHI. Zhao et al. (2014)

showed that humid areas with higher vegetation cover have lower cooling efficiency than arid regions, making temperature extremes worse. Although many studies have shown that daytime UHI is higher than nighttime UHI, certain research demonstrates variations in SUHI across different cities, and it is not necessarily the case that nighttime UHI is higher or daytime UHI is higher (Peng et al., 2012; Memon et al., 2009; Jin et al., 2005).

In addition, Wienert & Kuttler (2005) found that the higher the latitude, the higher the UHI. By analyzing the UHI in 28 cities situated in northern West Siberia at the 60º north latitude, Miles & Esau (2017) discovered that the average UHI is higher in winter than in summer, and they also noted a strong correlation between the UHI of high-latitude cities and population density and surrounding temperature. Furthermore, Welegedara et al. (2021) also discovered that the influencing factors for UHI in Edmonton, a high-latitude city, include vegetation, water bodies, urban density, population density, and household income.

Moreover, the UHI also can be affected by some socio-economic factors arising from the process of urbanization and industrialization. Estoque et al. (2017) found out that the size, shape, and density of impervious surfaces and green spaces have a significant impact on the distribution of surface temperature. Oke (1973) showed that the logarithm of the population is related to the UHI intensity. Later, Li et al. (2017) also stated that urban size significantly affects UHI intensity. However, Buyantuyev & Wu (2010) found that socioeconomic factors such as median household income have a much greater impact on UHI during the daytime than during the nighttime.

2.3 Research method

MODIS and Landsat remote sensing satellite imagery are frequently used to calculate UHI, and each type of imagery has its own advantages and limitations. MODIS data offers a higher temporal coverage (twice daily), providing data for both daytime and nighttime UHI. On the other hand, Landsat data has a better spatial resolution (resampled to 30 m), enabling a clearer identification of hotspots (Sidiqui et al., 2016). In pursuit of extensive and detailed data, many researchers have used Landsat data in the study of UHI. For example, Rajasekar and Weng (2009) conducted research on the spatiotemporal variations of UHI in Indianapolis over a fifteen-

year period using Landsat data, while Peng et al. (2018) analyzed the seasonal variations and influencing factors of UHI intensity in Shenzhen, China, using Landsat data. However, due to MODIS only becoming operational on the Aqua satellite in 2002, its archive data available for research is limited (Tomlinson et al., 2012). Nevertheless, the high temporal resolution of MODIS (twice daily for each satellite) has led many researchers to consider MODIS data as an ideal choice for studying UHI (Tomlinson et al., 2012).

Most of the previous studies used linear regression models to examine the driving factors of SUHI intensity (Zhou et al., 2014; Li & Zhou, 2019; Mohammad & Goswami, 2021). At the same time, geographically weighted regression also can be applied to the UHI studies similar to studies conducted to understand the regional patterns of crime, regional characterization of the prevalence of specific diseases, and key influences on the frequency of forest fires (Martínez-Fernández, Chuvieco & Koutsias, 2013; Cahill & Mulligan, 2007; Fotheringham, Charlton & Brunsdon, 1998; Fotheringham, Brunsdon & Charlton, 2003).

Chapter 3. Research area, Data and Methodology

3.1 Study area

The purpose of this study is to investigate the spatial and temporal variation of UHI under different geographical and climatic conditions as well as to analyze relevant factors affecting UHIs. Canada is a vast country, spanning a large area from north to south and east to west. However, the population of Canada is small, especially in the northern area. In this study, I selected five major Canadian cities, including Toronto, Montreal, Vancouver, Edmonton and Calgary, as case studies. These cities are located in different regions of the country and have different geographic features. For instance, Edmonton and Calgary are prairie cities. Vancouver is on the west coast of Canada and is a coastal city, while Montreal and Toronto are in the center area of the country and situated next to the Great River and the Great Lakes, respectively.

Edmonton is the northernmost city in North America with a million population. Edmonton is also the capital of the Alberta province and the center of the Edmonton metropolitan area. Edmonton is located on the North Saskatchewan River, at an elevation of 670 meters above sea level (Young et al., 1994). Edmonton is located near 53 degrees north latitude in central Alberta and covers an area of 765.61 square kilometers (Census Profile, 2021 Census of Population, n.d.). Edmonton is the furthest north of these five cities. Statistics Canada census data indicates that in 2021, the city of Edmonton has a population of 1,010,899, with a population density of 1320.4 persons per square kilometer, placing Edmonton as the fifth largest city in Canada (Census Profile, 2021 Census of Population, n.d.). Edmonton is characterized by a humid continental climate, with dry and cold winters and warm and sunny summers.

Calgary is also located in the province of Alberta, and it is the largest city in Alberta and the largest metropolitan area in the provinces of Alberta, Saskatchewan and Manitoba. Statistics Canada census data for 2021 shows that Calgary has a population of 1,306,784, with a population density of 1592.4 persons per square kilometer, and covers an area of 820.62 square kilometers (Census Profile, 2021 Census of Population, n.d.). Calgary is the third largest city in Canada. Calgary is located at 51 degrees north latitude at the confluence of two rivers, the Bow and Elbow, and at an elevation of 1,060 meters above sea level (Young et al., 1994). In addition, the city is bordered by the foothills of the Rocky Mountains to the west and the Canadian

Prairies region to the east, resulting in a subarctic climate in the western part of Calgary and a semi-monsoon humid continental climate in the east, with a warm summer and a cold, dry winter.

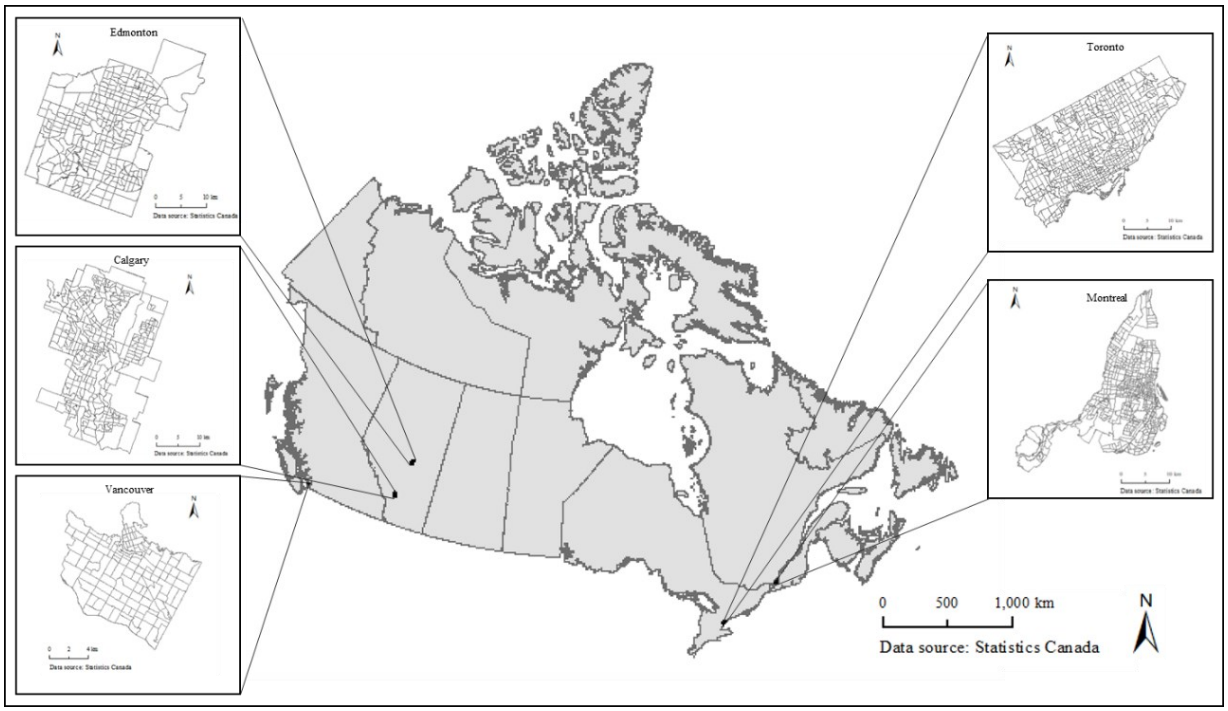

Figure 3.1 Study area

Vancouver, the most populous city in British Columbia, is located on the Burrard Peninsula in the Lower Mainland region at 49 degrees north latitude and covers an area of approximately 115.18 square kilometers (Vancouver, n.d.; Census Profile, 2021 Census of Population, n.d.). With an average elevation of 34 meters above sea level and bordering the Strait of Georgia, Vancouver has an oceanic climate with dry summers and rainy winters. Due to the influence of the Rocky Mountains and the warm currents of the Pacific Ocean, Vancouver is one of the warmest cities in Canada and the warmest of the five cities in this research. According to the 2021 Census, Vancouver has a total population of 662,248, making it the most densely populated of the five cities, with a population density of 5,749.9 persons per square kilometer (Census Profile, 2021 Census of Population, n.d.).

Toronto is located in the southern part of Ontario on the northwestern shore of Lake Ontario and is the capital of Ontario province. According to the 2021 census, Toronto has a total population of 2,794,356 and a total area of 631.10 square kilometers, resulting in a population density of 4427.8 persons per square kilometer, making it the largest city in Canada (Census Profile, 2021 Census, n.d.). Toronto is located at 43 degrees north latitude, which is the furthest north of the five cities in this study. With an average elevation of 76 meters above sea level (Elevation Schedule, n.d.), Toronto has a hot summer humid continental climate, with four distinct seasons throughout the year, and a small difference in daytime and nighttime temperatures due to the influence of Lake Ontario and urbanization.

Montreal is located on the Island of Montreal and surrounding islets in the St. Lawrence River in southwestern Quebec, surrounded by water. Montreal is the economic center of Quebec and the largest city in the Quebec province by area. According to the 2021 census, Montreal has a total population of 1,762,949 and a total area of 364.74 square kilometers, resulting in a population density of 4833.4 persons per square kilometer (Census Profile, 2021 Census, n.d.). Located at 45 degrees north latitude, with an average elevation of 112 meters above sea level, Montreal has a warm-summer humid continental climate with four clearly defined seasons. Influenced by several neighboring climate zones, Montreal receives abundant rainfall, with hot, rainy summers and cold, wet, snowy winters.

To understand the differences in UHI for each city in terms of geographic areas,
I use the census tracts of each city to analyze the spatial differences in UHI and their associated factors. In addition, this allows us to obtain the factors influencing the UHI of each city in different urban contexts.

3.2 Data

This study used data from the year 2021, as this year was marked by its exceptional warmth, providing an excellent opportunity to investigate the spatial and temporal distribution patterns of UHIs and their influencing factors in high-latitude Canadian cities. The details of the data used to derive different variables are presented in Table 3.1.

Table 3.1 A summary of a variables and data sources

Number	Variable	Dataset	Source	Spatial resolution
1	Land use/land cover data	MCD12Q1	Esri Inc.	500m
2	Land surface temperature data (Daytime)	MOD11A1	MODIS(GEE)	1000m
3	Land surface temperature data (Nighttime)	MYD 11A1	MODIS(GEE)	1000m
4	Vegetation data	MOD13A1	MODIS(GEE)	500m
5	Water data	MOD 09GA	MODIS(GEE)	500m
6	Night time light	Annual VNL V1	Earth Observation Group (EOG)	500m
7	Socio-economic statistics	Census data 2021	Statistics Canada	
8	Digital boundary data	2021 Census – Boundary files	Statistics Canada	

3.2.1 Land use/land cover data

In this study, I used Moderate Resolution Imaging Spectroradiometer (MODIS) MCD12Q1 land use/cover data acquired by the Terra satellite in 2021 with a spatial resolution of 500m available at https://www.arcgis.com. In addition, referring to the land classification methodology of Schneider et al. (2009) and based on the surface classification scheme of this project, I combined different land use classes into eight main categories that are built-up, croplands, trees, shrubs and grasslands, flooded vegetation, bare grounds, surface water bodies, as well as snow and ice.

3.2.2 Land surface temperature data

MODIS land surface temperature (LST) data contain data derived from Terra and Aqua satellites (Zhu et al., 2013). In this study, I used the MYD11A1 data that was obtained by the Aqua satellite to get the daytime LSTs, and MOD11A1 data that was obtained by the Terra satellite to get the nighttime LSTs. The spatial resolution of MODIS LST data is 1km. The calculation formula of surface temperature is as follows:

$$T = (DN \times 0.02) - 273.15 \quad \text{(Equation 3-1)}$$

Where, DN is the brightness value of the pixel, and T is the surface temperature (^{0}C) (Wan, 2014). Through Google Earth Engine codes, I directly downloaded the day and night LST data from MOD11A2 and MYD11A2, and calculated the monthly average LST data by using the GEE codes.

3.2.3 Enhanced Vegetation Index

I used the Enhanced Vegetation Index (EVI), which is the MOD13A1 product, to obtain vegetation data. The product has a production interval of 16 days and a resolution of 500 meters. Based on the attributes of leaf area, leaf chlorophyll and leaf crown structure, it provides a consistent spatial and temporal comparison of vegetation canopy greenness (NASA, n.d.). MODIS has two vegetation indices: the Normalized Difference Vegetation Index (NDVI) and the Enhanced Vegetation Index (EVI). "Two vegetation indices are derived from atmospherically-corrected reflectance in the red, near-infrared, and blue wavebands: The normalized difference vegetation index (NDVI), which provides continuity with NOAA's AVHRR NDVI time series record for historical and climate applications, and the enhanced vegetation index (EVI), which minimizes canopy-soil variations and improves sensitivity over dense vegetation conditions." (NASA, n.d.). Due to the strong urbanization of these five cities, I chose to use EVI as the vegetation index to analyze the relationship with UHI. The formulas for calculating the EVI is as follows:

$$EVI = 2.5 \times \frac{\rho_{NIR} - \rho_{RED}}{\rho_{NIR} + 6.0\rho_{RED} - 7.5\rho_{BLUE} + 1} \quad \text{(Equation 3-2)}$$

Where, ρ_{NIR}, ρ_{RED} and ρ_{BLUE} represent the reflectance of the near-infrared (NIR), red and blue bands, respectively (Esri, n.d.).

3.2.4 Normalized Difference Water Index

The Normalized Difference Water Index (NDWI) is also generally considered to be an important factor of SUHII. In this research, I use the MODIS NDWI product downloaded from the GEE as the water index to study the effect of water on the UHI. The formulas for calculating the NDWI is as follows:

$$NDWI = \frac{\rho_{GREEN} - \rho_{NIR}}{\rho_{GREEN} + \rho_{NIR}} \quad \text{(Equation 3-3)}$$

Where, ρ_{NIR} and ρ_{GREEN} represent the reflectance of the near-infrared (NIR) and green bands, respectively (Esri, n.d.; McFeeters, 1996).

3.2.5 Nighttime light data

In recent years, nighttime light images have become an effective tool for measuring the level of urbanization (Henderson et al., 2003; Elvidge et al., 2010). In this study, I used the global nighttime light product from the Earth Observation Group (EOG) as an index of urban development intensity. The EOG produced the high-quality global nighttime light products using nighttime light data from the sensors (Operational Linescan System, OLS) carried by the Defense Meteorological Satellite Program (DMSP) of the United States, and the Visible and Infrared Imaging Suite (VIIRS) Day Night Band (DNB) on board of Joint Polar-orbiting Satellite System (JPSS) available at https://eogdata.mines.edu/products/vnl/#v1.

3.2.6 Socio-economic data

In this research, I obtained socio-economic data including total population, population density and median after-tax income of households from Statistics Canada to understand the relationship between socio-economic conditions and UHI.

3.3 Methodology

3.3.1 Methodological Framework

The flow chart of the research methodology is shown in Figure 3.2. It has four major components: collecting data from different datasets, data processing, understanding influencing factors and different statistical and geospatial analyses.

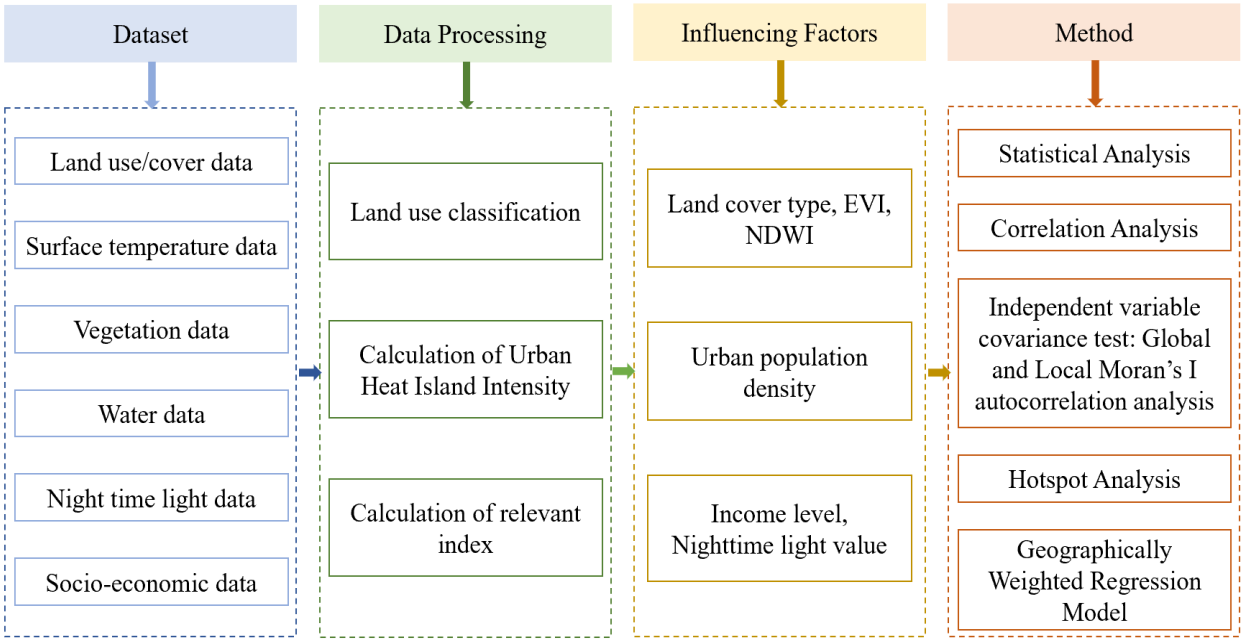

Figure 3.2 Research Methodology

3.3.2 Calculation of urban heat island intensity

In this study, I demarcated the urban boundary of each city based on the built-up surfaces in residential, industrial, transportation and other construction areas within the city. Then, the rural area of each city was demarcated by creating buffer zones that extended outward from the built-up boundaries. The buffer zone radius varies depending on the size of each city. The buffer zone radius for Vancouver is 10 kilometers from the city boundary, for Edmonton it is 5 kilometers, for Toronto it is 15 kilometers, for Montreal it is 10 kilometers, and for Calgary it is 5 kilometers. However, due to urban development and expansion, built-up areas may also exist within the buffer zones or rural areas, which may affect the results of UHI intensity calculations. The built-up area refers to the non-agricultural production construction area developed through construction in the administrative area (Zhang et al., 2018). Therefore, I defined the buffer zones without the urban, transportation and other built-up lands as rural areas, and removed the urban land, transportation land and other construction land from the rural area. The schematic representation of urban area, rural area and related indicators of UHIs is shown in Figure 3.3.

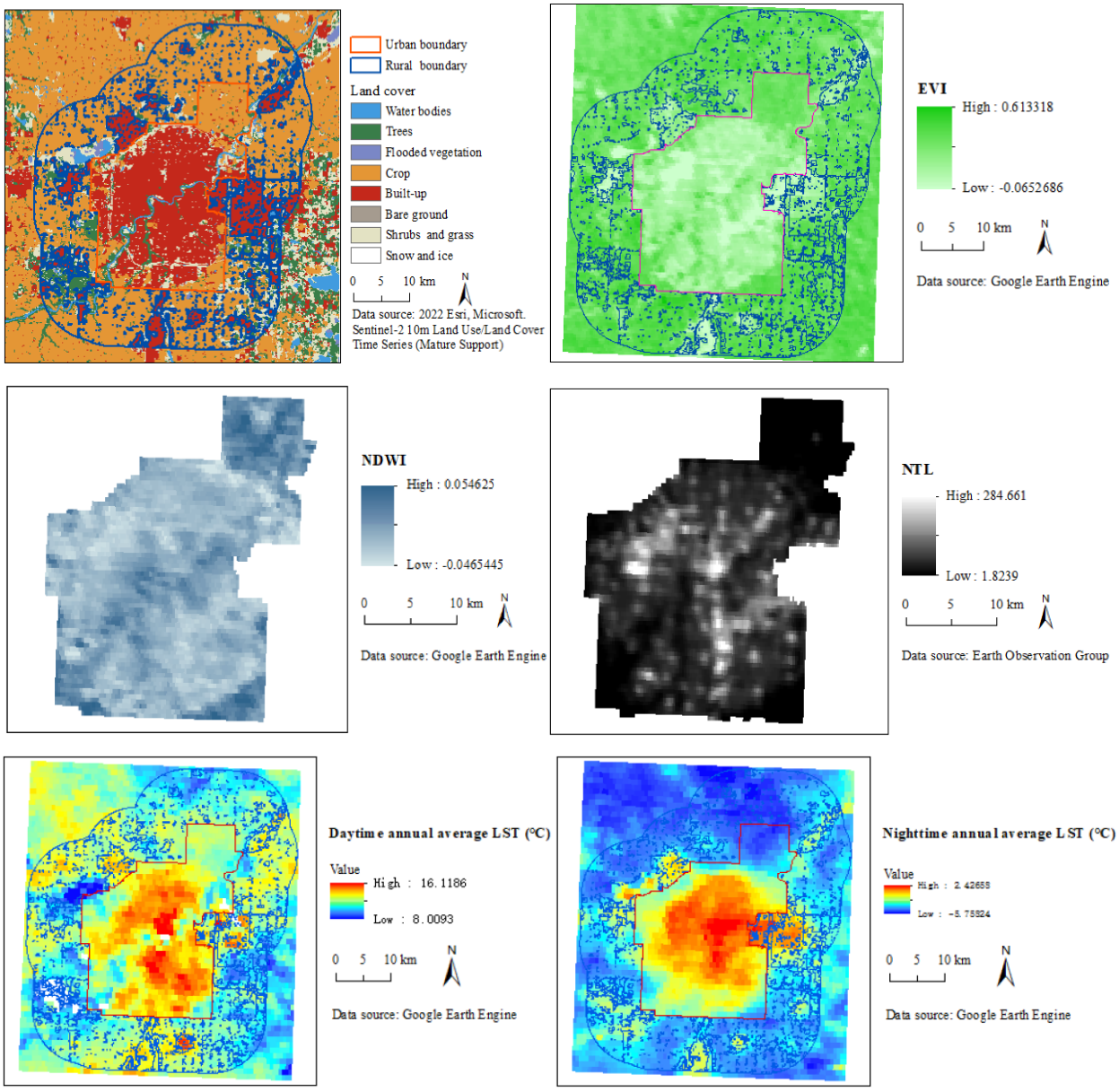

Figure 3.3 Schematic diagram of urban, rural and the relevant indicators for UHI (take Edmonton as an example)

I derived the UHI intensities in each city using MODIS land surface temperature data as indicated in equation 3-4 to compare UHI intensities in different cities.

$$SUHII = T_u - T_s \qquad \text{(Equation 3-4)}$$

Where, $SUHII$ is the intensity of the surface urban heat island; T_u is the urban surface temperature; T_s is the rural surface temperature. Positive UHI intensity indicates that the urban

area is experiencing higher temperature than that of the rural areas. In contrast, negative intensity indicates an urban heat sink or cooler urban areas than rural (Clinton & Gong, 2013).

In order to analyze the similarities and differences of UHI in the five cities, I calculated the monthly and annual averages, and seasonal day and night UHI averages for each considered city. I have considered four seasons which are: June, July and August as summer; September, October and November as autumn; December, January and February as winter; and March, April and May as spring.

3.3.3 Correlation analysis

Correlation analysis is used to analyze the strength and direction of linear relationship between two or more variables. The correlation coefficient is used to indicate the intensity and direction of the relationship between two variables. The correlation coefficient is generally represented by the symbol "r". The formula for calculating the correlation coefficient (r) is as follows:

$$r = \frac{\sum(X - \bar{X})(Y - \bar{Y})}{\sqrt{\sum(X - \bar{X})^2}\sqrt{\sum(Y - \bar{Y})^2}} \quad \text{(Equation 3-5)}$$

where X and Y represent two variables, $\overline{X}$ is the mean value of X, $\overline{Y}$is the mean value of Y, and the value of r is between -1 and 1. When the value of r is positive, it means that the two variables are positively correlated, and when the value of r is negative, it means that the two variables are negatively correlated. The absolute value of r reflects the closeness of the correlation between the two variables, and the larger the absolute value is, the closer the correlation is. When the absolute value of r is equal to 1, the two variables are completely correlated, and when r is equal to 0, it means that there is no correlation between the two variables. The confidence level is used to test for statistical significance and is expressed as p. When $p < 0.05$, it means that the correlation coefficient is statistically significant, and when $p > 0.05$, it means that the correlation coefficient is not statistically significant. However, in some cases it is considered to indicate that the coefficients are statistically significant when $p < 0.01$, and in some cases when $p < 0.1$ can also indicate that the coefficients are statistically significant.

3.3.4 ANOVA

Analysis of variance (ANOVA), also known as "F-test", is used to test the significance of the difference between the means of two or more categories/classes. The basic principle of ANOVA is to consider more than two classes that cause differences between the means of different experimental groups, which are the experimental conditions and the random error. The experimental condition is the difference caused by the different treatments, called the difference between groups, which is expressed as the sum of the squared deviations of the mean of each group variable from the total mean, denoted as SSb. The calculation formula is as follows:

$$SSb = k \times \sum(\bar{x} - \bar{X})^2 \quad \text{(Equation 3-6)}$$

where k represents the number of groups, $\bar{x}$ represents the mean of each group, and $\bar{X}$ represents the overall mean (St & Wold, 1989).

Random errors, such as differences due to measurement errors or differences between individuals, are called differences within groups, which is expressed as the sum of the squared deviations of the mean of each group variable from the values of the variables within that group, denoted as SSw. The calculation formula is as follows:

$$SSw = \sum(x - \bar{x})^2 \quad \text{(Equation 3-7)}$$

where x represents the values of the variables within each group and $\bar{x}$ denotes the mean within each group (St & Wold, 1989).

The formula for calculating the F-statistic of ANOVA is:

$$F = \frac{SSb/(m-1)}{SSw/(n-m)} \quad \text{(Equation 3-8)}$$

where n represents the total number of samples and m represents the number of subgroups. If the p-value of the F statistic is less than a certain threshold (usually taken as 0.05), the difference in the means of the groups can be considered significant (St & Wold, 1989).

3.3.5 Regression analysis

Regression analysis is a statistical analysis method to determine the quantitative interdependent relationships between two or more variables, which focuses on building regression models to express the quantitative relationships between variables in functional form (Draper & Smith, 1998). In this paper, I used linear regression analysis to analyze the linear correlation between

the daytime and nighttime UHI intensity and the influencing factors in each city, and the equation expressions are shown in Equation 3-9:

$$Y = a + bx + e \quad \text{(Equation 3-9)}$$

where a denotes the intercept, b denotes the slope of the line, and e is the error term. The fitness of the regression model was measured by R^2, and the larger the R^2, the better the fit of the regression model. In this paper, SPSS 21 software was used for the analyses.

3.3.6 Spatial autocorrelation analysis

Spatial autocorrelation refers to the potential interdependence between observations of some variables within the same distribution. In order to analyze the influence of the structural configurations on the UHI of each city, I conducted the spatial autocorrelation analysis. Tobler (1970) pointed out the first law of geography, which states that everything is related to everything else, but the closer things are to each other, the greater the connection. Spatial autocorrelation methods are broadly classified into two types by function, which are global spatial autocorrelation and local spatial autocorrelation. The commonly used spatial autocorrelations are Moran's I, Geary's C, Getis, Join count, etc. (Fortin et al., 2002; Myint, 2003; Yin et al., 2018; Sun et al., 2020).

The global spatial autocorrelation is used to describe the overall distribution of a phenomenon and to determine whether the phenomenon has aggregation characteristics in space, but it does not exactly indicate in which areas the aggregation exists. The global spatial autocorrelation is expressed by the global Moran I index, which is calculated as follows:

$$GlobalMoran's\ I = \frac{n \sum_{i=1}^{n} \sum_{j=1}^{n} W_{i,j} (x_i - \bar{x}) (x_j - \bar{x})}{S_0 \sum_{j=1}^{n} (x_i - \bar{x})^2} \quad \text{(Equation 3-10)}$$

where x_i represents the attribute of element i and x_j represents the attribute of element j; n represents the total number of samples; $W_{i,j}$ represents the spatial weight, defined by the adjacency criterion, when i and j are adjacent, $W_{i,j} = 1$, otherwise, $W_{i,j} = 0$; $i = 1, 2, \dots, n$; $j = 1, 2, \dots, m$ (Wang, 2018); $\underline{x}$ is the average of x; S_0 is the aggregation of all spatial weights, and the formula is as follows:

$$S_o = \sum_{i=1}^{n} \sum_{j=1}^{n} W_{ij} \quad \text{(Equation 3-11)}$$

The value of global Moran's I ranges from -1 to 1, when $I > 0$, it indicates a positive spatial correlation, and the closer the value is to 1, the stronger the positive spatial autocorrelation, and the values of the objects are aggregated; when $I < 0$, it indicates a negative spatial correlation, and the closer the value is to -1, the stronger the negative spatial autocorrelation, and the values of the objects are discrete and mutually exclusive (high values are excluded around high values, and low values are excluded around low values); when $I = 0$, the values of the objects are randomly distributed, indicating no spatial correlation. (Esri, n.d.)

The p-value represents the probability and the Z-score represents the multiple of the standard deviation. The calculation formula of the Z-score is as follows:

$$Z = \frac{I - E(I)}{\sqrt{Var(I)}} \quad \text{(Equation 3-12)}$$

where,

$$E(I) = \frac{-1}{n-1} \quad \text{(Equation 3-13)}$$

$$Var(I) = E(I^2) - E(I)^2 \quad \text{(Equation 3-14)}$$

when $|Z| > 1.65$, indicating that the data have significant spatial autocorrelation; when $|Z| > 1.96$, it means there is 95% probability that the data have significant spatial autocorrelation; when $|Z| > 2.58$, it means there is 99% probability that the data have significant spatial autocorrelation, as shown in Figure 3.4. (Esri, n.d.)

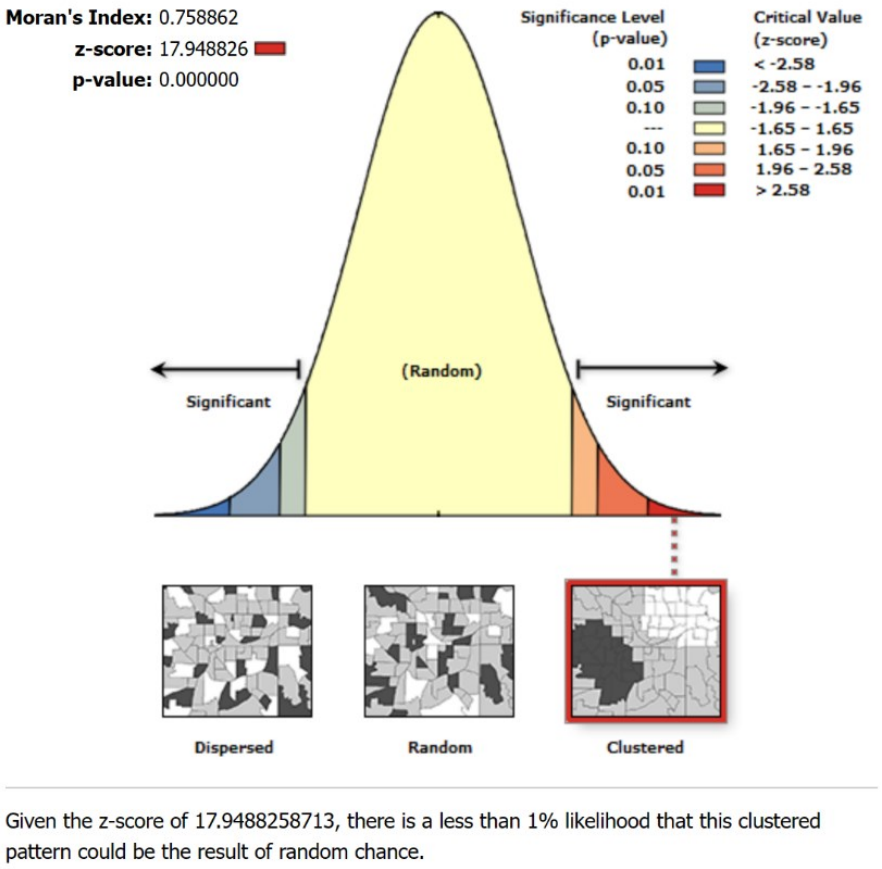

Figure 3.4 Schematic diagram of significance level and critical value of global spatial autocorrelation

However, partial spatial positive correlation and partial spatial negative correlation may coexist in the overall study area, and Local Indicators Spatial Autocorrelation (LISA) is needed to reveal the possible spatial variability (Li, M., Ou, J., & Li, X., 2016). Local spatial autocorrelation is the study of spatial correlation in different areas of the study area. LISA mainly uses local Moran's I coefficients and Getis coefficients to respond to the degree of spatial clustering of the variables at the local area scale. Local Moran's I is calculated as follows:

$$LocalMoran's\ I\ = \frac{x_i - \bar{x}}{S_i^2} \sum_{j=1, j\neq i}^{n} W_{i,j}\ (x_i - \bar{x}) \qquad \text{(Equation 3-15)}$$

$$S_i^2\ = \frac{\sum_{j=1, j\neq i}^{n} (x_i - \bar{x})^2}{n-1} \qquad \text{(Equation 3-16)}$$

where x_i is the attribute of element i; $\bar{x}$ is the average of x; $W_{i,j}$ represents the spatial weight between element i and element j; n represents the total number of samples. (Esri, n.d.)

The calculation formula of Z-score is as follows (Esri, n.d.):

$$Z = \frac{I - E(I)}{\sqrt{Var(I)}} \quad \text{(Equation 3-17)}$$

where,

$$E(I) = \frac{-\sum_{j=1, j\neq i}^{n} W_{i,j}}{n-1} \quad \text{(Equation 3-18)}$$

$$Var(I) = E(I^2) - E(I)^2 \quad \text{(Equation 3-19)}$$

The spatial association pattern of LISA is represented by four types of High-High (H-H), High-Low (H-L), Low-High (L-H), Low-Low (L-L) clusters. Among them, High-High and Low-Low clusters indicate positive spatial correlation, that is, high UHI in one community will affect surrounding communities' UHI to become higher. High-low and low-high clusters indicate negative spatial correlations, that is, high UHI in one community will affect surrounding communities' UHI to become lower.

The calculation formula of Getis is as follows:

$$Getis = \frac{\sum_{j=1}^{n} W_{i,j}\, x_j - \bar{x} \sum_{j=1}^{n} W_{i,j}}{S\sqrt{\frac{\left[n\sum_{j=1}^{n} W^2{}_{i,j} - \left(\sum_{j=1}^{n} W_{i,j}\right)^2\right]}{n-1}}} \quad \text{(Equation 3-20)}$$

$$\underline{x} = \frac{\sum_{j=1}^{n} x_j}{n} \quad \text{(Equation 3-21)}$$

$$S = \sqrt{\frac{\sum_{j=1}^{n} x^2{}_j}{n} - (\bar{x})^2} \quad \text{(Equation 3-22)}$$

where x_j represents the attribute of element j; $W_{i,j}$ represents the spatial weight between element i and j; n represents the total number of samples. (Esri, n.d.)

Since Getis is z-scored, no further calculation is required. Compared to local Moran's I, Getis is more sensitive to weights but only calculates p-values and z-scores.

3.3.7 Geographically weighted regression

Geographically weighted regression (GWR) is one of the spatial regression methods. The GWR model is currently used in a variety of disciplines such as geography, economics, natural resource management, medicine, etc. GWR is a type of linear regression oriented to local modeling, which is used to reflect the spatial heterogeneity and spatial relationships and changes

in spatial non-stationarity. The Monte Carlo significance test is generally considered to perform spatial non-stationarity tests (Brunsdon, Fotheringham & Charlton, 1996; Gollini et al., 2013).

GWR explores the spatial variability of a study target at a certain scale and related influencing factors by establishing local regression equations at each point in the spatial scale, and can be used to make predictions about future outcomes. Thus, the regression coefficients of independent variables of this model vary with spatial location. These independent equations were constructed in the GWR model by combining the dependent and explanatory variables for the elements that are located within the neighboring area of each target element. The geographically weighted regression is an extension of the ordinary linear regression model with the addition of geographic location parameters, which are calculated as follows:

$$y_i = \beta_0(u_i, v_i) + \sum_{k=1}^{p} \beta_k (u_i, v_i)\, x_{ik} + \varepsilon_i \qquad \text{(Equation 3-23)}$$

where, (u_i, v_i) is the coordinate of point i; $\beta_0(u_i, v_i)$ is the intercept of point i; $\beta_k (u_i, v_i)$ is the k-th localized estimate coefficient of the independent variable x_i, $i = 1, 2, \dots, n$. (Esri, n.d.)

It is often assumed that features that are closer have a stronger correlation, i.e., the concept of distance decay (Guo et al., 2018; Wheeler & Tiefelsdorf, 2005). GWR calibrates the model by weighting all observation points around the sample point. Therefore, the core of the GWR model is the spatial weight matrix, and the common spatial weight functions are: 1. Distance threshold method; 2. Inverse distance method; 3. Gaussian function method, etc. Among them, the Gaussian function method represents the relationship between weights and distances by selecting a continuous monotonically decreasing function. Compared with the other two methods, Gauss function overcomes the disadvantage of discontinuity of spatial weight function and there are many functions that can fulfill the requirements, so Gaussian function is widely used, and its function form is as follows:

$$W_{ij} = exp\left(-\left(\frac{d_{ij}}{b}\right)^2\right) \qquad \text{(Equation 3-24)}$$

where, W_{ij} represents the weight of j observed from point i; d_{ij} represents the distance between observation points i and j; b represents a non-negative decay parameter that describes the functional relationship between weights and distance, called the bandwidth. (Esri, n.d.)

The larger the bandwidth, the slower the weights decay with distance, and conversely the smaller the bandwidth the faster the weights decay. The bandwidth is very important for the weight function in GWR. An excessive bandwidth can lead to an excessive bias in the regression parameter estimates, while a tiny bandwidth can lead to an excessive variance in the regression parameter estimates. The AIC criterion is widely used to select the optimal bandwidth. Akaike (1974) proposed a general model selection criterion, called Akaike Information Criterion (AIC), by modifying the parameter estimation method of the great likelihood principle. Afterwards, Brunsdon, Fotheringha & Charlton (2000) further used it for weighting function bandwidth selection in GWR analysis.

The results of the GWR analysis in ArcGIS provide the following various model diagnostic parameters for significance testing (Esri, n.d.).

1. Sigma-Squared. This is the sum of squares of the residuals of the model. The smaller the value of this statistic the better the GWR model fits. Sigma squared is used in AICc calculations.
2. Sigma-Squared MLE. This is the maximum likelihood estimate (MLE) of the variance of the residuals. The smaller the value of this statistic, the better.
3. Effective Degrees of Freedom. This is a compromise between the variance of the fitted values and the deviation of the coefficient estimates. As the neighborhood tends to infinity, the geographic weight assigned to an observation tends to 1. In contrast, as the neighborhood becomes smaller and gets closer to 0, the geographic weight will approach 0 (except for the regression point itself).
4. R^2. Its value varies between 0 and 1, with the larger the value the better the fit of the model.
5. $AdjR^2$. This is the Adjusted R^2 value, which is the result of compensating for the number of model variables.
6. AICc. This is the measure used to test model performance and compare regression models. The lower the AICc value, the better the model fits the observed data.

Chapter 4. Spatial and temporal distribution patterns of UHI in Vancouver, Edmonton, Calgary, Toronto, and Montreal

Based on the understanding of the current state of UHI research worldwide and in Canada and research methodologies, as well as a primary analysis of the selected study area, this chapter focused on the analysis of spatial and temporal distribution patterns of both LST and UHI in Vancouver, Edmonton, Calgary, Toronto, and Montreal. This chapter describes the spatial and temporal distribution patterns of LST and UHI, the relationship between different land cover types and LST, as well as the spatial and temporal trends of the monthly, seasonal and annual average daytime and nighttime UHII in these five cities at the urban and census tracts scales.

4.1 Spatial and temporal distribution patterns of LST

4.1.1 Spatial and temporal distribution patterns of day and night LST

Figure 4.1 shows the distribution of land cover types in five cities. These land use data were obtained using ESA Sentinel-2 imagery (Esri, 2022). As shown in the figure, the built-up areas of Vancouver, Toronto and Montreal make up the majority of the urban area, while the cities of Calgary and Edmonton are surrounded by large crop areas around the city in addition to built-up areas. Also, it can be seen that Vancouver, Toronto and Montreal have more tree cover and fewer shrub and grass lands within their cities, while Calgary and Edmonton have more shrub and grass landa than tree cover. Vancouver and Montreal have large, concentrated tree areas, while the other three cities have less tree areas.

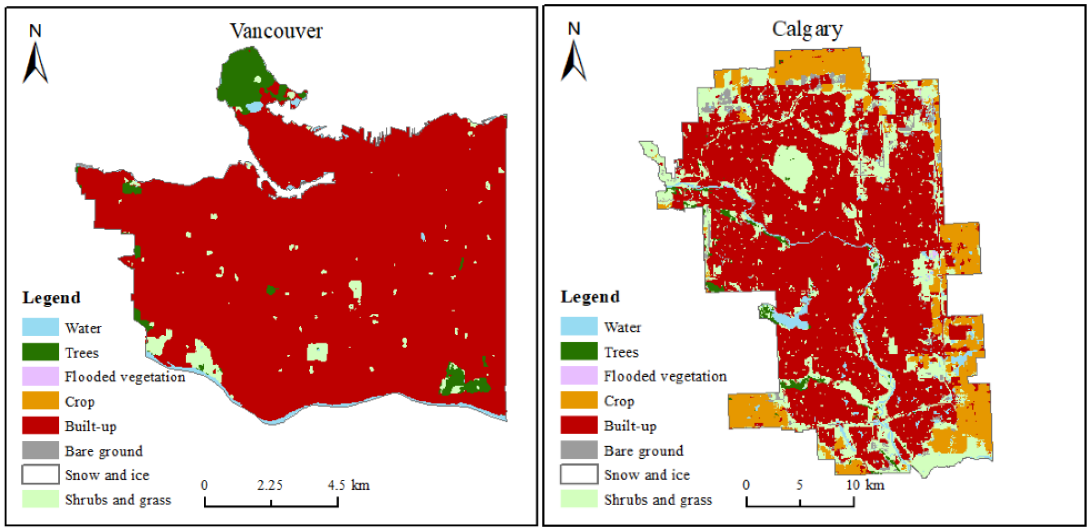

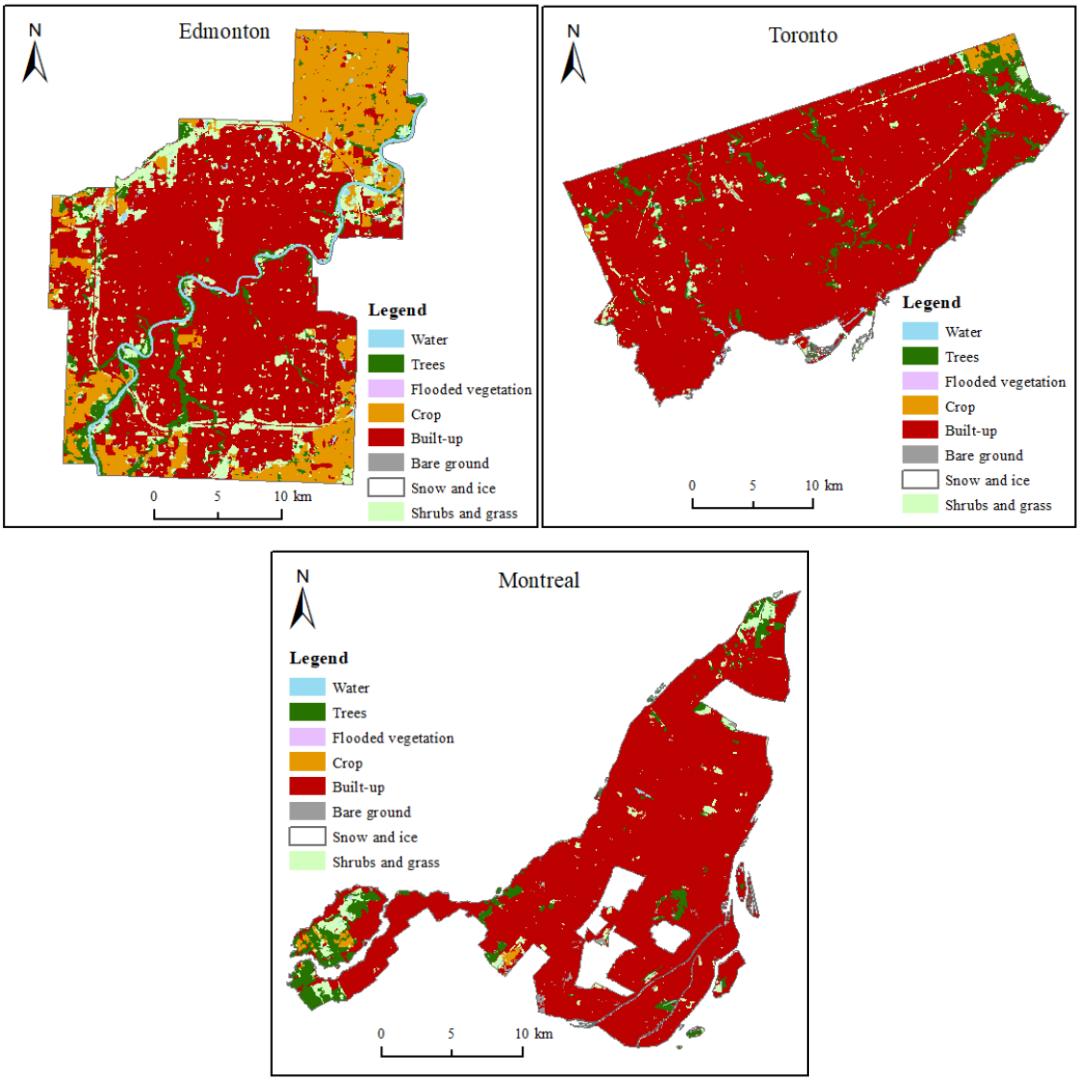

Figure 4.1 Land use land cover maps

Figure 4.2 illustrates the distribution of the annual average day and night LST of each city in 2021 observed by the MODIS satellite. The LST fluctuates with the surface energy balance and is controlled by surface radiation and thermodynamic properties, including surface humidity, thermal conductivity and surface emissivity, surface radiation input from the solar energy and atmosphere, as well as the influence of the near-surface atmosphere and the turbulent effect of ground gases (Voogt & Oke, 2003). As shown in Figure 4.2, the land surface temperature in all five cities is high in the downtown area and relatively low near the surface water bodies such as ocean, lakes or rivers. However, the distribution of the LST varies from city to city, with Vancouver having high daytime temperatures concentrated in the southeast part of the city and

high nighttime temperatures in the downtown areas; Calgary having high daytime temperatures in the east-central part of the city and high nighttime temperature in the central region of the city, and spreading outward in a radial pattern; Edmonton having high daytime temperatures in two major areas, respectively in the northwest, southeast and the central areas of the city, and having high nighttime temperature in the entire central part of the city; Toronto experience high surface temperatures within the entire city limits, with extreme daytime temperatures in the southwest and extreme nighttime temperature in the middle part, i.e., the downtown area; and Montreal having high daytime and nighttime temperatures mainly in the central part of the city, and having high nighttime temperature in some places near the water.

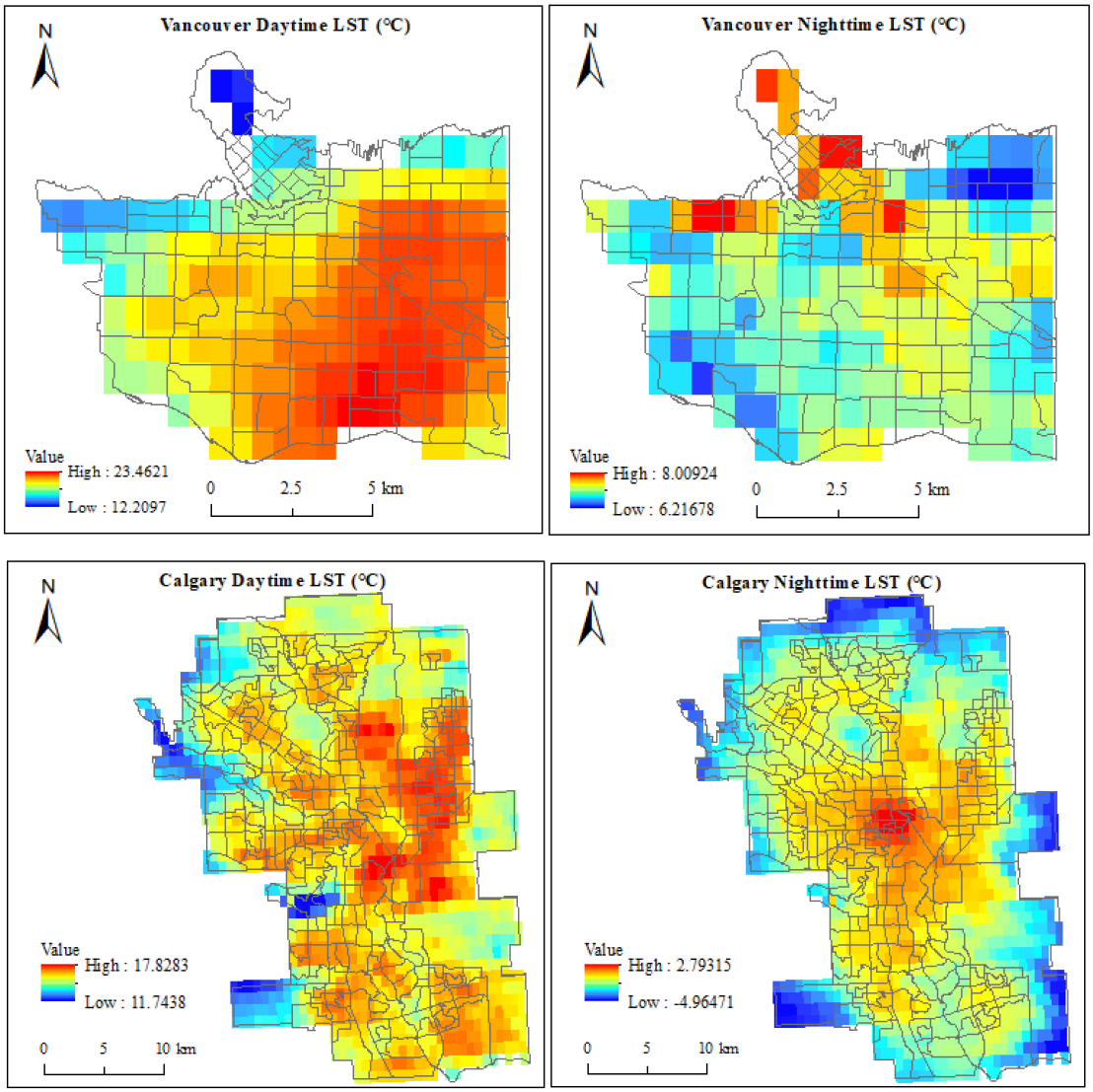

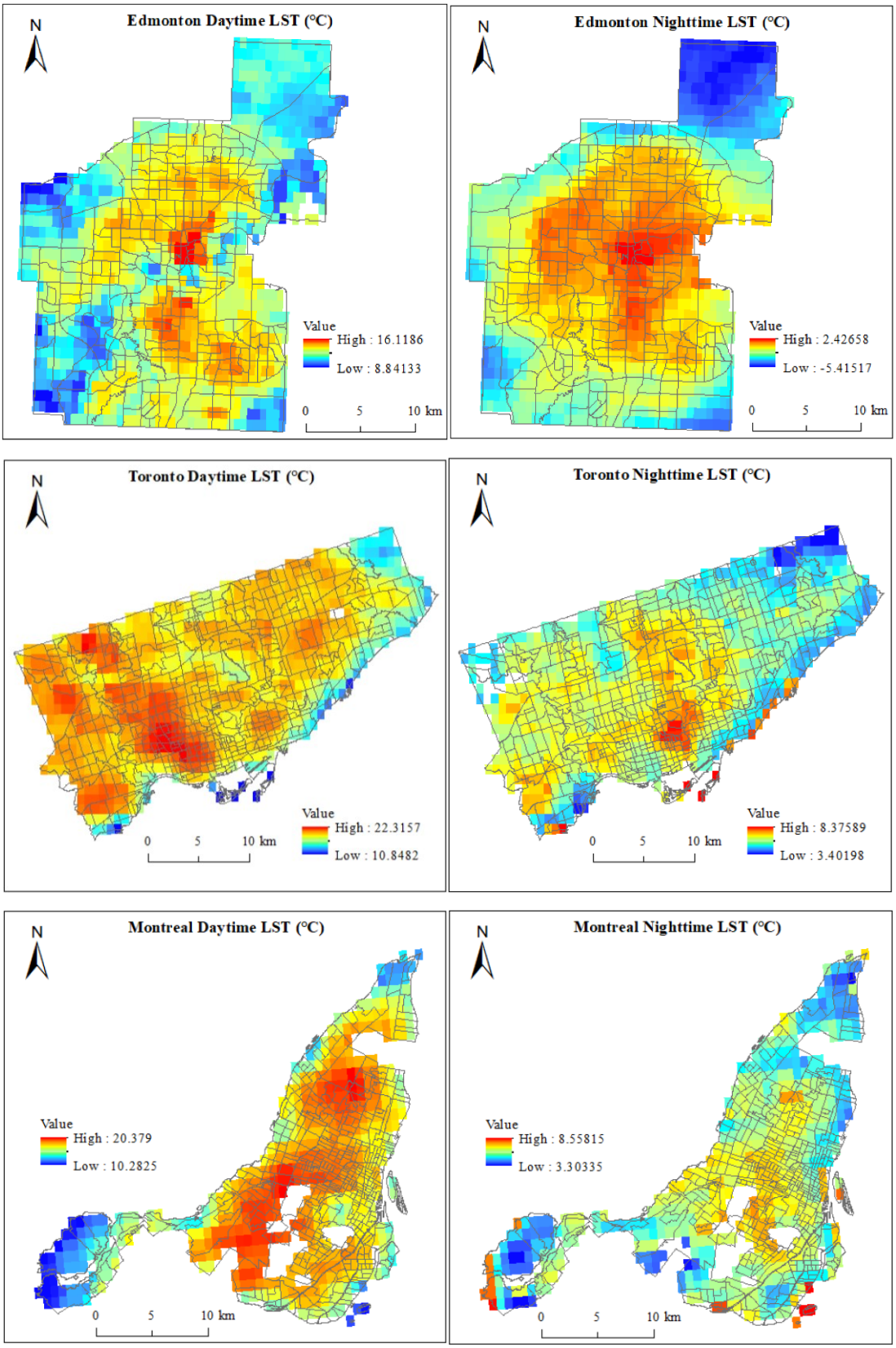

Figure 4.2 Annual average day and night LST distribution map

As shown in Table 4.1, the annual average of daytime LST is higher than nighttime LST in all five cities, with Calgary having the largest temperature difference between day and night at 16.86 ℃, followed by Edmonton and Toronto, while Montreal has the smallest temperature difference between day and night at 11.43 ℃. The city with the highest annual average LST at both the night and day is Vancouver, followed by Toronto, and the city with the lowest annual average LST during the day is Edmonton and the city with the lowest annual average LST at night is Calgary.

Table 4.1 Annual average day and night LST (℃) for each city

City	Vancouver	Edmonton	Calgary	Toronto	Montreal
Day LST	20.17	12.94	15.81	19.54	17.00
Night LST	7.15	-1.01	-1.05	5.67	5.57

The difference in temperature between the city with the highest daytime temperature and the city with the lowest daytime temperature is 7.2 ℃, while the difference in temperature between the city with the highest nighttime temperature and the city with the lowest nighttime temperature is 8.2 ℃. These differences may be linked to the geography and the latitude of the city of these five cities, the city located at higher latitudes, like Edmonton which experiences longer cold periods, has lower annual average land surface temperatures and the cities located at relatively low latitudes, such as Vancouver and Toronto, have higher annual average land surface temperatures.

4.1.2 Effect of Land cover type on LST

In this research, I calculated the average day and night surface temperatures for different land cover types. Snow and ice were not considered as their temperatures are always below 0 and are not affected by other factors. In addition, flooded vegetation and shrubs and grass are combined into one category, making a total of six land types, as shown in Table 4.1. In general, the highest daytime LST was observed in the built-up area, and the lowest daytime LST was observed in the vegetated areas. In Vancouver, the highest daytime LST was found in the grass areas, followed by the built-up areas, but the standard deviation of the daytime LST in the grass areas is 2.52℃, indicating that the data has huge variation, i.e., the difference of the daytime LST between different grass area is large.

From Figure 4.2, it can be seen that most of the grass areas in Vancouver are scattered within built-up areas, which means that the grass areas in downtown might be influenced by the surrounding built-up areas and heat is trapped in these grass areas, which make the daytime LST higher. In Edmonton, Calgary and Toronto, daytime LST is highest in built-up areas, while in Montreal, daytime LST is highest in bare ground, followed by built-up areas. In Vancouver, bare grounds have the lowest daytime LST and tree areas have relatively lower daytime LST, however, the standard deviation of the daytime LST of the tree areas in Vancouver is 5.13℃, demonstrating that there is a huge variation of the data, i.e., the daytime LST in the trees area fluctuated greatly. In terms of Vancouver's geographic characteristics, trees close to the ocean are affected by cold air, making the temperature lower in these tree areas, and therefore, the temperature difference in tree areas is greater compared to tree areas in the downtown area that are affected by buildings. In Calgary, tree areas have the lowest daytime LST. In addition, in Edmonton, Toronto and Montreal, the crop areas have the lowest daytime LST, which is likely because in all three cities, the crop is distributed at the edge of the city, making their daytime LST lower than that of the city center areas.

Table 4.2 Annual average day and night LST for different land cover types

		Daytime					
City		Built-up	Crop	Trees	Grasses	Bare ground	Water body
Vancouver	Mean (℃)	20.26	17.90	15.62	20.81	15.32	17.48
	Std dev.	2.33	0.00	5.13	2.52	0.37	0.00
Edmonton	Mean (℃)	13.36	12.11	12.23	12.90	13.33	12.32
	Std dev.	1.00	0.80	1.08	1.15	1.29	1.26
Calgary	Mean (℃)	16.04	15.26	14.69	15.48	14.92	15.30
	Std dev.	0.88	0.96	1.23	1.07	1.02	1.29
Toronto	Mean (℃)	19.70	16.20	18.22	19.17	17.85	17.39
	Std dev.	1.38	0.35	2.07	1.90	0.00	2.59
Montreal	Mean (℃)	17.48	13.01	13.35	14.89	18.93	15.02
	Std dev.	1.93	3.31	2.54	2.91	1.03	2.95

Nighttime							
City		Built-up	Crop	Trees	Grasses	Bare ground	Water body
Vancouver	Mean (℃)	7.14	6.86	7.57	7.07	7.40	7.03
	Std dev.	0.33	0.00	0.41	0.22	0.58	0.00
Edmonton	Mean (℃)	-0.13	-3.31	-1.36	-1.18	-1.41	-0.52
	Std dev.	1.26	1.24	1.65	1.26	0.94	1.53
Calgary	Mean (℃)	-0.52	-3.21	-1.65	-1.59	-1.74	-1.25
	Std dev.	1.06	1.01	1.39	1.15	0.70	1.22
Toronto	Mean (℃)	5.70	3.84	5.51	5.56	6.71	6.12
	Std dev.	0.61	0.35	0.76	0.77	0.00	0.85
Montreal	Mean (℃)	5.64	4.82	5.13	4.76	6.14	5.72
	Std dev.	0.69	1.40	1.37	0.73	1.12	0.97

During the night, in Edmonton and Calgary, it is still the built-up areas that have the highest LST and the crop areas that have the lowest LST. In Vancouver, the highest LST at night is in the trees area which might be due to heat-trapping within the area, followed by the bare ground, and the lowest LST at night is in the crop area, which is different from the daytime situation. All of these results indicate that the distance to large water bodies is significant, and there is variability in land use classifications based on location. In Edmonton and Calgary, the highest nighttime LST are found in the built-up areas and the lowest nighttime LST is found in the crop areas. The land type with the highest nighttime land surface temperatures in Montreal remain the same as during the daytime, and remain bare ground, while the lowest nighttime LST in Montreal is found in grasses areas. In Toronto, it is also the bare ground that has the highest nighttime LST, yet it is the crop areas that has the lowest nighttime LST.

In addition, Vancouver's built-up areas have the highest daytime LST, followed by Toronto, and Edmonton's built-up areas have the lowest daytime LST. Although, Vancouver's built-up areas continues to have the highest LST at night, followed by Toronto. However, different from daytime, Calgary's built-up area have the lowest LST at night. From this, it can be seen that the annual average daytime and nighttime LST in the built-up areas of each city is essentially consistent with the overall situation of the annual average daytime and nighttime land surface

temperature in each city described above. In this case, the LST in built-up area mainly influences the overall LST value.

4.2 Spatial and temporal distribution patterns of urban heat island

4.2.1 Annual average day and night urban heat island characteristics

Figure 4.3 illustrates the spatial distribution characteristics of the annual average urban heat island intensity (UHII) for the five cities during daytime and nighttime. As shown in the daytime UHII distribution, Vancouver, Toronto and Montreal have higher UHII than Calgary and Edmonton. The UHII is above 9.9 ℃ in southeast Vancouver and mostly above 6.5 ℃ in the central regions of Montreal and Toronto. The central area of the northern Edmonton has an UHII of over 5.6 ℃. Nevertheless, in the vast majority of Calgary, the UHII does not exceed 3.9 ℃. In addition, as shown in the figure, each city shows a negative UHII in some areas, which indicates that the urban heat sink occurs in some areas of each city (Clinton & Gong, 2013). For example, the UHI intensity is negative in the Edmonton Valley region and west of Calgary due to the influence of water bodies. Moreover, in certain areas of Vancouver and Montreal, the UHII is even below -5.4 ℃. The distribution of nighttime UHII is the opposite of that during the day, Calgary and Edmonton have higher UHII than Vancouver, Toronto and Montreal. The nighttime UHII in the central parts of Edmonton and Calgary is above 5.2 ℃, while the nighttime UHII in most parts of Vancouver and Montreal is below 2.8 ℃. As shown in Figure 4.4, the annual average daytime UHIIs are higher than the annual average nighttime UHIIs in Vancouver, Toronto, and Montreal, with the exception of Calgary and Edmonton, where the nighttime UHIIs are higher than the daytime UHIIs.

The surface energy balance can be viewed as:

$$Q + Q_A = E + H + G \qquad \text{(Equation 4-1)}$$

where, Q is full-wave net radiation; Q_A is anthropogenic heat emissions; E is latent heat flux; H is sensible heat flux; G is ground heat flux (Clinton & Gong, 2013; Friedl, 2002; Price, 1985; Rizwan et al., 2008; Taha, 1997). The daytime UHII is widely considered to be the result of a decrease in latent heat flux and an increase in sensible heat flux due to a decrease in surfaces such as vegetation and soil and an increase in impermeable surfaces (Voogt and Oke, 2003). In addition, the research of Zhao et al. (2014), who studied the daytime UHI in various regions of

North America that are in different climatic contexts, found that the daytime urban-rural temperature difference is also influenced by two things: convective efficiency, which is related to aerodynamic forces and drag, as well as air humidity. They argue that in humid climate zones, heat dissipation through convection is lower in urban areas than in rural areas, thereby increasing the temperature in urban areas and resulting in the heat island effect (Zhao et al., 2014). In this regard, this could explain the high UHII in southeast Vancouver.

Rural areas in humid regions have low aerodynamic drag due to abundant precipitation and high vegetation cover, thus dissipating heat well. However, in arid areas, the opposite is true. Convective efficiency in urban areas is stronger than in rural areas, so temperatures in urban areas are lower than those in rural areas, leading to a negative heat island (Zhao et al., 2014). This may be due to the fact that urban built-up areas located in arid inland cities have higher soil moisture and more vegetation cover compared to the surrounding rural areas, which lead to the lower LST in the urban areas than the rural areas. So, the daytime UHII in the arid inland cities is lower. These could explain the phenomenon of urban heat sink in more areas of Calgary that appeared in the results of this study. In contrast, Toronto, which is in the Great Lakes region, and Vancouver, which is on the coast, have stronger UHII during the day.

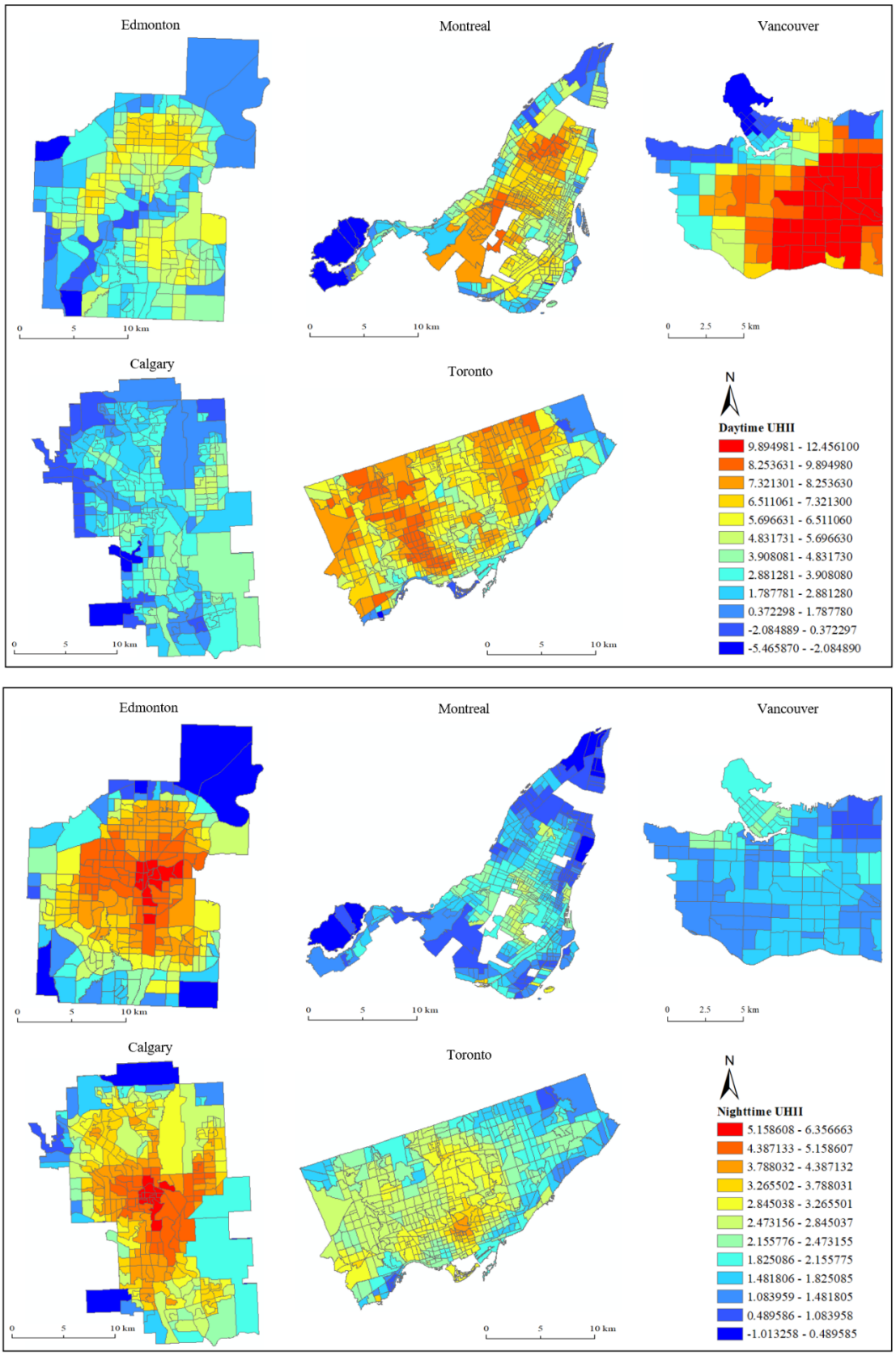

Figure 4.3 Annual average day and night UHI distribution map

At night, the flux to the air generally comes from radiative transfer, i.e. the thermal release of heat stored in urban areas during the day as well as the increase of anthropogenic heat emissions during the night (Masson, 2000; Rizwan et al., 2008; Clinton & Gong, 2013). During the day, building materials absorb thermal radiation for heat storage, and at night, the thermal release of this stored heat is a major contributor to nighttime UHII (Oke, 1982; Oke, 1988). Therefore, the nighttime UHII is dependent on the size of the urban areas (Sobstyl et al., 2018). The heat released at night usually enters the lower atmosphere. As the air passes through urban areas, the longer the distance from the edge of the urban area to the center of the city, the more heat accumulates in the air (Soltan & Sharifi, 2017). Thus, the larger the city, the higher the nighttime UHII. It appears that, under approximately the same climatic conditions, altitudes and geographic location, the total area of Toronto and its surrounding built-up area is about 1,570 square kilometers, while the total area of Montreal and its surrounding built-up area is about 966 square kilometers, resulting in a higher UHI intensity in Toronto than in Montreal, as shown in Figure 4.4.

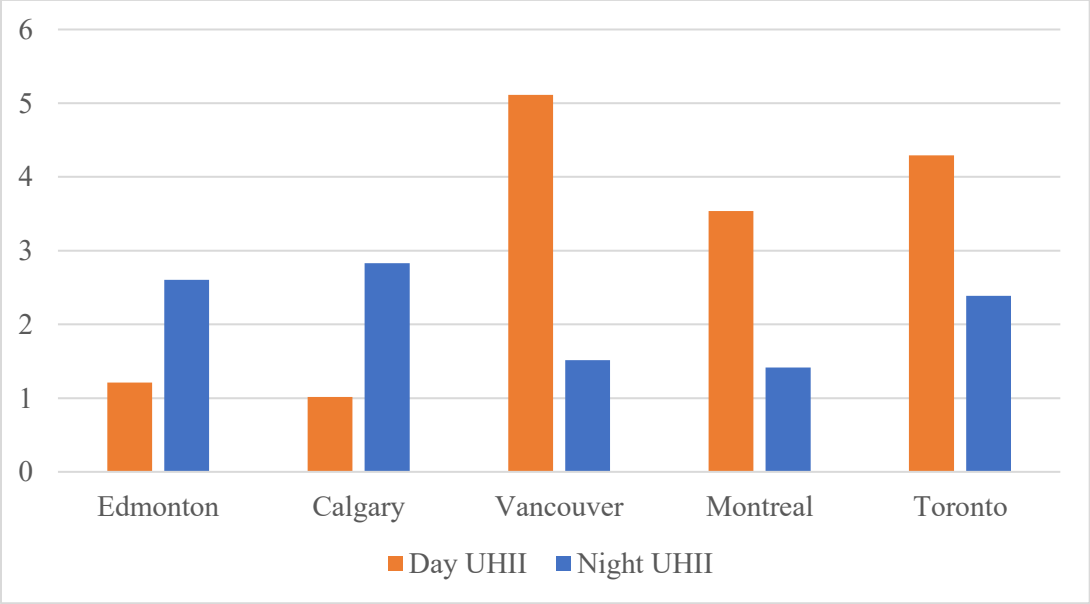

Figure 4.4 Annual average day and night UHII

Urbanization has transformed land cover from natural or semi-natural vegetative cover to impervious surface cover. Vegetation conducts transpiration during the day, which has a cooling

effect, while impervious surfaces absorb the energy of solar radiation, which leads to high daytime temperatures in the urban areas and low temperatures in the rural areas, creating a large daytime temperature difference between urban and rural areas. Daytime UHII is also influenced by the degree of urbanization (Zhou & Chen, 2018). However, the vegetation has a smaller effect on nighttime UHII, because vegetation does not conduct transpiration at night. In addition, the elevation differences between urban and rural areas, topographic features of the city and surrounding areas, and the type of land use in the surrounding areas of the city all have an impact on the UHI (Tang et al., 2022; Chen et al., 2017; Sun et al., 2019; Badaro-Saliba et al., 2021).

4.2.2 Spatial autocorrelation of annual average day and night urban heat island

4.2.2.1 Annual average day and night urban heat island global Moran's I index

In order to study the spatial autocorrelation of the daytime and nighttime UHI in the five cities, I first used the distance decay weighting method to establish a spatial weight matrix for the vector data of the annual average daytime and nighttime UHI in the five cities. This weight matrix assigns greater weights to the locations that are closer to the observation points. Next, this spatial weight matrix is used to calculate the global and local Moran's I index.

Table 4.3 Global Moran's I index summary

	City	Moran's Index	Z score	P value
Daytime	Montreal	0.318	27.325	0.000
	Toronto	0.437	30.079	0.000
	Calgary	0.300	15.639	0.000
	Edmonton	0.421	25.462	0.000
	Vancouver	0.837	17.240	0.000
Nighttime	Montreal	0.498	40.648	0.000
	Toronto	0.524	36.009	0.000
	Calgary	0.756	33.146	0.000
	Edmonton	0.531	36.072	0.000
	Vancouver	0.759	17.949	0.000

The global Moran's I index for the daytime and nighttime UHI in each of the five cities are shown in Table 4.3. The global Moran's I index for the daytime and nighttime UHII in the five cities are all greater than 0, with z-scores exceeding 2.58 and *p*-values less than 0.01. This result indicates that the UHII at the census tract scale in these five cities have significant positive spatial autocorrelation.

4.2.2.2 Annual average day and night urban heat island hot spots analysis

As shown in Figures 4.5 and 4.6, the spatial clustering patterns of daytime and nighttime UHI among the five cities are generally similar, with some slight differences. In Edmonton, during the day, the hot spots (high-high clustering) are mainly distributed in the northern and southeastern regions, while the cold spots (low-low clustering) are primarily located in the western and southwestern regions. The not significant values are scattered in the central and northern areas. During the nighttime, the hot spots (high-high clustering) are distributed in the entire central part of Edmonton and the cold spots (low-low clustering) are distributed in the north and south region. In Calgary, during the daytime, the hot spots (high-high clustering) are mainly concentrated in the central area, while the cold spots (low-low clustering) are primarily distributed in the northwestern and southwestern parts. The Not significant values are clustered in the northern and southern areas. At night, as in Edmonton, the hot spots (high-high clustering) are concentrated throughout the center of Calgary and the cold spots (low-low clustering) are primarily distributed in the north part.

For Toronto, during the day, the hot spots (high-high clustering) are mainly found in the northwestern and northeastern parts, and the cold spots (low-low clustering) are mainly distributed in the southern lakeside areas. The Not significant values are primarily concentrated in the central area. At night, hot spots (high-high clustering) are found in the central part, and the cold spots (low-low clustering) are mainly distributed in the northeast and southeast areas. In Montreal, the spatial clustering patterns of daytime and nighttime UHI are generally similar, the hot spots (high-high clustering) are concentrated in the central area of the city, while the cold spots (low-low clustering) are scattered around the city's periphery. The not significant values are also scattered around the city's periphery. As for Vancouver, the clustering pattern of the daytime UHII is relatively straightforward, with hot spots (high-high clustering) concentrated in

the southeastern region and cold spots (low-low clustering) in the northwestern area. The Not significant values are distributed in the areas between the cold and hot spots. However, the hot spots (high-high clustering) of the nighttime UHII mainly concentrated in the downtown area and cold spots (low-low clustering) mainly located in the northeast part.

Overall, the daytime and nighttime UHI in these five cities demonstrate spatial clustering patterns with distinct hotspots and coldspots, indicating the presence of significant spatial autocorrelation in the UHI phenomenon. Combined with the global Moran's I index, this reveals the presence of both global and local spatial autocorrelation, and indicates that there is spatial non-stationarity in the dataset.

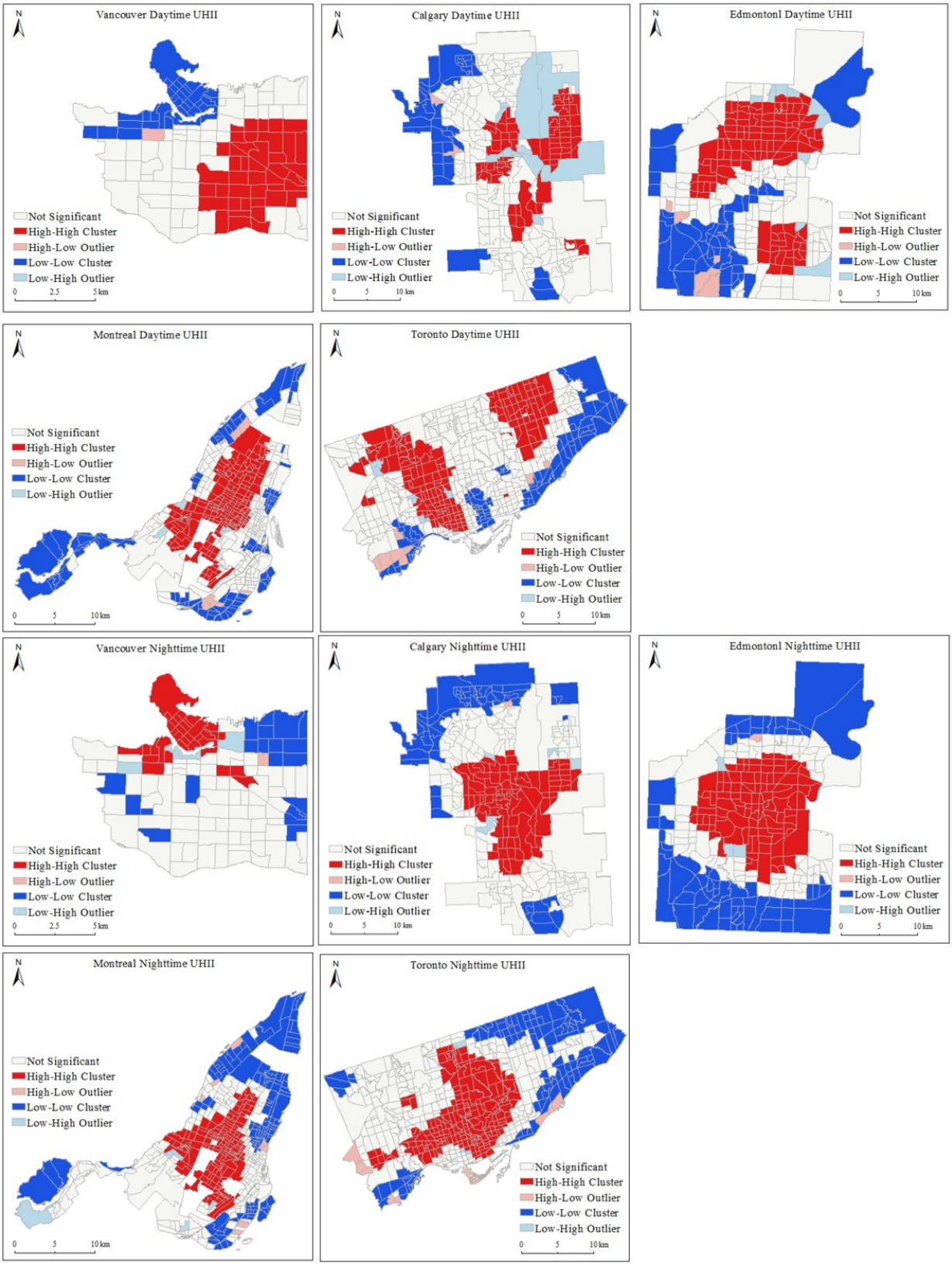

Figure 4.5 Daytime and Nighttime UHII LISA map

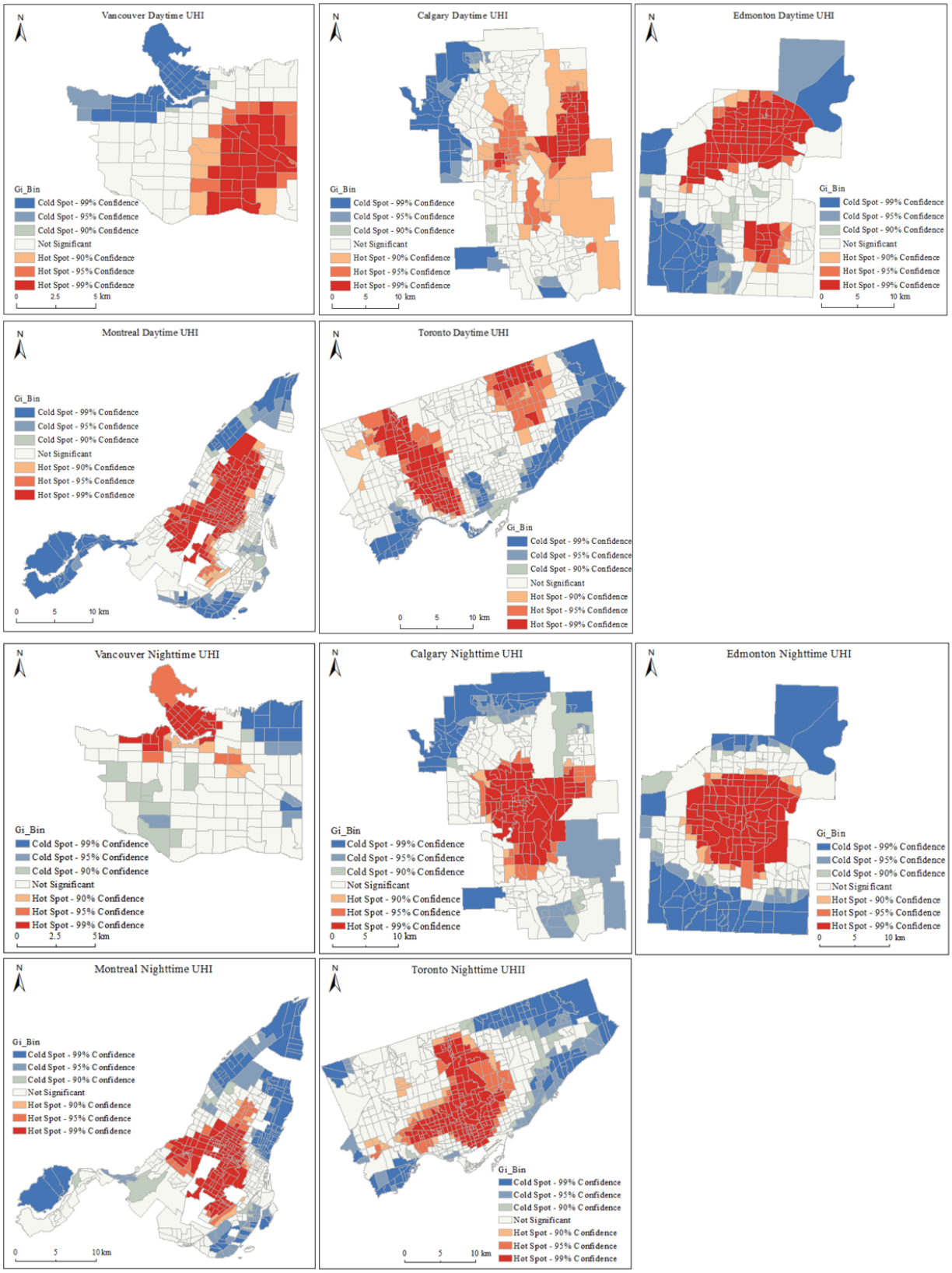

Figure 4.6 Daytime and Nighttime UHII Hot spots map

4.2.3 Seasonal influence on day and night urban heat island

As shown in Figures 4.7 and 4.8, the daytime and nighttime UHII shows obvious seasonal characteristics due to climatic influences and vegetation changes, and there are certain spatial differences in the UHII across the four seasons. Notably, Edmonton and Calgary exhibit the most significant seasonal variations in UHI. During the summer, fall, and spring, their UHII distribution trends are similar, but in the winter, they display contrasting patterns of UHII distribution. Specifically, areas with higher UHII in the summer, fall, and spring become lower UHII areas throughout the cities in the winter, particularly during daytime in Calgary and nighttime in Edmonton. On the other hand, Vancouver, Toronto, and Montreal exhibit consistent patterns of UHI distribution across all four seasons, although they also experience lower UHII values for the entire city during winter.

During the day, the highest summer UHII value is found in Vancouver, reaching up to 12.46℃, and a region near Lake Ontario in Toronto has the lowest value at -8.30℃. Obviously, in summer all five cities experience remarkably high daytime UHII values encompassing their entire urban areas. In the fall, the daytime UHII starts to decline in all cities, and the regions showing relatively high UHII values experience a substantial reduction in each city. Nevertheless, even during this season, the highest daytime UHII values exceeded 3℃ in all cities. Moreover, both the highest value and the lowest value are in Vancouver at 6.39℃ and at -4.82℃. During the winter months, the daytime UHII values are lowest. However, in winter Vancouver is still warmer than other cities, and different from the other seasons, in winter the daytime UHII of Vancouver greater than 0℃ across its entire city. This phenomenon is likely attributed to the very wet winter in Vancouver, which diminish the capacity of urban areas to dissipate heat. Additionally, Calgary and Edmonton experience higher maximum daytime UHII during the winter months compared to all other seasons. But the central regions of Calgary and Edmonton's urban areas display significant urban heat sinks. The low UHII observed in Edmonton and Calgary during winter might be attributed to the climate effects and air pollution. Both cities experience excessively harsh winters. At the same time, much of the power is generated by coal, which leads to increased emissions of air pollutants and thus reduces the absorption of shortwave solar radiation within urban areas (Zhou et al., 2015). Consequently, a combination of climatic causes and human activities reduces the LST in urban areas and leads to the urban heat sink

during winter. In the spring, the daytime UHII starts to increase. Similar to summer, the highest daytime UHII value is found in Montreal, reaching 10.42℃, while the lowest value is still observed along the lake in Toronto at -9.70℃.

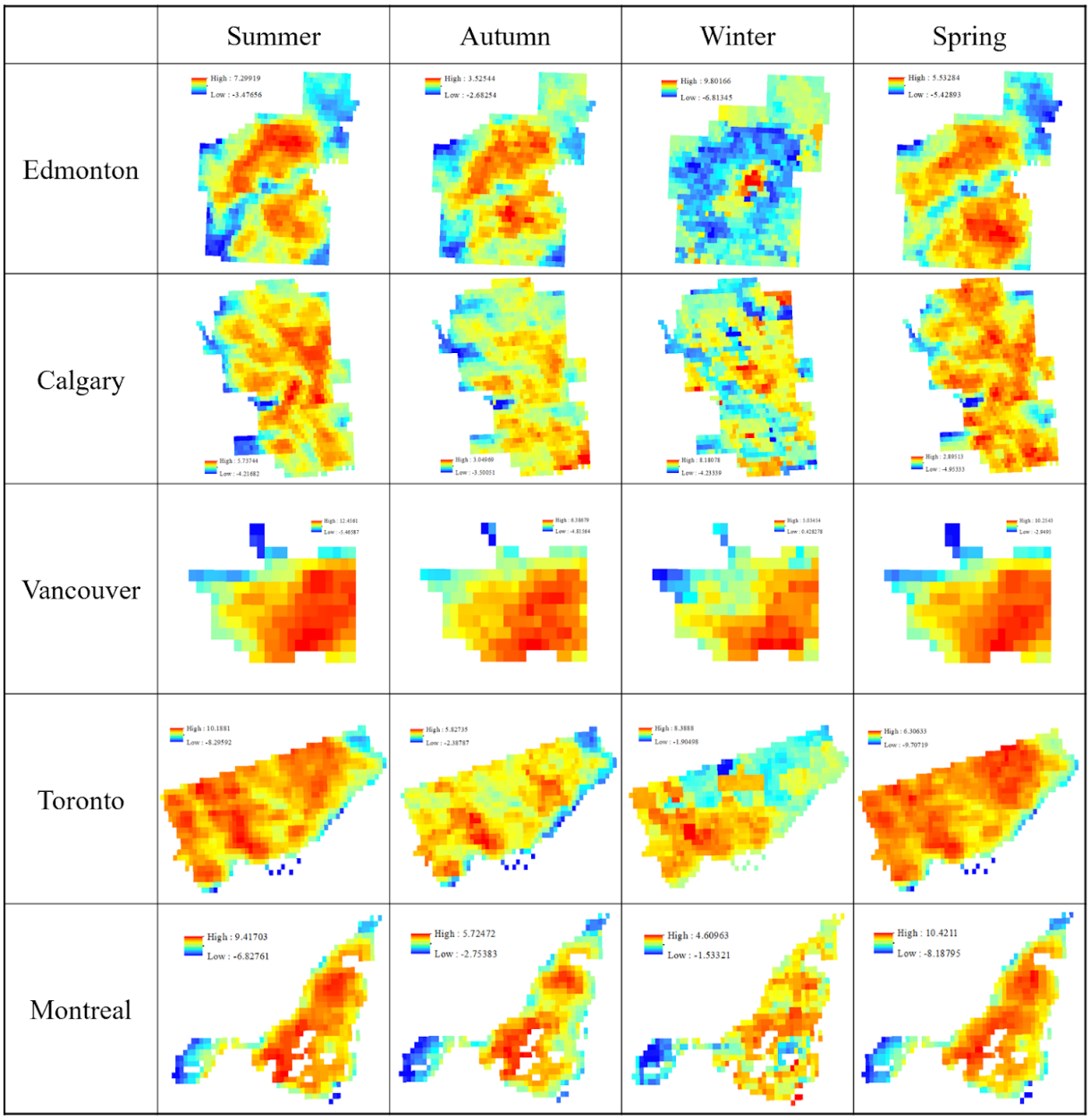

Figure 4.7 Four-season daytime UHI distribution map

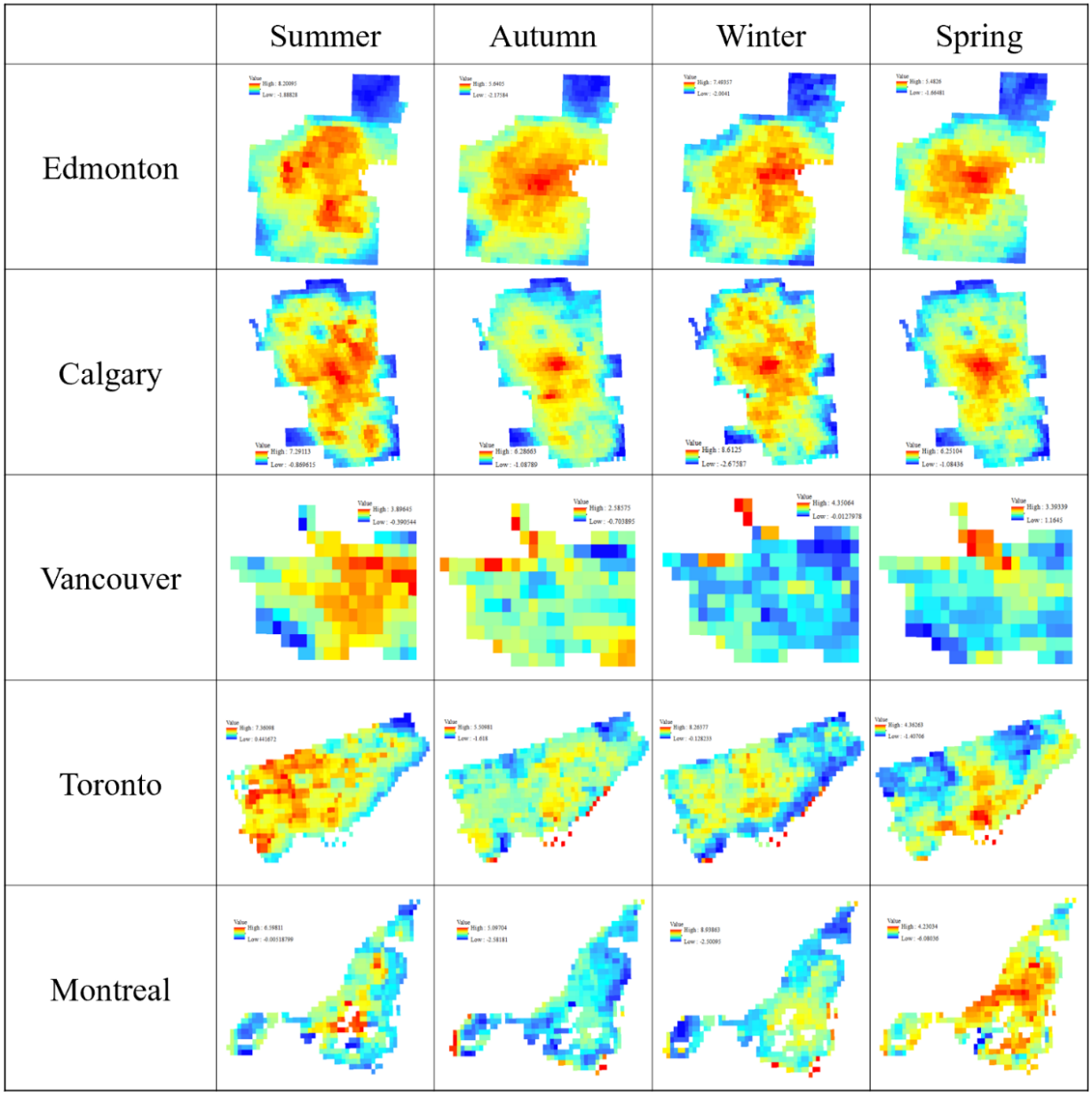

Figure 4.8 Four-season nighttime UHI distribution map

During the nighttime, all cities except Vancouver have a maximum summer UHII value of 6.5℃ or higher. Edmonton reaches its peak summer UHII value of 8.20℃, while Toronto and Calgary also experience a peak summer UHII value of over 7.3℃. Moreover, in Edmonton, regions near the surrounding rural areas still maintain a lower nighttime UHII value in the summer, at -1.89℃, respectively. In the fall, the peaks of the nighttime UHII were substantially decreased in all cities. In Vancouver, the highest recorded nighttime UHII value is only 2.59℃, which is

almost half of the peaks of other four cities. Meanwhile, in Montreal, regions near the water surfaces have the lowest nighttime UHII in the fall, at -2.58℃. During the winter season, Calgary and Edmonton show the significant nighttime UHI, that the central parts of cities exhibit extreme high nighttime UHII values. Besides, the highest nighttime UHII values among the five cities is observed in Montreal, at 8.94℃ and the lowest nighttime UHII values is observed in Calgary, at -2.68℃. During winter, the nighttime UHII in Vancouver remains above -0.01 ℃ across the entire urban area. During the spring season, the nighttime UHII significantly increased in Calgary, where the highest values reached 6.25℃ from -3.82℃. But the distribution patterns of spring nighttime UHII in all five cities remain consistent with the rest of the seasons.

As shown in Figure 4.9, with the exception of Edmonton, the seasonal trends in UHII for the other four cities are roughly the same during the day and at night. During the daytime, Toronto, Montreal, Vancouver and Calgary have relatively minimal seasonal variation in UHII, while Edmonton has more substantial seasonal fluctuations. Edmonton's daytime UHII value is below -1℃ during the winter months, while by nighttime it is instead higher than the UHII values during the fall and spring months. The relative stability of UHII values in Toronto, Montreal, Vancouver and Calgary during the day may be attributed to their proximity to bodies of water, as water bodies tend to have a temperature-regulating effect, helping to moderate the daytime UHII. Additionally, compared to cities with harsh winters such as Edmonton and Calgary, Vancouver has milder winters which may result in less variation in the daytime UHII during the winter months.

In contrast, the seasonal changes in nighttime UHII are smooth in all cities. In Edmonton, the nighttime UHII remains above 1℃ in all four seasons, which are higher than during the day. Calgary exhibits the nighttime UHII values above 2℃ for all seasons. In addition, Figure 4.9 illustrates that the summer season exhibits the highest daytime and nighttime UHII values. All five cities have average daytime UHII values greater than 2℃, and average nighttime UHII values greater than 1.6℃. Among them, Vancouver, Toronto and Montreal are particularly notable for having daytime UHII values exceeding 4℃, and the daytime UHII values are above 6℃ in both Vancouver and Toronto. In addition, the nighttime UHII values of Edmonton and Calgary are above 3℃ during the summer months, making the UHI effect particularly significant

during this period. This is the same result as the study findings of Li et al. (2017) on UHI in the continental United States. Furthermore, Edmonton, Calgary and Toronto had higher nighttime UHII values in winter compared to the fall and spring, mainly attributable to lower LST in rural areas, while all other cities had the lowest winter UHII values of the year.

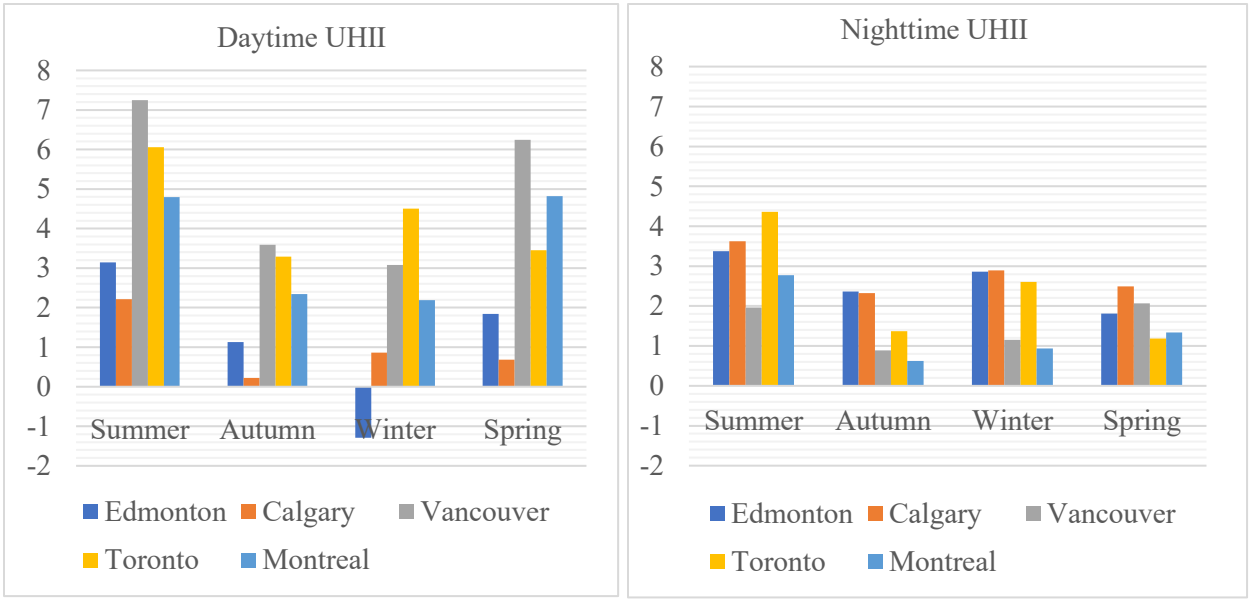

Figure 4.9 Annual average four-season day and night UHII

4.2.4 Monthly variation of average day and night urban heat island

In Figures 4.10, the shifting trends of monthly average daytime and nighttime land surface temperatures (LST) and urban heat island (UHII) are presented. As shown in Figure 4.8, daytime LST in the five cities are approximately the same from April through September, with Vancouver experiencing higher temperatures from January through March and Toronto experiencing higher temperatures from October through December. However, Vancouver's daytime UHII values only higher than other cities from April to July, while Calgary's daytime UHII values consistently maintain the lowest all year, except for January and December when it is the lowest in Edmonton.

In addition, Montreal has a very large increase in daytime UHII in March, and a small increase in Edmonton and Calgary. This phenomenon might be attributed to the extremely cold winters in

all three cities, with daytime land surface temperatures falling below -10℃, and nighttime land surface temperatures even below -20℃ in Edmonton and Calgary in February. As temperatures warmed up in March, the snow in the cities was cleared, while the rural areas still retained snow and ice. This created a substantial temperature difference between the urban areas and the rural areas, contributing to the significant increase in daytime UHII in Montreal and a relatively smaller rise in Edmonton and Calgary.

In comparison to the daytime, the fluctuations in both LST and UHII during the nighttime are more pronounced in all five cities, with larger ups and downs. As shown in Figures 4. 11, the trends in nighttime LST vary across the five cities, with only Calgary and Edmonton being roughly the same, but all of the nighttime UHII trends are quite different. Among them, Toronto has the most fluctuating trend in the nighttime UHII variation, while Vancouver has the smoothest UHII variation trend. This may account for small city size of Vancouver which makes it susceptible to the influence of the surrounding ocean on temperature moderation. The nighttime UHII in Toronto has a large drop in October and this is due to the fact that rural areas around Toronto are warmer than urban areas in October.

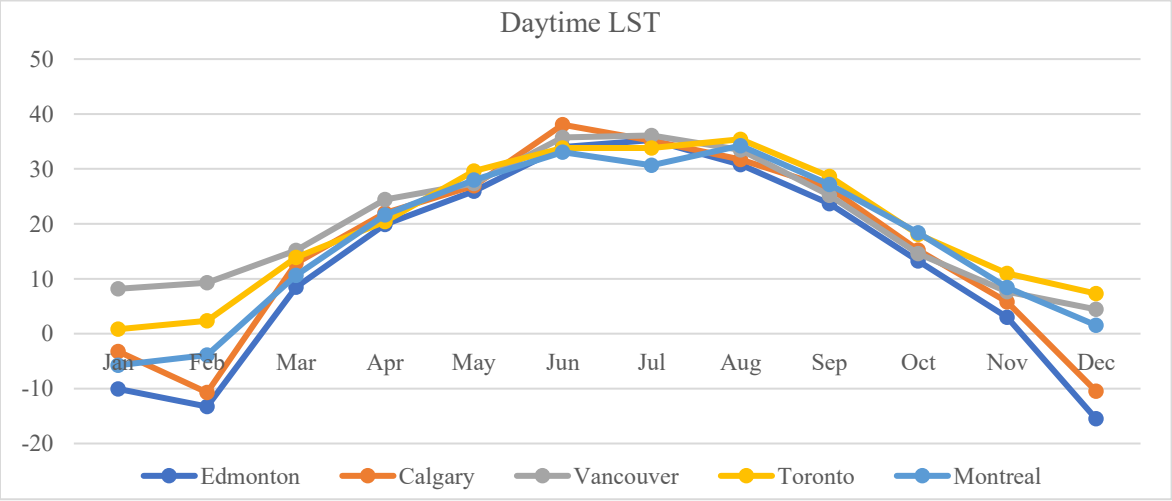

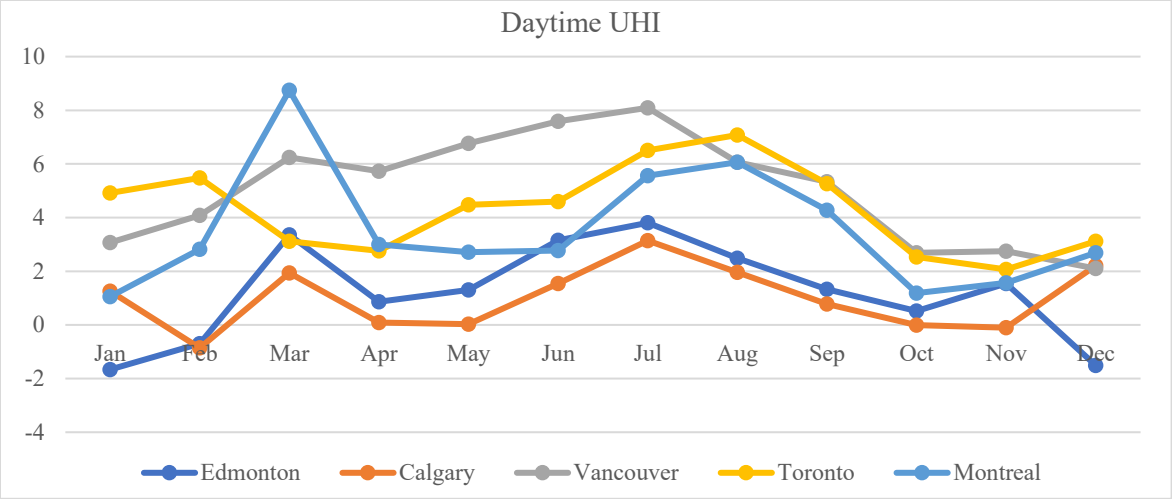

Figure 4.10 Monthly average daytime LST and UHII

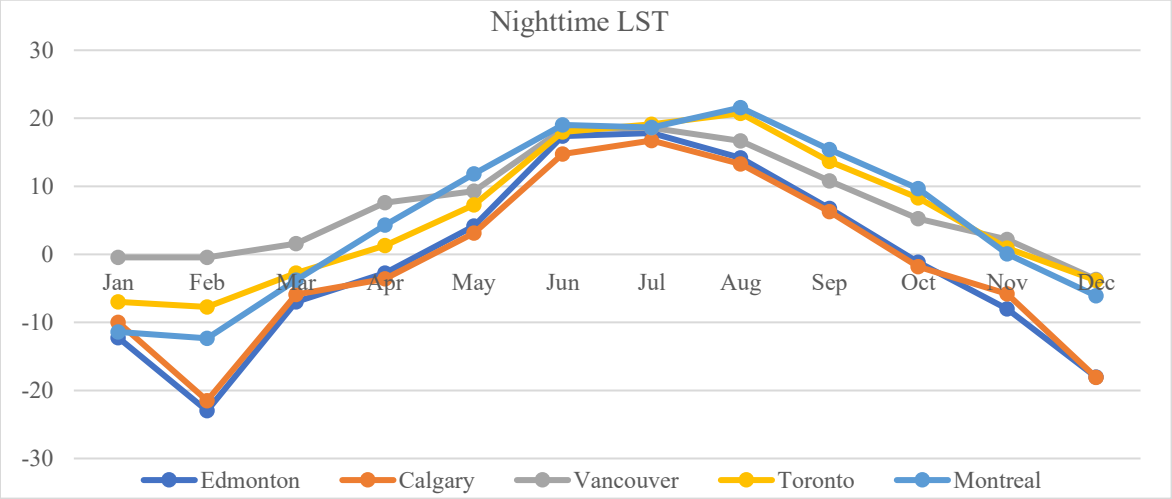

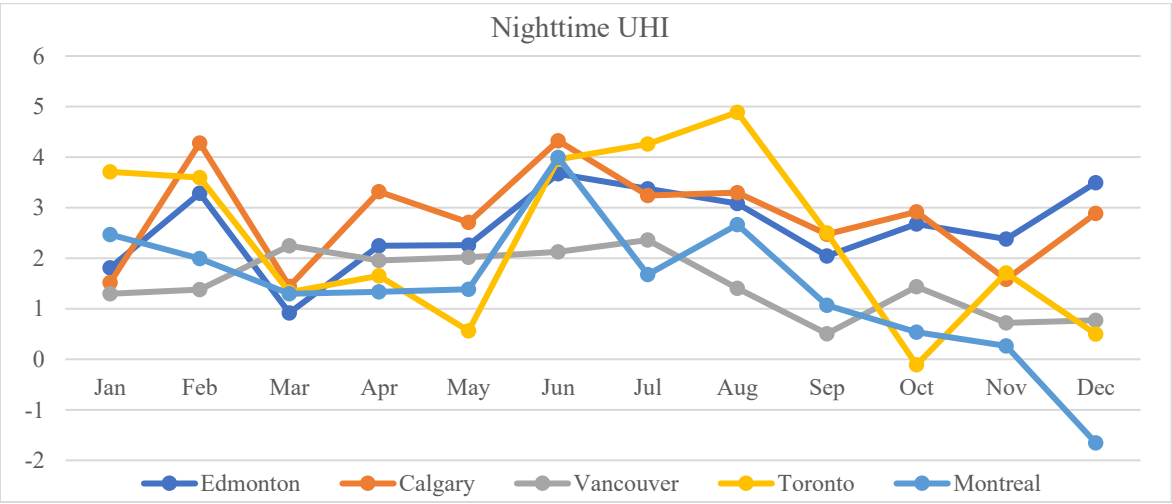

Figure 4.11 Monthly average nighttime LST and UHII

Considering that the daytime and nighttime UHII in Vancouver and Toronto are significantly higher than in other cities, possibly due to the influence of nearby water bodies (i.e., the North Pacific Ocean and Lake Ontario), this study conducted an analysis of the variations in the annual average LST for both urban and rural areas at different distances from the water bodies in these two cities. Additionally, the study also examines the differences in LST between the urban and rural regions at the same distance from the water bodies. To achieve this, buffer zones were created at 1-kilometer intervals around the water bodies to obtain urban and rural area bands at varying distances from the water bodies, thus acquiring the LST for each area band, as well as the temperature differences between the urban and rural area bands at the same distance from the water bodies.

As shown in Figure 4.12, in Vancouver, during the daytime, the closer the distance to the water bodies, the lower the LST in the urban area and the higher the LST in the rural area. Therefore, the daytime LST difference between the urban and rural areas at the same distance from the water bodies increases with the distance, indicating that the North Pacific Ocean has a significant influence on the daytime UHII in Vancouver. On the other hand, the variation trend of the nighttime LST in urban area is not very different from that in rural areas, so the variation of the LST difference between the urban and rural areas is not very significant at night. Thus, the impact of the North Pacific Ocean on the nighttime UHII in Vancouver is not significant. As shown in Figure 4.13, in Toronto, the daytime LST in the urban area decreases as the distance to Lake Ontario gets closer, but beyond 4 kilometers, the daytime LST in the urban area does not vary with distance. However, in the rural areas of Toronto within 2 kilometers from the water body, the daytime LST is lower when closer to the water body, and beyond 2 kilometers, the daytime LST decreases as the distance from the water body increases. Therefore, although Lake Ontario has little impact on the daytime LST in Toronto's urban area, it still influences the daytime LST in the rural areas to some extent, indicating that Lake Ontario has an effect on the daytime UHII in Toronto. Furthermore, at night, although the variation trend of the LST in urban area is smooth, the LST in rural areas decreases significantly as the distance from the water body increases, leading to the increase of the LST difference. Therefore, Lake Ontario also has an effect on the nighttime UHII in Toronto. In this regard, oceans have a greater impact on UHI than lakes during the day, while lakes have a greater impact on UHI than ocean at night.

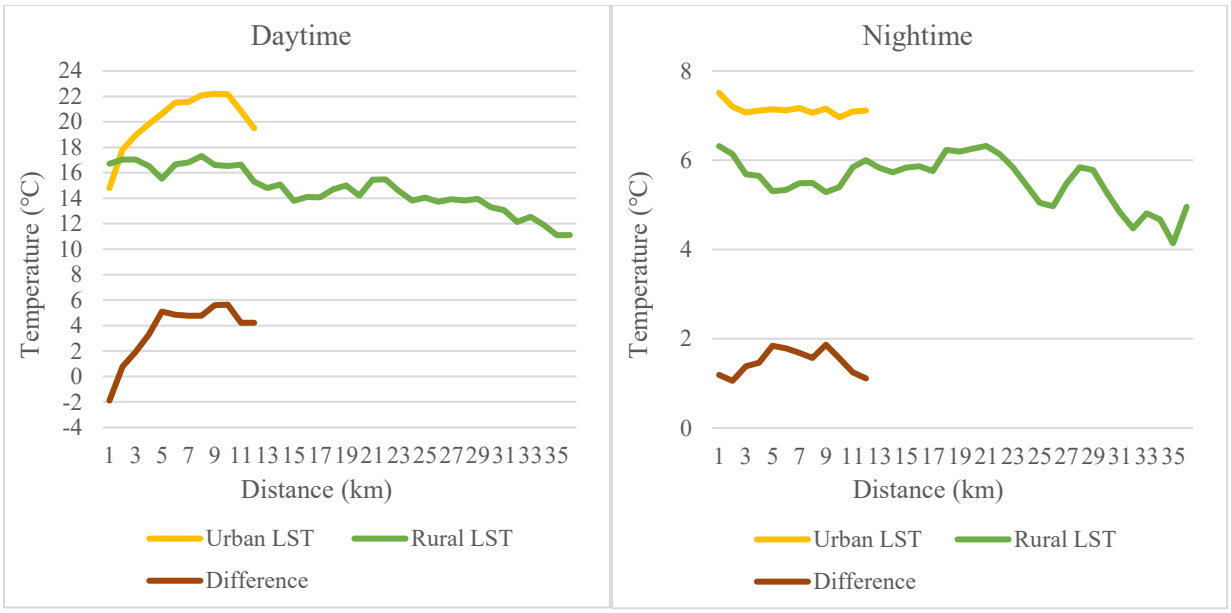

Figure 4.12 Urban and rural LST at different distances from water bodies in Vancouver

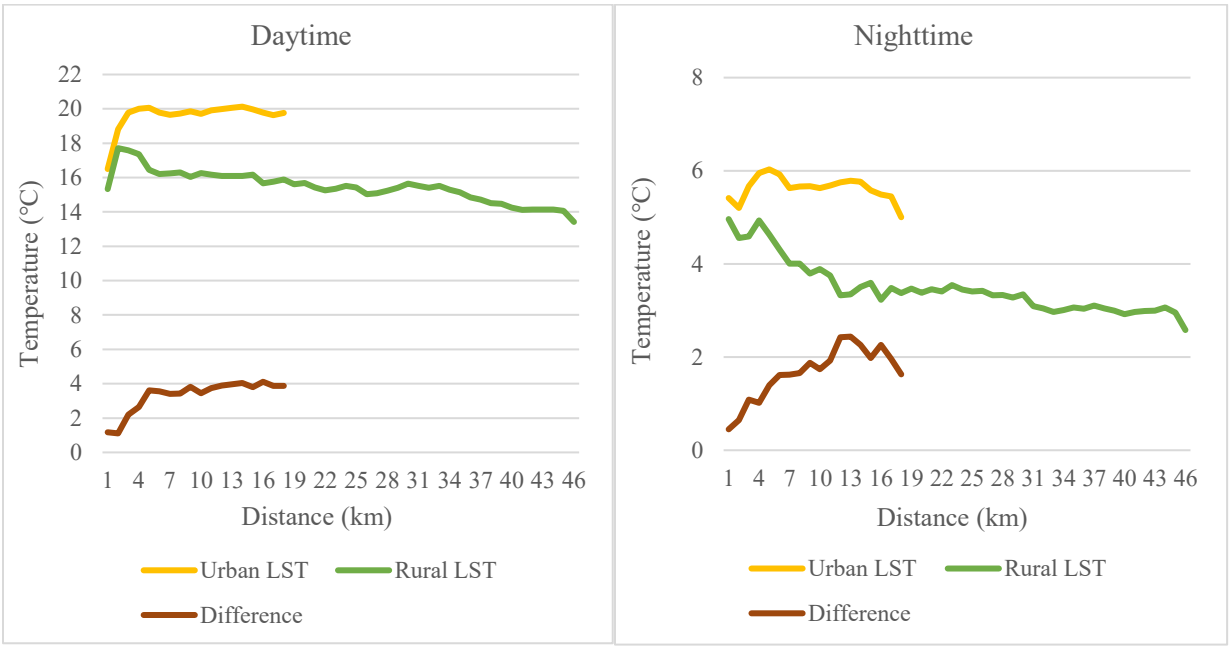

Figure 4.13 Urban and rural LST at different distances from water bodies in Toronto

4.3 Chapter Summary

This chapter analyzed the spatial and temporal distribution patterns of daytime and nighttime UHI in these five cities, as well as the effects of different land cover types on LST, based on MODIS LST data and land use data.

It was found that the daytime and nighttime UHII in all these five cities had significant seasonal and monthly variations. Vancouver and Toronto have the highest daytime UHII among the five cities, and Edmonton and Calgary have the highest nighttime UHII among the five cities. Large water bodies such as oceans or lakes have a certain impact on the UHI in the waterfront areas of Vancouver and Toronto, but the overall influence is not significant. Moreover, the LST trends for different land cover types in cities were different between daytime and nighttime, and built-up areas had the higher daytime and bare grounds had higher nighttime LST of the six land cover types. Besides, the influence of the ocean on LST within Vancouver's build-up area is minimal. In Vancouver and Toronto, grasslands do not provide much cooling effect. However, the ocean and lake can impact both daytime and nighttime UHI in these cities. In addition, the daytime and nighttime UHI intensities of all five cities have significant spatial autocorrelation.

Chapter 5. Factors influencing urban heat islands in Vancouver, Edmonton, Calgary, Toronto, and Montreal

Chapter 4 of this study delved into the spatial and temporal distribution of land surface temperature and UHIs, and then identified noticeable seasonal variations in UHIs. In this chapter, I further investigated the six environmental and socio-economic influencing factors contributing to the UHI. I conducted spatial effect analysis and developed the spatial regression models at the scale of census tracts to quantify the influential factors of the day and night UHI in the five cities in this study to gain a deeper understanding of the drivers of UHIs and their spatial patterns across these urban areas.

5.1 Effects of demographic factors

Two demographic factors were selected for this study, that are total urban population and urban population density. As shown in Figures 5.1 and 5.2, in each city, there are several neighborhoods with high population totals, exceeding 6,400 individuals. But no clear pattern of aggregation is represented. In contrast, when it comes to high population densities, only Montreal and Toronto have some neighborhoods with high population densities of more than 13,947.7 persons per square kilometer, all of which are concentrated in their respective downtown areas. Vancouver also has a few neighbourhoods with high population densities in the northern part of the city. In contrast, the population densities of both Edmonton and Calgary neighborhoods generally remain below 5,412.9 persons per square kilometer.

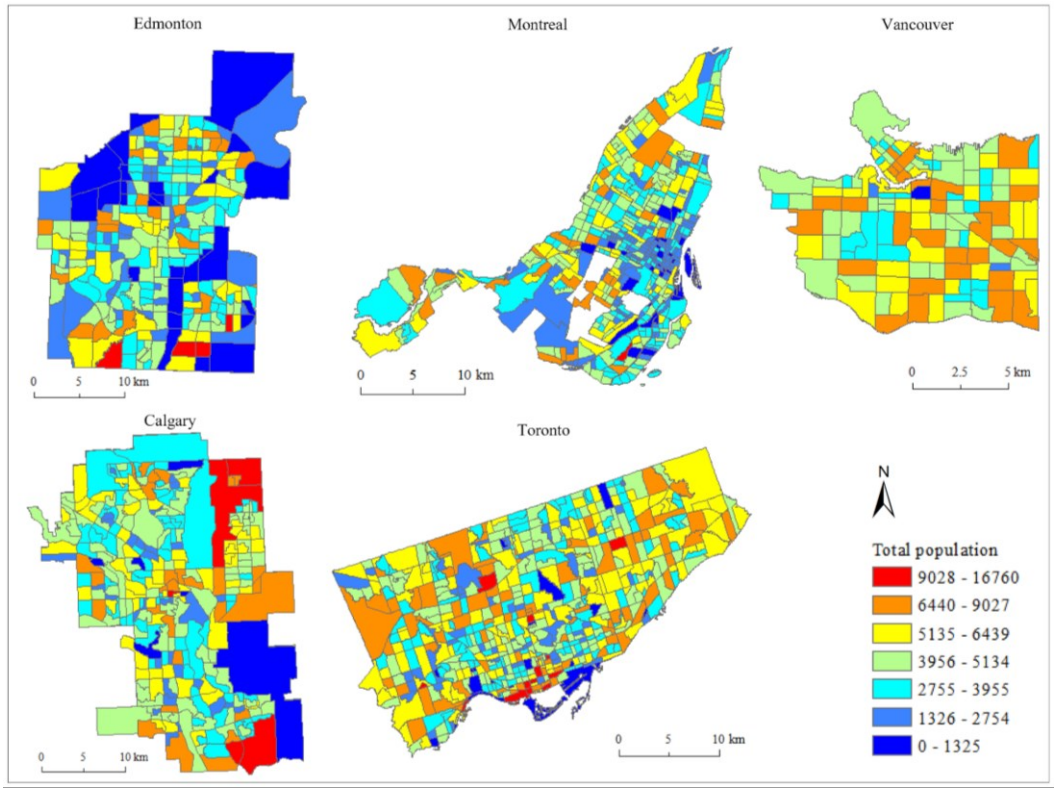

Figure 5.1 Total population distribution map

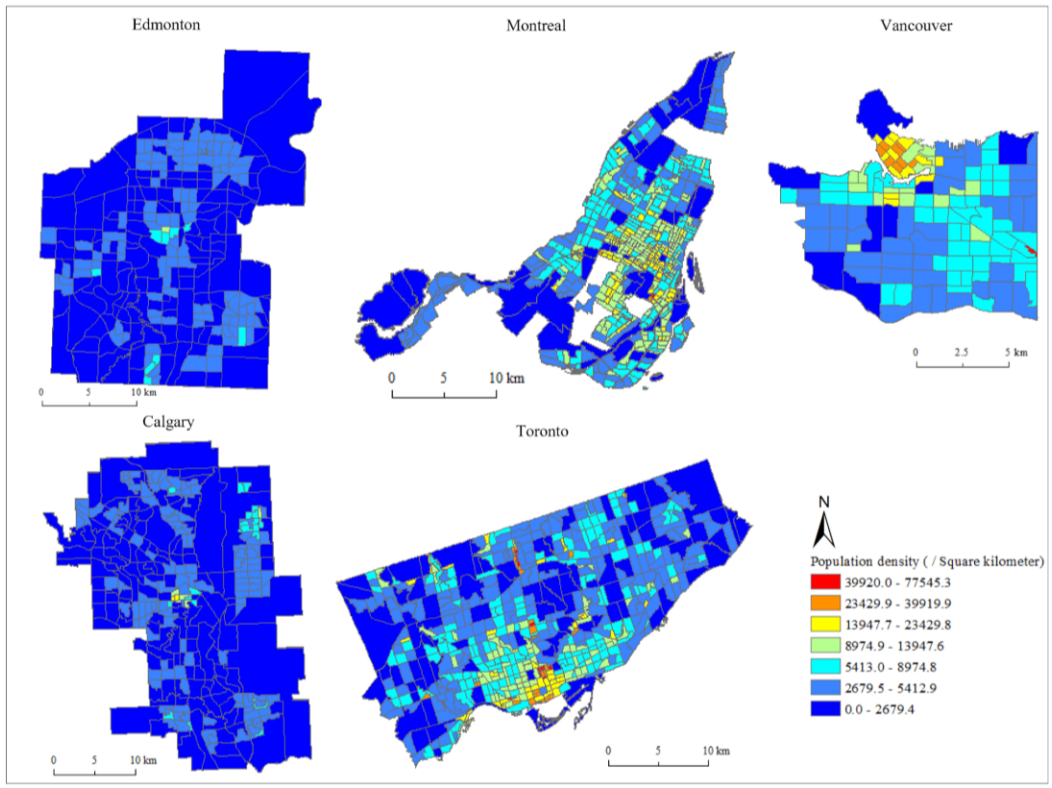

Figure 5.2 Population density distribution map

5.2 Socioeconomic factors

Due to the income inequality among individuals, median income is often considered a more reliable measure than average income, especially when the income gap is significant (Manitoba Collaborative Data Portal, 2018). This preference is due to its ability to withstand the influence of extreme values or outliers, ensuring a more accurate representation of the central income level in such scenarios. Hence, this study used the 2020 median after-tax income of households as an economic influencing factor. As presented in Figure 5.3, Calgary has the highest median after-tax income of households in 2020 at $85,000, followed by Edmonton at $79,500, while Montreal reports the lowest median after-tax income at $56,000.

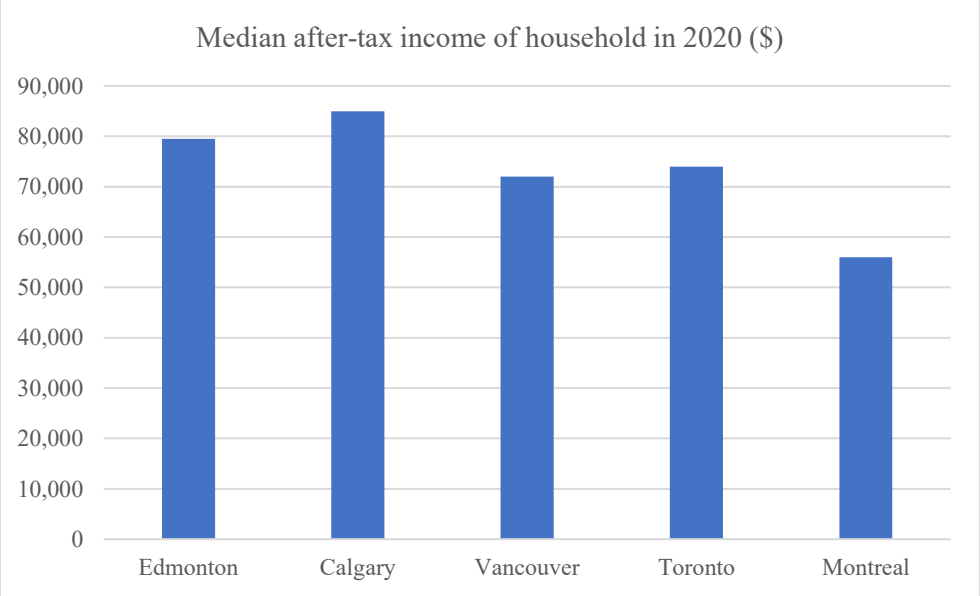

Figure 5.3 Median after-tax income of households in 2020 in five cities

As can be seen in Figure 5.4, similar to the cities' overall median after-tax income of households, Montreal's neighborhoods generally exhibit lower median after-tax incomes, essentially below $56,800, with only a few neighborhoods above $71,500. However, neighborhoods in Edmonton, Calgary, Vancouver and Toronto, with the exception of a few sparsely populated areas, have median after-tax incomes that are largely above $71,500. In Edmonton, Calgary and Toronto, there are several communities where the median after-tax income exceeds $111,000.

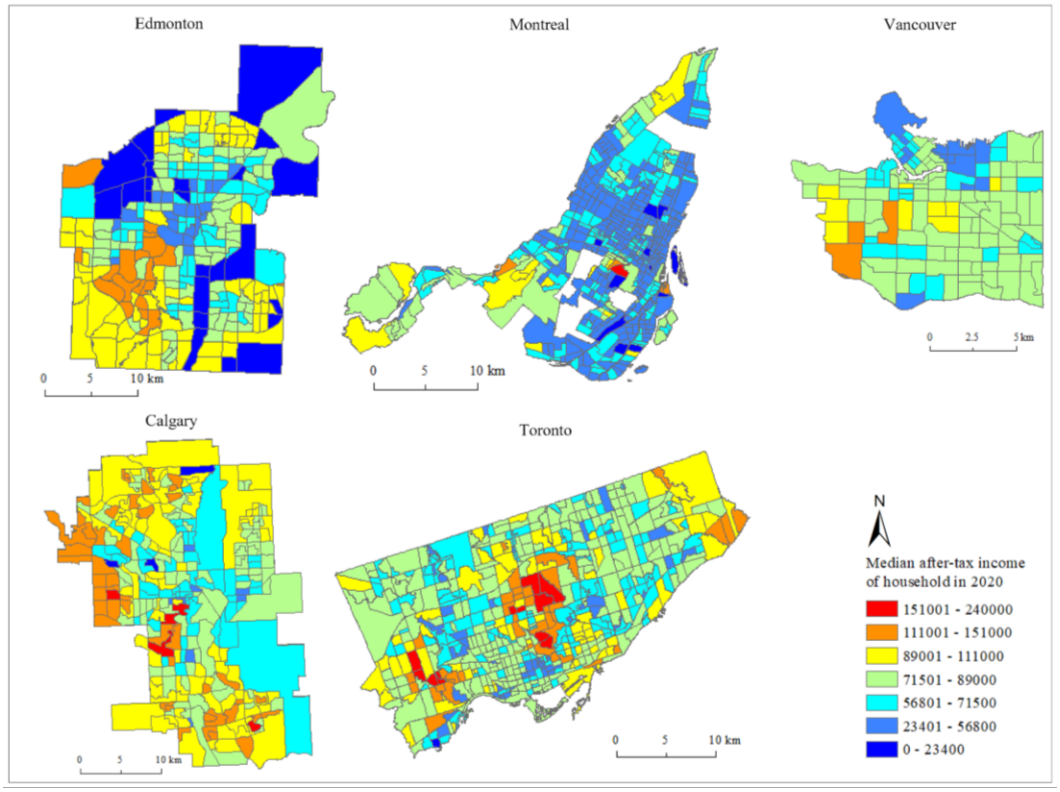

Figure 5.4 Median after-tax income of household distribution map

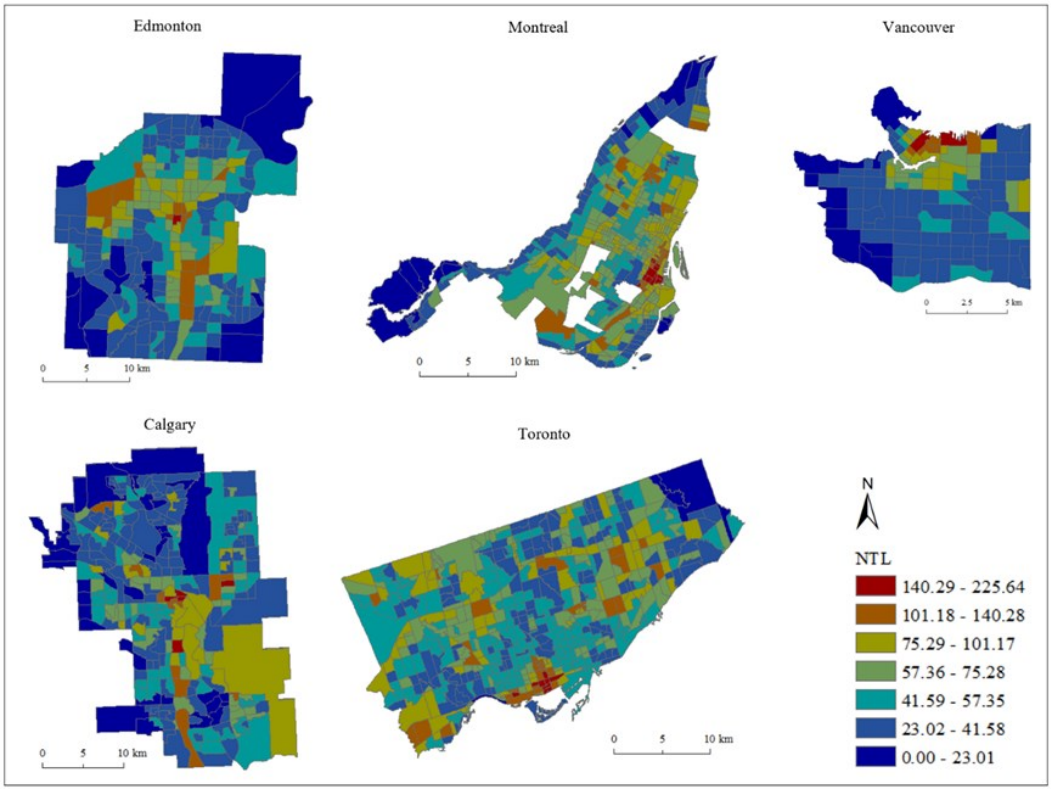

Figure 5.5 Nighttime light (NTL) value distribution map

The nighttime light (NTL) value can to some extent reflect the level of urbanization and socio-economic development (Zhao et al., 2019), and an increasing number of people are using nighttime light values to predict the intensity of UHIs (Sun et al., 2020; Sun et al., 2019). As shown in Figure 5.5, in the central part of Edmonton, the southwestern area of Calgary, and the central area of Montreal, the nighttime light values are relatively high, with NTL values generally reaching 75.29 and above in these areas. The areas with high NTL values in Vancouver are mainly concentrated in the downtown area, while in Toronto, the distribution of NTL values is more scattered, but the highest NTL values are also concentrated in the downtown area.

5.3 Natural environmental factors

The natural environment plays a crucial role in influencing the UHI. Vegetation including trees and green spaces in urban areas, can provide shade and cooling through evapotranspiration. These natural elements help to absorb and dissipate heat, reducing overall UHI intensity. Moreover, the configuration and distribution of green spaces in cities affect the spatial distribution and intensity of UHI. In addition, natural features such as water bodies, rivers and lakes can influence UHII. Water bodies have a cooling effect and can moderate temperature fluctuations in the surrounding urban areas, thereby mitigating the UHI effect.

Figures 5.6 and 5.7 display the distribution maps of Enhanced Vegetation Index (EVI) and Normalized Difference Water Index (NDWI) for the five cities. Typically, an area is considered a water body when the NDWI value is greater than 0.2 (EOS Data Analytics, 2023). However, as can be seen from Figure 5.7, all values are less than 0.1, so there are no water bodies at the neighborhood level in these five cities.

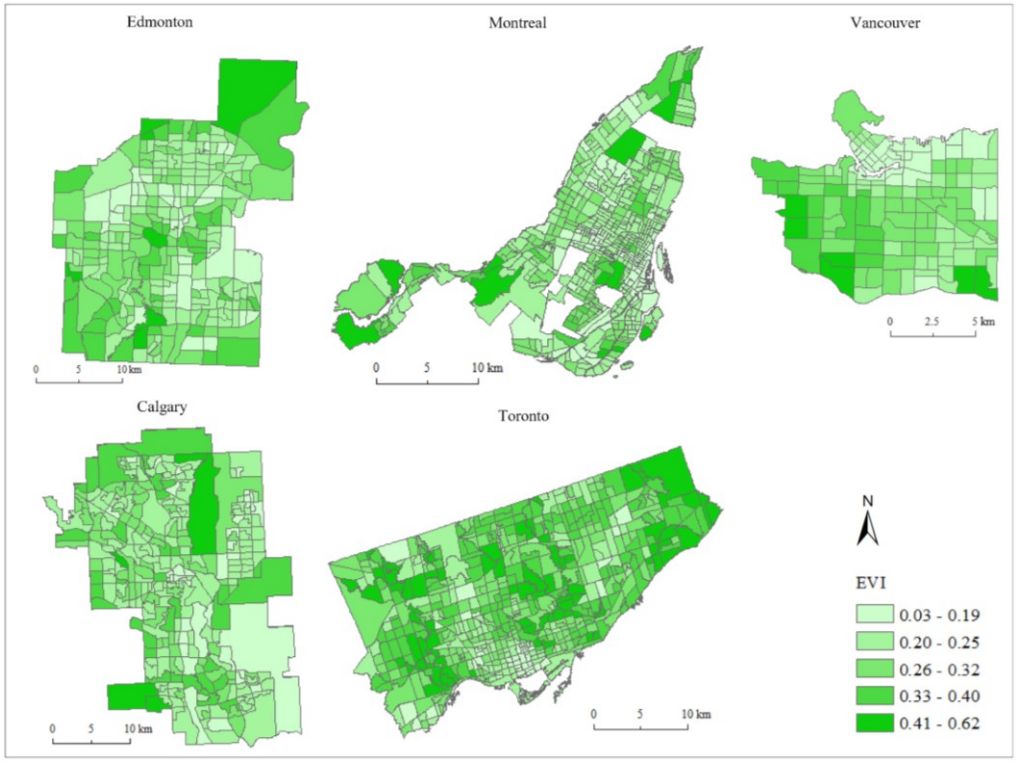

Figure 5.6 EVI distribution map

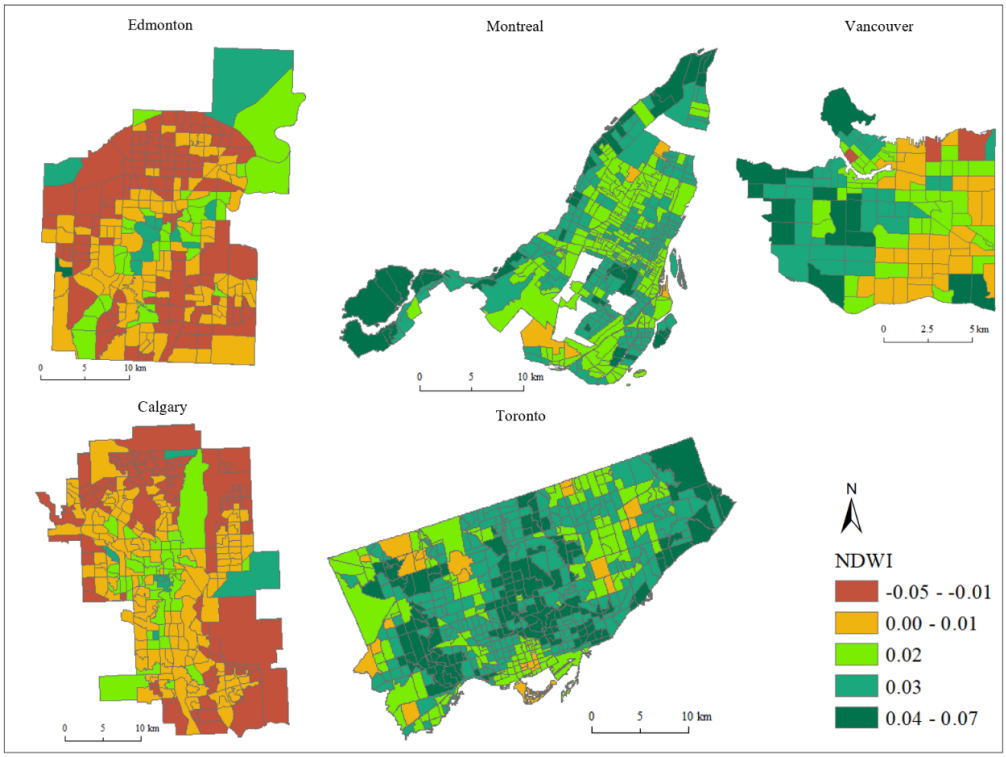

Figure 5.7 NDWI distribution map

As shown in Figures 5.6 and 5.7, Toronto has generally higher values for both vegetation index and water index, indicating more extensive vegetation cover and water presence. On the other hand, both Edmonton and Calgary exhibit overall lower values for the water index, indicating relatively less water presence in these two cities.

5.4 Establishment of indicator system

The larger the city, the higher the level of urbanization. City size is positively correlated with the rate of increase in UHII (Zhao et al., 2016), and besides being influenced by solar radiation, the UHI is also affected by the level of urbanization. However, due to the possibility of collinearity, this study chose nighttime light value data as the indicator representing the degree of urbanization. In other words, areas with higher levels of development have higher nighttime light values. I selected six natural environmental and socio-economic factors that influence the UHI, as shown in Table 5.1.

Table 5.1 Urban heat island influencing factor indicator system

Number	Type of indicator	Catalog
1	Socio-economic factors	Total population
2		Population density
3		Income (after-tax)
4		NTL
5	Natural environmental factors	NDWI
6		EVI

5.5 Regression model

5.5.1 Correlation analysis

Before conducting regression analysis, the correlation between daytime and nighttime UHII and the independent variables is analyzed, and the correlation coefficients between daytime and nighttime UHII and the independent variables are shown in Tables 5.2 and 5.3. From Table 5.2, it can be observed that the daytime UHII in Edmonton has a significant correlation with all six variables, while the daytime UHII in Montreal has a significant correlation with all variables except the total population, which did not pass the 5% significance level test. Similarly, the

daytime UHII in Calgary has a significant correlation with all variables except total population and NDWI, which did not pass the significance level test. The daytime UHII in Vancouver has a significant correlation with population density, median after-tax income of households, NDWI and EVI. Toronto's daytime UHII shows significant correlations with median after-tax income of households, NTL, NDWI and EVI.

Overall, the daytime UHII shows the strongest correlation with median after-tax income of households and EVI, both of which exhibit significant negative relationships with the daytime UHII in all cities except Vancouver. This indicates that areas with higher vegetation coverage or higher income population tend to have lower daytime UHII values. This could be attributed to wealthier residential areas having higher vegetation coverage, leading to lower UHII in those regions. Similarly, there is a significant negative correlation between NDWI and the daytime UHII, meaning that areas with more water bodies tend to have lower daytime UHII values. On the contrary, NTL shows a positive correlation with daytime UHII, indicating that areas with higher levels of urbanization tend to have stronger daytime UHII.

Interestingly, population density exhibits a significant positive correlation with the daytime UHII in Montreal, Edmonton, and Calgary, while it shows a significant negative correlation with daytime UHII in Vancouver. This suggests that in Montreal, Edmonton, and Calgary, higher population density is associated with stronger daytime UHII, while in densely populated areas of Vancouver, the daytime UHII is lower. Similarly, when the nighttime UHII in other cities shows a significant negative correlation with EVI and median after-tax income of households, in Vancouver, it shows a significant positive correlation with EVI and median after-tax income of households. The reason for this difference may be due to the fact that in Vancouver, most people reside in areas where is close to the coastline, and as previously found in Chapter 4, areas closer to water bodies in Vancouver tend to have lower daytime UHII values. In addition, because the downtown area in Vancouver is located near the coast, and high-income individuals tend to reside in areas away from the downtown area. As a result, the downtown area with higher population density experiences lower daytime UHII due to the influence of the ocean. On the other hand, areas where high-income individuals reside have higher vegetation cover, but since they are located further away from the coastline, they experience higher daytime UHII.

Table 5.2 Correlation coefficient between daytime UHII and independent variables

	Montreal	Edmonton	Calgary	Toronto	Vancouver
Total population	-0.042	-0.151*	-0.032	-0.049	0.072
Population density	0.246**	0.265**	0.303**	-0.016	-0.372**
Income (after-tax)	-0.141**	-0.286**	-0.418**	-0.098*	0.261**
NTL	0.301**	0.391**	0.426**	0.190**	-0.086
NDWI	-0.538**	-0.515**	0.098	-0.342**	-0.344**
EVI	-0.281**	-0.597**	-0.479**	-0.337**	0.195*

* Significant at the 0.05 level. ** Significant at the 0.01 level.

The correlation coefficients between nighttime UHII and the independent variables are shown in Table 5.3. different with the daytime UHI, the nighttime UHII in Edmonton is significantly correlated with only four independent variables, that is population density, median after-tax income of households, NTL and EVI. In Montreal, the nighttime UHII also shows significant correlations with four out of six independent variables, excluding median after-tax income of households and NTL. In Calgary, the nighttime UHII shows significant correlations with five out of six independent variables, except for total population. However, unlike daytime UHI, the nighttime UHII in Toronto shows significant correlations with only three independent variables, that is, population density, NTL and NDWI. In Vancouver, the nighttime UHII is significantly correlated with population density, median after-tax income of households, NTL, and EVI.

Table 5.3 Correlation coefficient between nighttime UHII and independent variables

	Montreal	Edmonton	Calgary	Toronto	Vancouver
Total population	-0.128**	-0.079	-0.079	-0.035	0.049
Population density	0.218**	0.204**	0.298**	0.318**	0.389**
Income (after-tax)	-0.046	-0.240**	-0.450**	0.067	-0.252**
NTL	0.060	0.584**	0.586**	0.111**	0.323**
NDWI	-0.208**	0.107	0.561**	0.153**	0.058
EVI	-0.141**	-0.439**	-0.302**	-0.067	-0.311**

* Significant at the 0.05 level. ** Significant at the 0.01 level.

From the overall nighttime UHI situation, nighttime UHII exhibits the strongest correlations with population density, which shows significant positive correlation with nighttime UHII in all five cities. NTL also shows a significant positive correlation with nighttime UHII in four cities, except for Montreal. EVI is significantly negatively correlated with nighttime UHII in four cities, except for Toronto. However, there are some differences between these cities. The nighttime UHII in Calgary and Edmonton show a significant positive correlation with NDWI, while in Montreal, it shows a significant negative correlation with NDWI. This might be because that the climate in Calgary and Edmonton is more arid, and water bodies have an insulating effect as the temperature drops slowly at night.

5.5.2 Ordinary least squares (OLS)

Spatial autocorrelation analysis indicates that both the daytime and nighttime UHI in the five cities show significant spatial dependence. To compare with the geographic weighted regression (GWR), this study also establishes global regression models using ordinary least squares (OLS) regression for the daytime and nighttime UHII in each city. Exclude variables that did not pass the 5% significance test in the correlation analysis and conduct spatial regression analysis on the remaining independent variables and daytime and nighttime UHI.

Furthermore, it is crucial to conduct multicollinearity tests because high correlations and interrelationships among independent variables in the regression model can seriously affect the analysis results. In this paper, the variance inflation factor (VIF) is used to test for multicollinearity among independent variables. When VIF > 7.5, it indicates the presence of multicollinearity issues among variables (Zhu, 2016). Based on the VIF test, no multicollinearity problems were found among these independent variables, allowing for further regression analysis. Then, by performing a significance test and removing the nulls, the best-fitting models were established.

Table 5.4 presents the detailed results of the OLS estimation for the daytime and nighttime UHI. The AIC test of the OLS models indicates the optimal bandwidth and the goodness of fit R^2 for daytime and nighttime UHII in each city. A higher R^2 value and a smaller AIC value indicate a better fit of the model. For the daytime UHI, the OLS model of Edmonton shows the best

explanatory effect with an R^2 of 0. 455 and a AIC of 1019.722, followed by Vancouver. For the nighttime UHI, the OLS model of Calgary exhibits the best explanatory effect with an R^2 of 0. 651 and an AIC of 560.181, followed by Edmonton. However, the R^2 for the OLS model of nighttime UHI in Montreal is only 0.092, indicating that the model cannot explain nighttime UHI in Montreal effectively. Further research is needed to identify the influencing factors of nighttime UHI in Montreal.

Table 5.4 Comparison of the goodness of fit for the OLS models of day and night UHI

		Montreal	Edmonton	Calgary	Toronto	Vancouver
Day	R^2	0.335	0.455	0.315	0.130	0.454
	Adjusted R^2	0.331	0.444	0.311	0.127	0.441
	AIC	2077.698	1019.722	985.596	2372.132	697.869
Night	R^2	0.092	0.375	0.651	0.167	0.263
	Adjusted R^2	0.087	0.367	0.646	0.163	0.245
	AIC	806.643	737.986	560.181	871.532	62.729

5.5.3 Geographically weighted regression (GWR)

Because regression models with statistically significant non-stationarity are often suitable for Geographic Weighted Regression (GWR) analysis, this study conducted GWR analysis separately for daytime and nighttime UHI in each of the five cities. As shown in Table 5.5, compared to the goodness of fit and AIC values of the OLS models, the GWR models have higher global R^2 values and lower AIC values. In particular, the nighttime UHI OLS model in Montreal shows a low R^2 value of 0.092, whereas the nighttime UHI GWR model exhibits a significantly higher R^2 value of 0.51. Therefore, it can be concluded that for the daytime and nighttime UHI in each city, the GWR models are more appropriate and show the best goodness of fit performance. Meanwhile, the GWR models also consider the spatial variations.

Table 5.5 Comparison of the goodness of fit for the GWR models of day and night UHI

		Montreal	Edmonton	Calgary	Toronto	Vancouver
Day	R^2	0.759	0.688	0.636	0.606	0.846
	Adjusted R^2	0.713	0.622	0.556	0.553	0.796
	AIC	1663.889	929.187	884.481	1986.287	581.457
	Bandwidth	2917.141	6282.316	4326.532	3535.025	2316.929
Night	R^2	0.506	0.804	0.753	0.758	0.531
	Adjusted R^2	0.464	0.772	0.722	0.699	0.448
	AIC	567.323	491.478	496.724	340.408	32.262
	Bandwidth	5139.201	5364.575	7544.095	2956.353	3294.304

Figure 5.8 displays the spatial distribution maps of the local R^2 for the GWR models of daytime and nighttime UHI in Edmonton, as well as the spatial distribution maps of intercepts and coefficients for the significant variables. As shown in Figure 5.8, the Local R^2 values for daytime UHI in Edmonton range from 0.21 to 0.86, with higher fit in the northern and western regions, indicating a more significant impact of explanatory variables on daytime UHI in those areas. Daytime UHI intensity in the northern region may be influenced more by factors such as vegetation coverage, and population density. For nighttime UHI in Edmonton, the Local R^2 values for the GWR models range from 0.18 to 0.86, with higher fit observed in the northern and southeastern areas, suggesting that explanatory variables have a stronger impact on nighttime UHI in these regions. Vegetation and NTL, i.e., degree of urban industrialization, have significant influence on nighttime UHI intensity in these areas.

Intercepts typically represent the strength of UHI, independent of influencing factors. As shown in Figure 5.8, the intercept values for daytime UHI are higher in the south and north regions, gradually decreasing towards the central areas. This suggests that when all explanatory variables are zero, the model predicts higher UHI values in the south and north regions. For nighttime UHI, the intercept values are higher in the northwestern regions, gradually decreasing towards the southeastern areas. Additionally, the coefficients of the five main variables related to daytime and nighttime UHI intensity exhibit significant spatial variability.

Regarding daytime UHI, the spatial distribution of the EVI coefficient indicates higher absolute values in the northern and western regions, while the southern and central regions display slightly lower absolute values, suggesting that vegetation has a greater impact on UHI in the northern and western regions compared to the southern and central regions, that is, vegetation plays a more significant role in mitigating UHI in the northern and western regions compared to the southern and central regions. The spatial distribution pattern of the NDWI coefficient differs from EVI and exhibits opposite correlations in different regions. In the central region, NDWI shows a significant negative correlation with daytime UHI, indicating that higher water body coverage leads to lower UHI values.

In contrast, in the northern and southern regions, NDWI shows a significant positive correlation with daytime UHI, suggesting that higher water body coverage leads to higher UHI values in these regions. This indicates that water bodies play a warming role in urban fringe areas with more vegetation, while in urban areas with more buildings and less vegetation, water bodies have a cooling effect, alleviating the UHI effect. Similarly, the spatial distribution of population density, total population and income correlate differently in various urban regions. In the north parts, population density and income exhibit a negative correlation with daytime UHI, while in the southern regions, population density and income and daytime UHI are positively correlated. This suggests that high population densities and low population incomes in the north parts of Edmonton exacerbate the UHI effect during the daytime.

For nighttime UHI, as shown in Figure 5.8, the spatial distribution patterns of EVI and population density coefficients in the GWR models is basically the same with those of daytime UHI. The coefficient values of NTL are higher in the northern and eastern regions and relatively lower in the western areas, indicating that the degree of urbanization has a greater influence on nighttime UHI in the northern and eastern regions and a relatively smaller impact in the western areas. Additionally, the smaller coefficients for NTL and population density are due to the difference in units between NTL, population density and UHII values, not that they are not significantly correlated with the UHI.

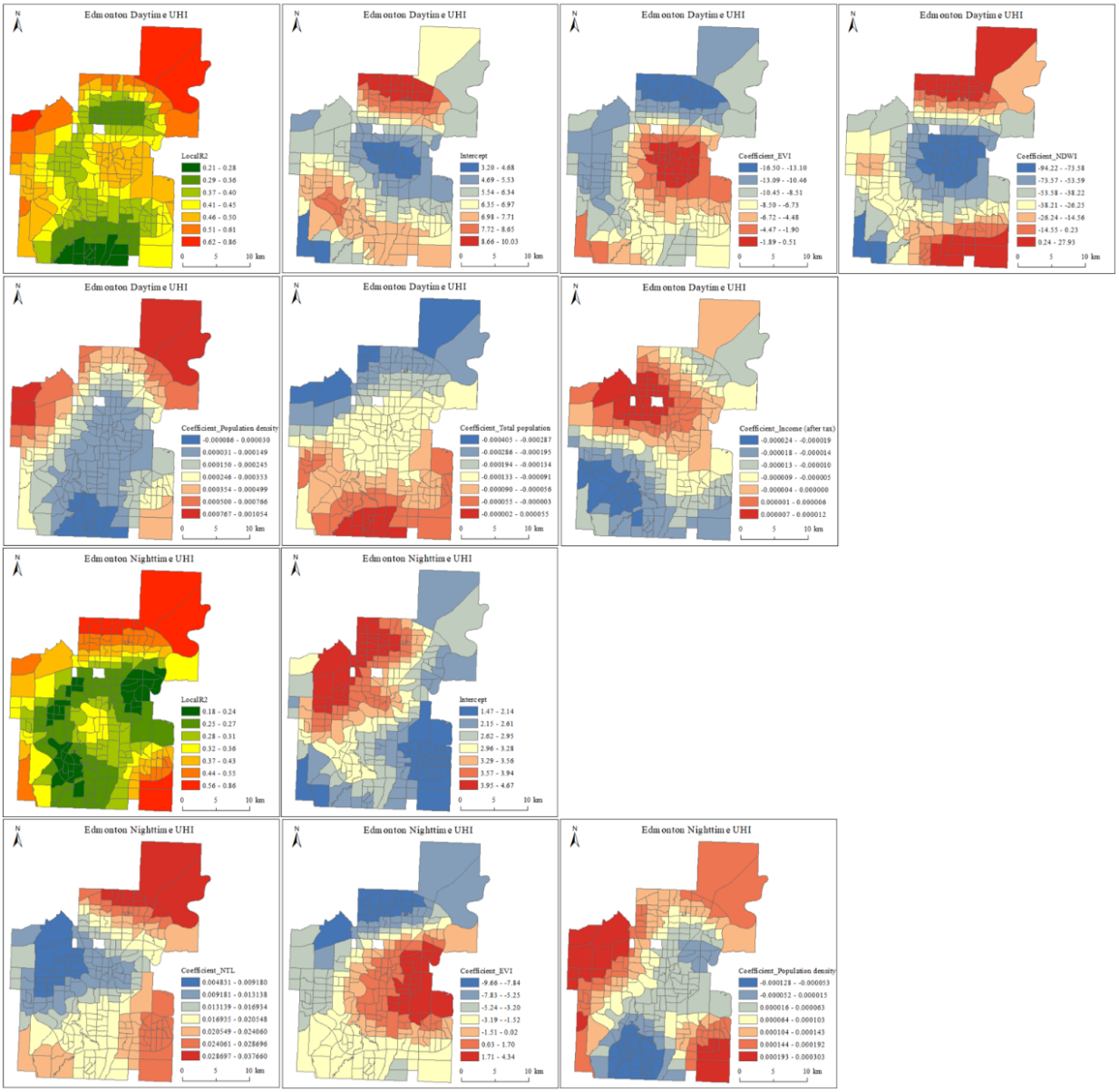

Figure 5.8 Spatial distribution maps of Local R^2, intercepts, and coefficients of the main variables for the GWR models of daytime and nighttime UHI in Edmonton

Figure 5.9 presents the spatial distribution maps of Local R^2, intercepts, and main variable coefficients for the GWR models of daytime and nighttime UHI in Calgary. As shown in Figure 5.9, the daytime UHI GWR model in Calgary exhibits a Local R^2 range of 0.01-0.76, with higher goodness of fit observed in the eastern and western regions, indicating a more significant impact of explanatory variables on daytime UHI in these areas. The daytime UHI intensity in these regions may be influenced more by EVI. For the nighttime UHI GWR model in Calgary, the

Local R^2 varies from 0.32 to 0.79, with higher goodness of fit observed in the central part of the city, suggesting a more significant impact of explanatory variables on nighttime UHI in these areas. NDWI has a more pronounced effect on nighttime UHI intensity in these regions. However, it is evident that the overall Local R^2 values for both daytime and nighttime UHI in Calgary are lower compared to Edmonton. As depicted in Figure 5.9, the intercept values for daytime UHI are higher in the northeastern and southwestern regions, gradually decreasing towards the central region. This indicates that the daytime UHI intensity is higher in the northeastern and southwestern part of Calgary. However, the intercept values at nighttime are higher in the western region and middle eastern region. Additionally, the coefficients of the main variables associated with daytime and nighttime UHI in Calgary also display substantial spatial variability.

Regarding the coefficients of EVI, it can be observed that the western region has higher absolute values, while the central region, where is the downtown area, has lower absolute values for daytime UHI, which indicate that the influence of vegetation is higher in the western regions compared to the central regions, indicating weaker associations between vegetation and daytime UHI in these areas. This situation is similar to the distribution of EVI coefficients in Edmonton, where the impact of vegetation is higher in areas with higher levels of urban economic development. Income exhibits a positive correlation with daytime UHI in the central and southeastern region and a negative correlation with daytime UHI in the northeastern and southwestern region, indicating a stronger influence of urban development on daytime UHI in northeastern and southwestern areas.

For the nighttime UHI GWR model in Calgary, the spatial distribution of EVI coefficients differ from daytime, where vegetation has a limited impact on nighttime UHI in the entire eastern region but a higher impact in western regions. The coefficients of NTL in the central-eastern region are greater than in the southern region. The trends in nighttime light values are often closely related to the intensity of urban economic development, and the central-eastern regions of Calgary generally have stronger nighttime light values. Moreover, higher income in the northeastern and southeastern region correspond to higher UHI values, while in the western region, higher nighttime light values are associated with lower UHI values. In contrast to other

cities, in Calgary, NDWI is significantly positively correlated with nighttime UHI, i.e., the more moisture, the higher the UHI value, and the effect of NDWI on nighttime UHI is greater in the western part of Calgary.

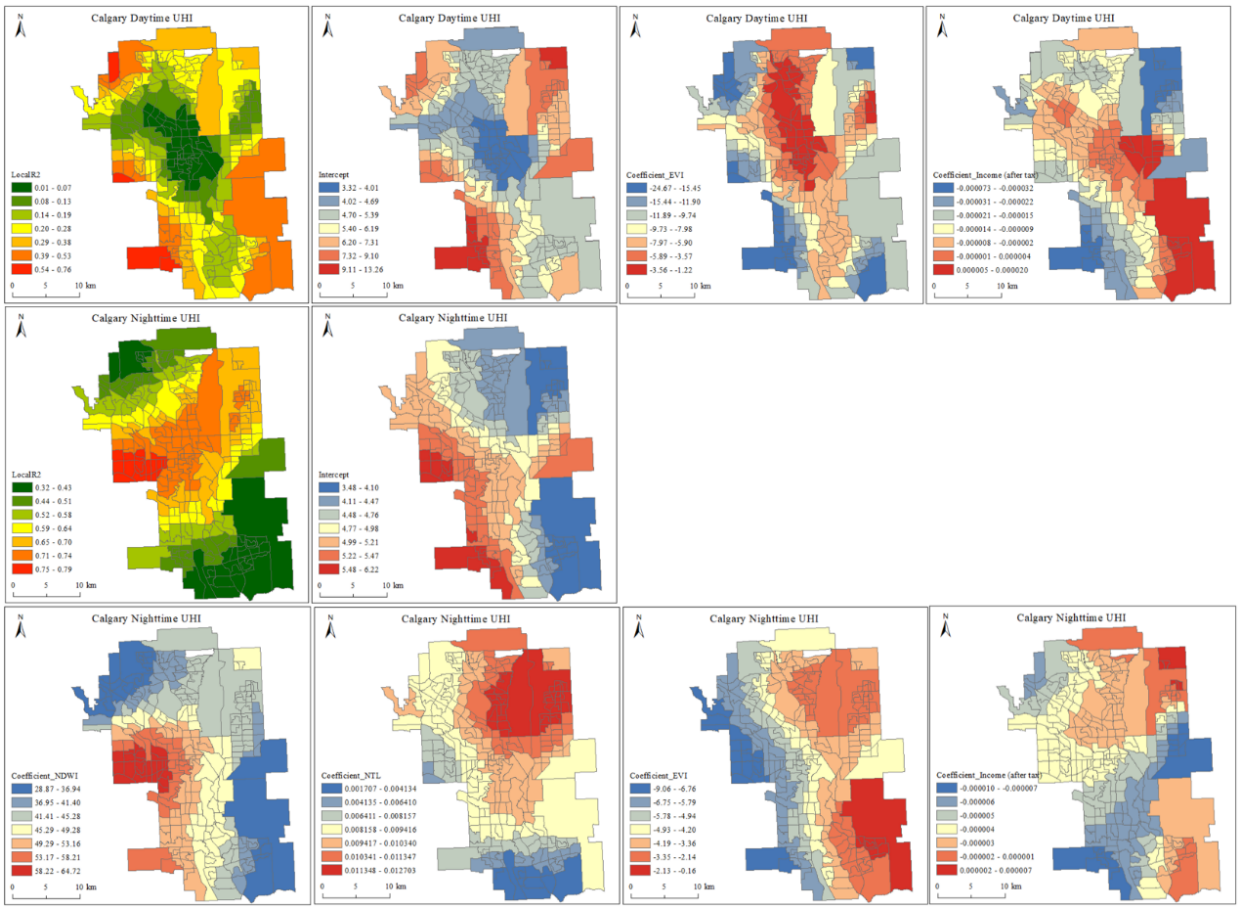

Figure 5.9 Spatial distribution maps of Local R^2, intercepts, and coefficients of the main variables for the GWR models of daytime and nighttime UHI in Calgary

Figure 5.10 presents the spatial distribution maps of Local R^2, intercepts, and main variable coefficients for the GWR models of daytime and nighttime UHI in Vancouver. As shown in Figure 5.10, the daytime UHI GWR model in Vancouver exhibits a Local R^2 range of 0.07-0.59, with higher goodness of fit observed in the central part and southern part of the city, indicating a more significant impact of explanatory variables on daytime UHI in these areas. For the nighttime UHI GWR model in Vancouver, the Local R^2 varies from 0.02 to 0.48, with higher goodness of fit observed in the western areas, suggesting a more significant impact of

explanatory variables on nighttime UHI in these regions. Population density, vegetation and water bodies are the main significant explanatory variables influencing both daytime and nighttime UHI intensity. As depicted in Figure 5.10, the intercept values for daytime UHI in Vancouver are higher in the southern regions and gradually decrease towards the northern regions, indicating higher daytime UHI intensity in the southern part of Vancouver. For the nighttime UHI, the intercept values are higher in the northwestern regions, indicating stronger nighttime UHI in these areas. Moreover, there is substantial spatial variability in the coefficients of the key variables associated with daytime and nighttime UHI intensity in Vancouver.

Regarding the daytime UHI, the spatial distribution of NDWI coefficients indicates higher absolute values in the western region and lower absolute values in the northeastern region. Moreover, in the western region, NDWI shows a negative correlation with the daytime UHI, indicating a stronger impact of water bodies on UHI mitigation in these areas. However, in the northeastern region of Vancouver, the influence of water bodies on daytime UHI is weaker and it can even exacerbate the UHI effect, suggesting the need for considering other measures to alleviate daytime UHI in this area. Similar, EVI in the central part of Vancouver has significant positive correlation with daytime UHI, which is different from most of the previous findings that vegetation has a negative correlation with the UHI (Tran et al., 2017; Zhang et al., 2013; Schwaab et al., 2021). Only in the very small part of the north and south areas can vegetation serve to mitigate the UHI. From the results in Chapter 4, this may be due to the fact that among the vegetation, it is the trees that have a mitigating effect on the UHI in Vancouver, whereas in Vancouver the LST of grasses, shrubs, and flood plants are even higher than the LST in built-up areas.

For the nighttime UHI GWR model in Vancouver, the spatial distribution of EVI coefficients shows that vegetation has a greater impact on nighttime UHI in the western regions than the eastern regions. However, it can be seen that during the nighttime EVI also has a significant positive correlation with the nighttime UHI in some parts of eastern region. The spatial distribution of NDWI coefficients for nighttime UHI is different with the daytime pattern. NDWI is significantly positively correlated with nighttime UHI throughout northern Vancouver, i.e., the more moisture, the higher the UHI value in these areas. Additionally, Vancouver's nighttime

UHI is significantly negatively correlated with EVI, with higher coefficient estimates in the western region, indicating a stronger impact of vegetation on nighttime UHI in this area.

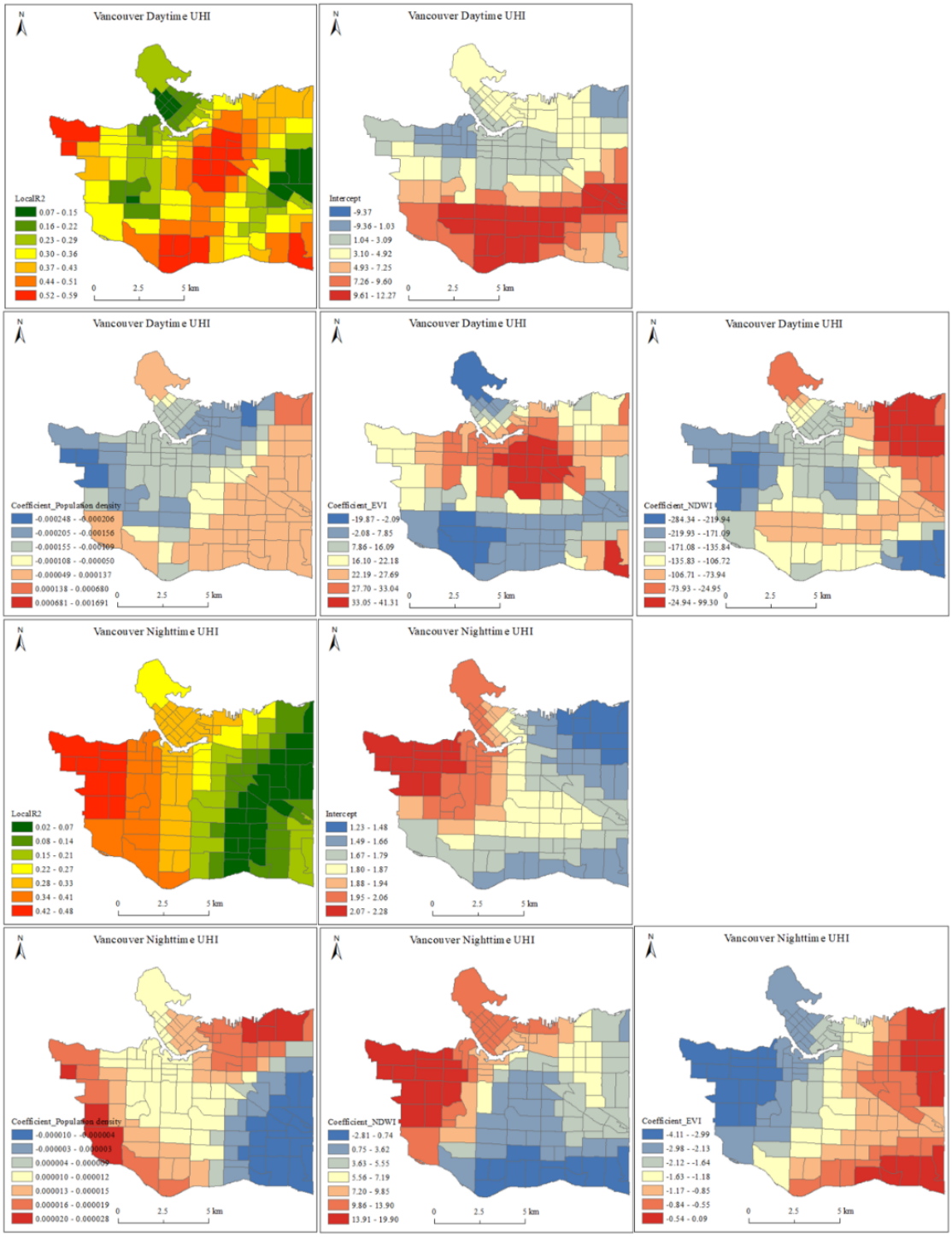

Figure 5.10 Spatial distribution maps of Local R^2, intercepts, and coefficients of the main variables for the GWR models of daytime and nighttime UHI in Vancouver

Figure 5.11 displays the spatial distribution maps of Local R^2, intercepts, and main variable coefficients for the GWR models of daytime and nighttime UHI in Toronto. As shown in Figure 5.11, the daytime UHI GWR model in Toronto exhibits a Local R^2 range of 0.02 to 0.64, with higher goodness of fit observed in the eastern and central-western parts, indicating a more significant impact of explanatory variables on daytime UHI in these areas. Water bodies and vegetation are the main significant explanatory variables influencing daytime UHI intensity in these regions. For the nighttime UHI GWR model in Toronto, the Local R^2 varies from 0.001 to 0.55, with higher goodness of fit observed in the northern region, suggesting a more significant impact of explanatory variables on nighttime UHI in these areas. NTL and water bodies are the main significant explanatory variables influencing nighttime UHI intensity in these regions. The GWR models for daytime and nighttime UHI in Toronto exhibit the widest range of Local R^2 values among the five cities.

As shown in Figure 5.11, the intercept values for daytime UHI in Toronto are higher in the northeastern and northwestern parts, indicating higher daytime UHI intensity in these areas, which is consistent with the spatial distribution of daytime UHI in Toronto. For the nighttime UHI, the intercept values are higher in the southeastern and western areas, indicating stronger nighttime UHI in these regions. Certainly, there is significant spatial heterogeneity in the coefficients of the key variables related to both daytime and nighttime UHI intensity in Toronto.

Regarding the daytime UHI, the spatial distribution of EVI coefficients indicates a positive correlation with UHI in the southeastern, and southwestern, northern parts, which means that higher vegetation cover is associated with higher daytime UHI values. This finding is consistent with the results of the study of Wang (2018) on the correlation between vegetation and daytime UHI in major cities in China. However, in the central-southern regions, vegetation cover exhibits a significant negative correlation with daytime UHI, indicating that vegetation can reduce daytime UHI intensity in these areas. This central-southern region corresponds to Toronto's downtown area, so increasing vegetation cover in downtown Toronto can effectively mitigate daytime UHI effects. The spatial distribution pattern of NDWI coefficients is opposite to EVI. NDWI exhibits a significant negative correlation with daytime UHI in the eastern and western parts, while showing a significant positive correlation in the downtown area. This may be

because Toronto's downtown area is adjacent to Lake Ontario, resulting in higher humidity, and thus poorer cooling effects during the daytime, leading to higher daytime UHI values where water bodies are more abundant and the environment is more humid.

The GWR model for nighttime UHI, in Toronto, NTL exhibits a similar spatial distribution of coefficients to the EVI. In the central area, NTL and NDWI have positive correlation with the nighttime UHI, while in the western and eastern region, they have negative correlation with the nighttime UHI. Additionally, the nighttime UHI in Toronto also shows a correlation with population density, with a positive correlation between population density and nighttime UHI in the most parts of Toronto, and a negative correlation in the southeastern parts.

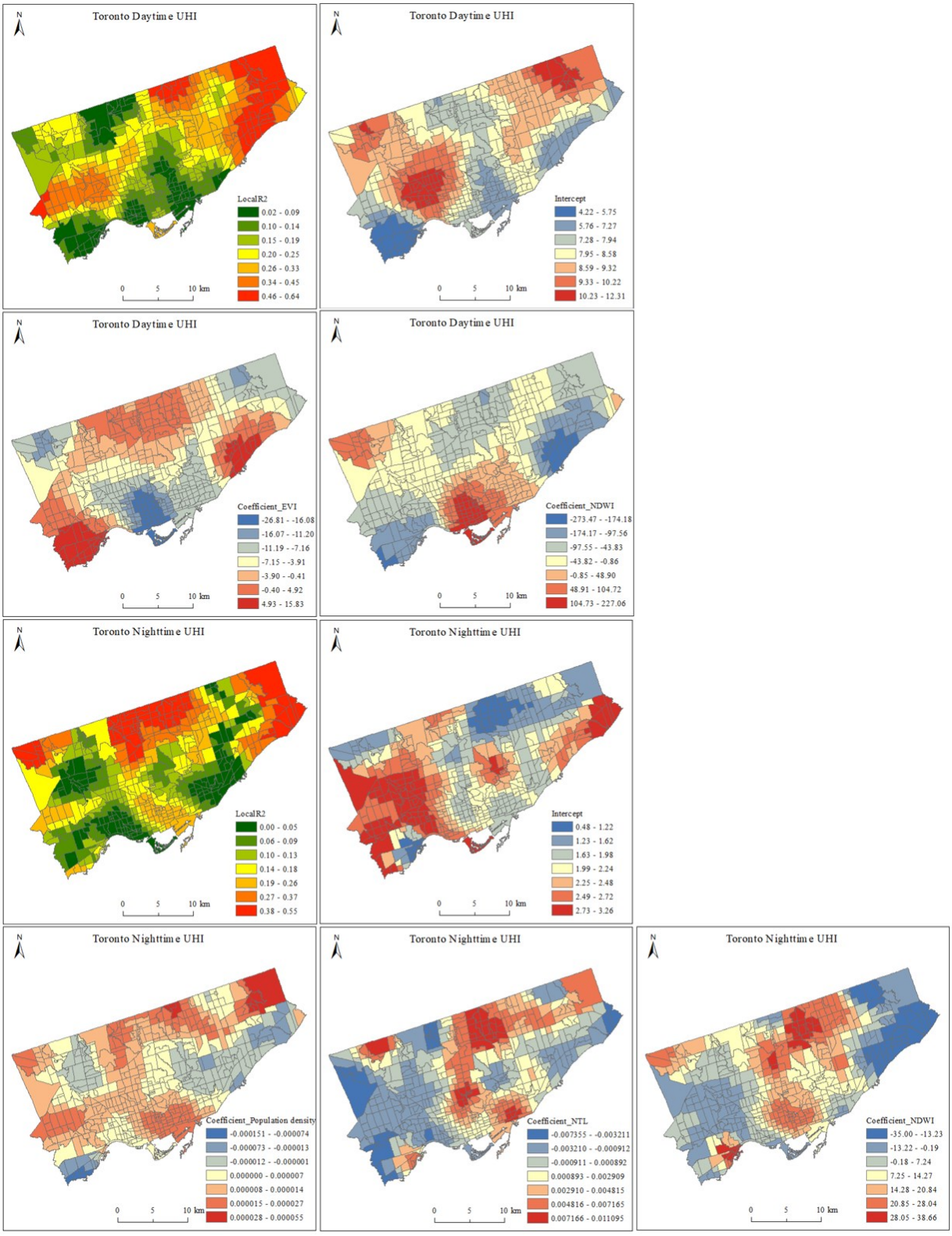

Figure 5.11 Spatial distribution maps of Local R^2, intercepts, and coefficients of the main variables for the GWR models of daytime and nighttime UHI in Toronto

Figure 5.12 displays the spatial distribution of the Local R^2, intercept, and coefficients of the key variables in the GWR model for daytime and nighttime UHI intensity in Montreal. As shown in the Figure 5.12, the Local R^2 values for daytime UHI in Montreal range from 0.01 to 0.89, with higher fit observed in the western and northern parts, indicating that the explanatory variables have a more significant impact on daytime UHI in these areas. The main variables that have a relatively significant impact on daytime UHI intensity are vegetation coverage, water bodies and population density. Similarly, for nighttime UHI, the Local R^2 values range from 0.001 to 0.88, with higher fit observed in the same western and northern regions, suggesting that the explanatory variables have a more pronounced influence on nighttime UHI in these areas. The key variables that have a relatively significant impact on nighttime UHI intensity are water bodies, population density and total population.

Furthermore, the intercept values for both daytime and nighttime UHI are higher in the western and central region and gradually decrease towards the south and northeast, as shown in Figure 5.12, indicating that daytime UHI intensity is higher in the central region compared to the southern, and northeastern areas, which aligns with the general distribution of daytime and nighttime UHI in Montreal. There is substantial spatial heterogeneity in the coefficients of the main variables strongly associated with both daytime and nighttime UHI.

Concerning daytime UHI, the EVI coefficients are higher in the fringe areas than in the central areas. In the northern and southern regions, EVI is significantly positively correlated with daytime UHI, while in the western region, it shows a significant negative correlation. As for NDWI coefficients, they are positive in the middle part of the south side and negative in the western and northern regions. This signifies a noteworthy correlation between water bodies and daytime UHI in Montreal, with a more pronounced overall impact in the northern areas. For nighttime UHI, the spatial distribution of NDWI and population density coefficients are generally consistent with the daytime patterns. This suggests that the factors influencing both daytime and nighttime UHI in Montreal are largely similar, allowing for a unified consideration of mitigation strategies without significant differences between daytime and nighttime UHI.

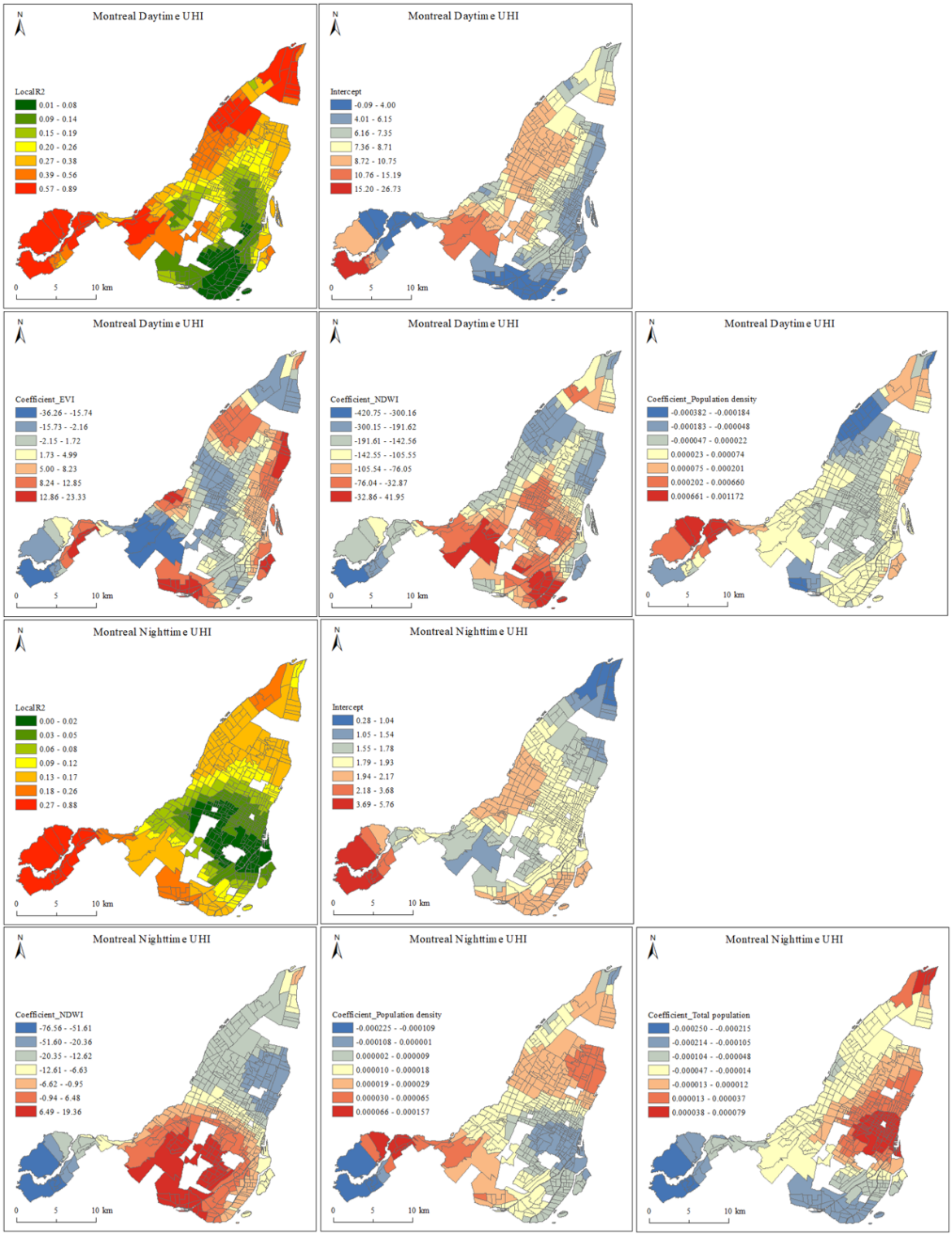

Figure 5.12 Spatial distribution maps of Local R^2, intercepts, and coefficients of the main variables for the GWR models of daytime and nighttime UHI in Montreal

5.6 Chapter Summary

This chapter investigated the relationship between UHI and each of the influencing factors in the five cities based on MODIS EVI and NDWI data, 2021 Census data, and VIIRS nighttime light values data. In all cities, correlation analyses revealed that the factors influencing daytime UHI are different with those influencing nighttime UHI.

The OLS results show the best model fit for explaining nighttime UHI in Calgary, suggesting that these factors (NTL, income, EVI and NDWI) explain Calgary's nighttime UHI well. From the GWR result, it can be seen that population density, EVI and NDWI are basically significantly correlated with both daytime and nighttime UHI in each city, which suggests that vegetation and water bodies in certain areas within these cities are able to mitigate and ameliorate UHI in the five cities and large population density can contribute to the exacerbation of UHI. In addition, NTL values were significantly positively correlated with nighttime UHI most of the time, indicating that the higher the degree of urbanization, the higher the intensity of UHI in these five cities.

Chapter 6. Conclusion and limitations

This chapter summarized the key findings of the entire study, reviewed and addressed the research questions, highlighted the novelty and findings of the study, acknowledged its limitations, and outlined future research directions.

6.1 Conclusion

The urban natural environment system plays a crucial role for urban residents, and with the continuous progress of urbanization, our concern for the entire global ecological environment is increasing. In this study, based on theories from geography and statistics, and utilizing remote sensing and geographic information systems, I analyzed the spatiotemporal patterns of daytime and nighttime UHI in five major Canadian cities in 2021, focusing on identifying their influencing factors. I selected two major categories of factors: natural environment and socio-economic factors, and used spatial models to analyze their impact on UHIs from a spatiotemporal perspective. Additionally, I investigated the spatiotemporal variations in UHIs among these cities. The main conclusions are as follows:

1. Using remote sensing data, I studied the SUHII in five major Canadian cities from both regional and seasonal perspectives and explored the spatiotemporal distribution patterns of UHI effects and their relationship with land use land covers. The results showed that the intensity of UHI exhibits clear seasonal variations, with the strongest UHI effect observed in summer and the weakest in winter in all cities. Besides, this study found that Vancouver, Toronto, and Montreal experience significantly higher daytime UHI effects across all four seasons compared to Edmonton and Calgary. However, during the nighttime, Edmonton and Calgary have higher UHI than the other three cities. In addition, among all types of land covers, built-up areas have the most significant impact on daytime LST in almost all cities, while bare ground has the most significant impact on nighttime LST in Toronto and Montreal.

2. Through analyzing the spatial distribution patterns of daytime and nighttime UHI in these five cities, differences and similarities were discovered among them. During the day, the spatial pattern of UHI in all cities except Edmonton is roughly the same across the four

seasons, while at night, all cities show a clear seasonal variation in the spatial pattern of UHI. In Edmonton, the spatial pattern of daytime UHI in winter was different from the other three seasons, with urban heat sinks occurring in winter. Additionally, the distribution patterns of UHI in these cities all exhibit an outward expansion from the city center, and the daytime and nighttime distribution patterns in each city are different.

3. Through spatial autocorrelation and heterogeneity tests, I found that both daytime and nighttime UHII demonstrate significant spatial dependence and heterogeneity. By comparing the indicators of ordinary least squares (OLS) and geographically weighted regression (GWR) models, I found that the GWR models consistently outperform the OLS models. The regression results indicate that the explanatory power of R^2 varies depending on the research subject and model, and the influencing factors of daytime and nighttime UHI differ among each city. Furthermore, the analysis showed that population density, EVI and NDWI were the most influential factors for all cities, but their impact on UHI varies with geographic location and between daytime and nighttime.

The spatiotemporal changes of UHI also reflect the temporal and spatial patterns of urbanization and industrialization in these cities. The changes in land use patterns and the interplay of natural and anthropogenic factors during the urbanization process have varying degrees of impact on the urban ecological environment.

6.2 Novelty

1. The study focused on five major Canadian cities situated in high-latitude regions. Examined the spatial distribution patterns of daytime and nighttime UHI across these cities at various temporal scales.

2. Using spatial regression models, the study investigated the influencing factors of daytime and nighttime UHI across the five cities at a neighbourhood level and explored their spatial differences.

6.3 Suggestions

According to the study, vegetation, water bodies and population density in these five cities have significant mitigating effects on daytime and nighttime UHI, but there is also spatial variability in each city. In Edmonton and Calgary, the EVI is significantly negatively correlated with UHI, so increasing vegetation cover can help to mitigate UHI in these two cities. Whereas in Vancouver, EVI is positively correlated with daytime UHI, which may be due to the fact that EVI characterizes all vegetation types, such as grass, shrubs, flooded vegetation, and trees. Based on the results of the study on the relationship between land use cover and LST, as indicated in Chapter 4, it is possible that a relative reduction in grass, shrub and flood vegetation cover or an increase in tree cover can help to mitigate the daytime UHI in Vancouver. However, in specific parts of northern and southern Montreal, as well as certain areas in the northern, southwestern, and southeastern parts of Toronto, EVI and daytime UHI showed a positive correlation. Therefore, these regions should be avoided when aiming to increase vegetation cover to alleviate daytime UHI. Conversely, in areas where EVI is negatively correlated with UHI, implementing measures such as constructing green roofs to augment vegetation cover can effectively mitigate UHI.

Moreover, the NDWI is significantly negatively correlated with daytime UHI in parts of Edmonton and Vancouver. Therefore, increasing water bodies would help mitigate the daytime UHI effect in these two cities. However, in parts of Vancouver, the NDWI is positively correlated with the daytime UHI, so water bodies are not effective in reducing daytime UHI in these regions. The same situation also applies to Toronto. However, in Montreal, the NDWI is significantly negatively correlated with both daytime and nighttime UHI in most areas, so adding water bodies or increasing vegetation with higher water in parts of Montreal could help alleviate UHI. Due to the different impacts of water bodies on UHI during the day and night, it is important to consider this when formulating policies.

Furthermore, in all cities except Calgary, population density is positively correlated with UHI. Therefore, within feasible limits, appropriately reducing population density, especially in areas where population density has a greater impact on UHI, can effectively mitigate UHI.

Therefore, this paper suggests that planners can target each neighborhood according to the different correlations between the UHI of different neighborhoods and the vegetation, water bodies and population density in order to improve the overall UHI of the whole city. Additionally, since the nighttime UHI effect is more pronounced in Edmonton and Calgary, and the daytime UHI effect is more evident in Vancouver, Toronto, and Montreal, it is recommended that more attention should be paid to factors affecting both daytime and nighttime UHI in Edmonton and Calgary, while in the other three cities, factors affecting daytime UHI should be given more consideration.

6.4 Limitations

In the process of completing this thesis, although efforts have been made to improve the relevant research, there are still some shortcomings.

1. Due to the relatively low spatial resolution of MODIS data, there may be errors in the results. Therefore, for more accurate research on each city, higher-resolution remote sensing data, such as Landsat data, would be required.

2. As these five cities are located in different spatial positions and have different climatic conditions, the study of factors influencing daytime and nighttime UHI needs further analyses. In future research, more influencing factors, such as humidity, elevation, PM 2.5 density, length of highway, and car ownership per capita, should be considered to provide a more accurate understanding of the factors influencing daytime and nighttime UHI.

With the ongoing urbanization process, the UHI effect remains a serious urban issue. The research on strategies to mitigate the UHI effect should continue, specifically considering the geographic location and environmental and socioeconomic factors. However, the implementation of new technologies and measures can offer assistance in alleviating the UHI situation.

References

Adopted, I. P. C. C. (2014). Climate change 2014 synthesis report. IPCC: Geneva, Szwitzerland.

Akaike, H. (1974). A new look at the statistical model identification. IEEE transactions on automatic control, 19(6), 716-723. doi: 10.1109/TAC.1974.1100705.

Badaro-Saliba, N., Adjizian-Gerard, J., Zaarour, R., & Najjar, G. (2021). LCZ scheme for assessing Urban Heat Island intensity in a complex urban area (Beirut, Lebanon). Urban Climate, 37, 100846. https://doi.org/10.1016/j.uclim.2021.100846

Bokaie, M., Zarkesh, M. K., Arasteh, P. D., & Hosseini, A. (2016). Assessment of urban heat island based on the relationship between land surface temperature and land use/land cover in Tehran. Sustainable Cities and Society, 23, 94-104. https://doi.org/10.1016/j.scs.2016.03.009

Brunsdon, C., Fotheringham, A. S., & Charlton, M. E. (1996). Geographically weighted regression: a method for exploring spatial nonstationarity. Geographical analysis, 28(4), 281-298. https://doi.org/10.1111/j.1538-4632.1996.tb00936.x

Brunsdon, C., Fotheringham, S., & Charlton, M. (2000). Geographically weighted regression as a statistical model.

Buyantuyev, A., & Wu, J. (2010). Urban heat islands and landscape heterogeneity: linking spatiotemporal variations in surface temperatures to land-cover and socioeconomic patterns. Landscape ecology, 25, 17-33. https://doi.org/10.1007/s10980-009-9402-4

Cahill, M., & Mulligan, G. (2007). Using geographically weighted regression to explore local crime patterns. Social Science Computer Review, 25(2), 174-193. https://doi.org/10.1177/0894439307298925

Cai, D., Fraedrich, K., Guan, Y., Guo, S., & Zhang, C. (2017). Urbanization and the thermal environment of Chinese and US-American cities. Science of the Total Environment, 589, 200-211. https://doi.org/10.1016/j.scitotenv.2017.02.148

Census Profile, 2021 Census of Population. (n.d.). Census Profile, 2021 Census of Population. https://www12.statcan.gc.ca/census-recensement/2021/dp-pd/prof/index.cfm?Lang=E

Che, H., Qi, B., Zhao, H., Xia, X., Eck, T. F., Goloub, P., ... & Zhang, X. (2018). Aerosol optical properties and direct radiative forcing based on measurements from the China Aerosol Remote Sensing Network (CARSNET) in eastern China. Atmospheric Chemistry and Physics, 18(1), 405-425. https://doi.org/10.5194/acp-18-405-2018

Chen, X. L., Zhao, H. M., Li, P. X., & Yin, Z. Y. (2006). Remote sensing image-based analysis of the relationship between urban heat island and land use/cover changes. Remote sensing of environment, 104(2), 133-146. https://doi.org/10.1016/j.rse.2005.11.016

Chen, Y. C., Chiu, H. W., Su, Y. F., Wu, Y. C., & Cheng, K. S. (2017). Does urbanization increase diurnal land surface temperature variation? Evidence and implications. Landscape and Urban Planning, 157, 247-258. https://doi.org/10.1016/j.landurbplan.2016.06.014

Chien, F., Hsu, C. C., Ozturk, I., Sharif, A., & Sadiq, M. (2022). The role of renewable energy and urbanization towards greenhouse gas emission in top Asian countries: Evidence from advance panel estimations. Renewable Energy, 186, 207-216. https://doi.org/10.1016/j.renene.2021.12.118

Clinton, N., & Gong, P. (2013). MODIS detected surface urban heat islands and sinks: Global locations and controls. Remote Sensing of Environment, 134, 294-304. https://doi.org/10.1016/j.rse.2013.03.008

Crutzen, P. J., 2004: New directions: The growing urban heat and pollution island effect—Impact on chemistry and climate. Atmos. Environ., 38, 3539–3540.

Dalby, S. (2002). Security and Ecology in the Age of Globalization. Environmental Change and Security Project Report, 8(101), 4.

Draper, N. R., & Smith, H. (1998). Applied regression analysis (Vol. 326). John Wiley & Sons.

Ejiagha, I. R., Ahmed, M. R., Hassan, Q. K., Dewan, A., Gupta, A., & Rangelova, E. (2020). Use of remote sensing in comprehending the influence of urban landscape's composition and configuration on land surface temperature at neighbourhood scale. Remote Sensing, 12(15), 2508. https://doi.org/10.3390/rs12152508

Elevation Schedule. (n.d.). Altitude Athletic Training. https://altitudeathletictraining.com/elevation-schedule-2/

Elvidge, C. D., Baugh, K. E., Kihn, E. A., Kroehl, H. W., Davis, E. R., & Davis, C. W. (2010). Relation between satellite observed visible-near infrared emissions, population, economic activity and electric power consumption. International Journal of Remote Sensing, 18(6), 1373-1379. https://doi.org/10.1080/014311697218485

EOS Data Analytics. (2023, May 25). NDWI: Index Formula, Value Range, And Uses In Agriculture. https://eos.com/make-an-analysis/ndwi/

Esri, Microsoft. (2022). Sentinel-2 10m Land Use/Land Cover Timeseries Downloader. [data set]. Sentinel-2 10m Land Use/Land Cover Timeseries Downloader (Mature Support) (arcgis.com)

Esri. (n.d.). EVI—ArcGIS Pro https://pro.arcgis.com/en/pro-app/latest/arcpy/spatial-analyst/evi.htm

Esri. (n.d.). Geographically Weighted Regression (GWR) (Spatial Statistics)—ArcGIS Pro https://pro.arcgis.com/en/pro-app/latest/tool-reference/spatial-statistics/geographicallyweightedregression.htm

Esri. (n.d.). How Cluster and Outlier Analysis (Anselin Local Moran's I) works—ArcGIS Pro https://pro.arcgis.com/en/pro-app/3.0/tool-reference/spatial-statistics/h-how-cluster-and-outlier-analysis-anselin-local-m.htm

Esri. (n.d.). How High/Low Clustering (Getis-Ord General G) works—ArcGIS Pro https://pro.arcgis.com/en/pro-app/3.0/tool-reference/spatial-statistics/h-how-high-low-clustering-getis-ord-general-g-spat.htm

Esri. (n.d.). How Spatial Autocorrelation (Global Moran's I) works—ArcGIS Pro https://pro.arcgis.com/en/pro-app/latest/tool-reference/spatial-statistics/how-geographicallyweightedregression-works.htm

Esri. (n.d.). NDWI—ArcGIS Pro https://pro.arcgis.com/en/pro-app/latest/arcpy/spatial-analyst/evi.htm

Estoque, R. C., Murayama, Y., & Myint, S. W. (2017). Effects of landscape composition and pattern on land surface temperature: An urban heat island study in the megacities of Southeast Asia. Science of the Total Environment, 577, 349-359. https://doi.org/10.1016/j.scitotenv.2016.10.195

Fortin, M. J., Dale, M. R., & ver Hoef, J. (2002). Spatial analysis in ecology. Encyclopedia of environmetrics, 4, 2051-2058. DOI: 10.1002/9780470057339.vas039

Fotheringham, A. S., Brunsdon, C., & Charlton, M. (2003). Geographically weighted regression: the analysis of spatially varying relationships. John Wiley & Sons.

Fotheringham, A. S., Charlton, M. E., & Brunsdon, C. (1998). Geographically weighted regression: a natural evolution of the expansion method for spatial data analysis. Environment and planning A, 30(11), 1905-1927. https://doi.org/10.1068/a301905

Friedl, M. A. (2002). Forward and inverse modeling of land surface energy balance using surface temperature measurements. Remote sensing of environment, 79(2-3), 344-354. https://doi.org/10.1016/S0034-4257(01)00284-X

Gaur, A., Eichenbaum, M. K., & Simonovic, S. P. (2018). Analysis and modelling of surface Urban Heat Island in 20 Canadian cities under climate and land-cover change. Journal of environmental management, 206, 145-157. https://doi.org/10.1016/j.jenvman.2017.10.002

Gollini, I., Lu, B., Charlton, M., Brunsdon, C., & Harris, P. (2013). GWmodel: an R package for exploring spatial heterogeneity using geographically weighted models. arXiv preprint arXiv:1306.0413. https://doi.org/10.48550/arXiv.1306.0413

Gunawardena, K. R., Wells, M. J., & Kershaw, T. (2017). Utilising green and bluespace to mitigate urban heat island intensity. Science of the Total Environment, 584, 1040-1055. https://doi.org/10.1016/j.scitotenv.2017.01.158

Guo, L., Ma, Z., & Zhang, L. (2008). Comparison of bandwidth selection in application of geographically weighted regression: a case study. Canadian Journal of Forest Research, 38(9), 2526-2534. https://doi.org/10.1139/X08-091

Hardin, A. W., Liu, Y., Cao, G., & Vanos, J. K. (2018). Urban heat island intensity and spatial variability by synoptic weather type in the northeast US. Urban climate, 24, 747-762. https://doi.org/10.1016/j.uclim.2017.09.001

Hayes, A. T., Jandaghian, Z., Lacasse, M. A., Gaur, A., Lu, H., Laouadi, A., ... & Wang, L. (2022). Nature-based solutions (nbss) to mitigate urban heat island (UHI) effects in Canadian cities. Buildings, 12(7), 925. https://doi.org/10.3390/buildings12070925

He, J. F., Liu, J. Y., Zhuang, D. F., Zhang, W., & Liu, M. L. (2007). Assessing the effect of land use/land cover change on the change of urban heat island intensity. Theoretical and applied climatology, 90, 217-226. https://doi.org/10.1007/s00704-006-0273-1

Health Canada. (2020). Reducing urban heat islands to protect health in Canada. Retrieved July 29, 2022 https://www.canada.ca/en/services/health/publications/healthy-living/reducing-urban-heat-islands-protect-health-canada.html

Henderson, M., Yeh, E. T., Gong, P., Elvidge, C., & Baugh, K. (2003). Validation of urban boundaries derived from global night-time satellite imagery. International Journal of Remote Sensing, 24(3), 595-609. https://doi.org/10.1080/01431160304982

Hondula, D. M., Balling, R. C., Andrade, R., Scott Krayenhoff, E., Middel, A., Urban, A., ... & Sailor, D. J. (2017). Biometeorology for cities. International journal of biometeorology, 61, 59-69. https://doi.org/10.1007/s00484-017-1412-3

Hoornweg, D., Sugar, L., & Trejos Gómez, C. L. (2011). Cities and greenhouse gas emissions: moving forward. Environment and urbanization, 23(1), 207-227. https://doi.org/10.1177/0956247810392270

Huang, C., Barnett, A. G., Wang, X., & Tong, S. (2012). The impact of temperature on years of life lost in Brisbane, Australia. Nature Climate Change, 2(4), 265-270. https://doi.org/10.1038/nclimate1369

Huang, X., & Wang, Y. (2019). Investigating the effects of 3D urban morphology on the surface urban heat island effect in urban functional zones by using high-resolution remote sensing data: A case study of Wuhan, Central China. ISPRS Journal of Photogrammetry and Remote Sensing, 152, 119-131. https://doi.org/10.1016/j.isprsjprs.2019.04.010

Imhoff, M. L., Zhang, P., Wolfe, R. E., & Bounoua, L. (2010). Remote sensing of the urban heat island effect across biomes in the continental USA. Remote sensing of environment, 114(3), 504-513. https://doi.org/10.1016/j.rse.2009.10.008

Jin, M., Dickinson, R. E., & Zhang, D. A. (2005). The footprint of urban areas on global climate as characterized by MODIS. Journal of climate, 18(10), 1551-1565. https://doi.org/10.1175/JCLI3334.1

Kalnay, E., & Cai, M. (2003). Impact of urbanization and land-use change on climate. Nature, 423(6939), 528-531. https://doi.org/10.1038/nature01675

Kornhuber, K., Osprey, S., Coumou, D., Petri, S., Petoukhov, V., Rahmstorf, S., & Gray, L. (2019). Extreme weather events in early summer 2018 connected by a recurrent hemispheric wave-7 pattern. Environmental Research Letters, 14(5), 054002. DOI 10.1088/1748-9326/ab13bf

Li, M., Ou, J., & Li, X. (2016). Spatio-temporal analysis of influenza A (H1N1) in China during 2009-2013 based on GIS. Geography Research, 35(11), 2139-2152. https://doi.org/10.11821/dlyj201611011

Li, X., & Zhou, W. (2019). Spatial patterns and driving factors of surface urban heat island intensity: A comparative study for two agriculture-dominated regions in China and the

USA. Sustainable Cities and Society, 48, 101518. https://doi.org/10.1016/j.scs.2019.101518

Li, X., Zhou, Y., Asrar, G. R., Imhoff, M., & Li, X. (2017). The surface urban heat island response to urban expansion: A panel analysis for the conterminous United States. Science of the Total Environment, 605, 426-435. https://doi.org/10.1016/j.scitotenv.2017.06.229

Maimaitiyiming, M., Ghulam, A., Tiyip, T., Pla, F., Latorre-Carmona, P., Halik, Ü., ... & Caetano, M. (2014). Effects of green space spatial pattern on land surface temperature: Implications for sustainable urban planning and climate change adaptation. ISPRS Journal of Photogrammetry and Remote Sensing, 89, 59-66. https://doi.org/10.1016/j.isprsjprs.2013.12.010

Manitoba Collaborative Data Portal. (2018). Median vs Average Household Income: What is the Difference Between These Indicators, and How to Interpret Them. http://www.mbcdp.ca/blog/median-vs-average-household-income-what-is-the-difference-between-these-indicators-and-how-to-interpret-them

Manley, G. (1958). On the frequency of snowfall in metropolitan England. Quarterly Journal of the Royal Meteorological Society, 84(359), 70-72. https://doi.org/10.1002/qj.49708435910

Martínez-Fernández, J., Chuvieco, E., & Koutsias, N. (2013). Modelling long-term fire occurrence factors in Spain by accounting for local variations with geographically weighted regression. Natural Hazards and Earth System Sciences, 13(2), 311-327. https://doi.org/10.5194/nhess-13-311-2013

Masson, V. (2000). A physically-based scheme for the urban energy budget in atmospheric models. Boundary-layer meteorology, 94, 357-397. https://doi.org/10.1023/A:1002463829265

McCarthy, M. P., Best, M. J., & Betts, R. A. (2010). Climate change in cities due to global warming and urban effects. Geophysical research letters, 37(9). https://doi.org/10.1029/2010GL042845

McFeeters, S. K. (1996). The use of the Normalized Difference Water Index (NDWI) in the delineation of open water features. International journal of remote sensing, 17(7), 1425-1432. https://doi.org/10.1080/01431169608948714

Memon, R. A., Leung, D. Y., & Liu, C. H. (2009). An investigation of urban heat island intensity (UHII) as an indicator of urban heating. Atmospheric Research, 94(3), 491-500. https://doi.org/10.1016/j.atmosres.2009.07.006

Miles, V., & Esau, I. (2017). Seasonal and spatial characteristics of urban heat islands (UHIs) in northern West Siberian cities. Remote sensing, 9(10), 989. https://doi.org/10.3390/rs9100989

Mohammad, P., & Goswami, A. (2021). Quantifying diurnal and seasonal variation of surface urban heat island intensity and its associated determinants across different climatic zones over Indian cities. GIScience & Remote Sensing, 1-27. https://doi.org/10.1080/15481603.2021.1940739

Myint, S. W. (2003). Fractal approaches in texture analysis and classification of remotely sensed data: Comparisons with spatial autocorrelation techniques and simple descriptive statistics. International Journal of remote sensing, 24(9), 1925-1947. https://doi.org/10.1080/01431160210155992

NASA. (n.d.). MODIS Vegetation Index Products (NDVI and EVI). https://modis.gsfc.nasa.gov/data/dataprod/mod13.php

Naserikia, M., Hart, M. A., Nazarian, N., & Bechtel, B. (2022). Background climate modulates the impact of land cover on urban surface temperature. Scientific Reports, 12(1), 15433. https://doi.org/10.1038/s41598-022-19431-x

Newbold, K. B. (2011). Urbanisation and the growth of the Canadian city. The changing Canadian population, 175-188.

Oke, T. R. (1973). City size and the urban heat island. Atmospheric Environment (1967), 7(8), 769-779. https://doi.org/10.1016/0004-6981(73)90140-6

Oke, T. R. (1982). The energetic basis of the urban heat island. Quarterly Journal of the Royal Meteorological Society, 108(455), 1-24. https://doi.org/10.1002/qj.49710845502

Oke, T. R. (1988). Street design and urban canopy layer climate. Energy and buildings, 11(1-3), 103-113. https://doi.org/10.1016/0378-7788(88)90026-6

Oke, T. R., & Maxwell, G. B. (1975). Urban heat island dynamics in Montreal and Vancouver. Atmospheric Environment (1967), 9(2), 191-200. https://doi.org/10.1016/0004-6981(75)90067-0

Parker, D. E. (2010). Urban heat island effects on estimates of observed climate change. Wiley Interdisciplinary Reviews: Climate Change, 1(1), 123-133. https://doi.org/10.1002/wcc.21

Peng, J., Jia, J., Liu, Y., Li, H., & Wu, J. (2018). Seasonal contrast of the dominant factors for spatial distribution of land surface temperature in urban areas. Remote sensing of Environment, 215, 255-267. https://doi.org/10.1016/j.rse.2018.06.010

Peng, S., Piao, S., Ciais, P., Friedlingstein, P., Ottle, C., Bréon, F. M., ... & Myneni, R. B. (2012). Surface urban heat island across 419 global big cities. Environmental science & technology, 46(2), 696-703. https://doi.org/10.1021/es2030438

Peng, S., Piao, S., Ciais, P., Friedlingstein, P., Ottle, C., Bréon, F. M., ... & Myneni, R. B. (2012). Surface urban heat island across 419 global big cities. Environmental science & technology, 46(2), 696-703. https://doi.org/10.1021/es2030438

Price, J. C. (1985). On the analysis of thermal infrared imagery: The limited utility of apparent thermal inertia. Remote sensing of Environment, 18(1), 59-73. https://doi.org/10.1016/0034-4257(85)90038-0

Rajasekar, U., & Weng, Q. (2009). Spatio-temporal modelling and analysis of urban heat islands by using Landsat TM and ETM+ imagery. International Journal of Remote Sensing, 30(13), 3531-3548. https://doi.org/10.1080/01431160802562289

Rinner, C., & Hussain, M. (2011). Toronto's urban heat island—Exploring the relationship between land use and surface temperature. Remote Sensing, 3(6), 1251-1265. https://doi.org/10.3390/rs3061251

Rizwan, A. M., Dennis, L. Y., & Chunho, L. I. U. (2008). A review on the generation, determination and mitigation of Urban Heat Island. Journal of environmental sciences, 20(1), 120-128. https://doi.org/10.1016/S1001-0742(08)60019-4

Sang, J., Liu, H., Liu, H., & Zhang, Z. (2000). Observational and numerical studies of wintertime urban boundary layer. Journal of Wind Engineering and Industrial Aerodynamics, 87(2-3), 243-258. https://doi.org/10.1016/S0167-6105(00)00040-4

Santamouris, M. (2015). Analyzing the heat island magnitude and characteristics in one hundred Asian and Australian cities and regions. Science of the Total Environment, 512, 582-598. https://doi.org/10.1016/j.scitotenv.2015.01.060

Schneider, A., Friedl, M. A., & Potere, D. (2009). A new map of global urban extent from MODIS satellite data. Environmental research letters, 4(4), 044003.

Schwaab, J., Meier, R., Mussetti, G., Seneviratne, S., Bürgi, C., & Davin, E. L. (2021). The role of urban trees in reducing land surface temperatures in European cities. Nature communications, 12(1), 6763. https://doi.org/10.1038/s41467-021-26768-w

Schwarz, N., Schlink, U., Franck, U., & Großmann, K. (2012). Relationship of land surface and air temperatures and its implications for quantifying urban heat island indicators—An application for the city of Leipzig (Germany). Ecological indicators, 18, 693-704. https://doi.org/10.1016/j.ecolind.2012.01.001

Sidiqui, P., Huete, A., & Devadas, R. (2016, July). Spatio-temporal mapping and monitoring of Urban Heat Island patterns over Sydney, Australia using MODIS and Landsat-8. In 2016 4th International Workshop on Earth Observation and Remote Sensing Applications (EORSA) (pp. 217-221). IEEE. doi: 10.1109/EORSA.2016.7552800.

Singh, N., Singh, S., & Mall, R. K. (2020). Urban ecology and human health: implications of urban heat island, air pollution and climate change nexus. In Urban Ecology (pp. 317-334). Elsevier. https://doi.org/10.1016/B978-0-12-820730-7.00017-3

Sobstyl, J. M., Emig, T., Qomi, M. A., Ulm, F. J., & Pellenq, R. M. (2018). Role of city texture in urban heat islands at nighttime. Physical review letters, 120(10), 108701. https://doi.org/10.1103/PhysRevLett.120.108701

Soltani, A., & Sharifi, E. (2017). Daily variation of urban heat island effect and its correlations to urban greenery: A case study of Adelaide. Frontiers of Architectural Research, 6(4), 529-538. https://doi.org/10.1016/j.foar.2017.08.001

St, L., & Wold, S. (1989). Analysis of variance (ANOVA). Chemometrics and intelligent laboratory systems, 6(4), 259-272. https://doi.org/10.1016/0169-7439（89）80095-4

Stewart, I. D. (2011). A systematic review and scientific critique of methodology in modern urban heat island literature. International Journal of Climatology, 31(2), 200-217. https://doi.org/10.1002/joc.2141

Sun, R., Lü, Y., Yang, X., & Chen, L. (2019). Understanding the variability of urban heat islands from local background climate and urbanization. Journal of cleaner production, 208, 743-752. https://doi.org/10.1016/j.jclepro.2018.10.178

Sun, Y., Gao, C., Li, J., Wang, R., & Liu, J. (2019). Evaluating urban heat island intensity and its associated determinants of towns and cities continuum in the Yangtze River Delta Urban Agglomerations. Sustainable Cities and Society, 50, 101659. https://doi.org/10.1016/j.scs.2019.101659

Sun, Y., Wang, S., & Wang, Y. (2020). Estimating local-scale urban heat island intensity using nighttime light satellite imageries. Sustainable Cities and Society, 57, 102125. https://doi.org/10.1016/j.scs.2020.102125

Taha, H. (1997). Urban climates and heat islands: albedo, evapotranspiration, and anthropogenic heat. Energy and buildings, 25(2), 99-103. https://doi.org/10.1016/S0378-7788(96)00999-1

Tang, J., Lan, X., Lian, Y., Zhao, F., & Li, T. (2022). Estimation of Urban–Rural Land Surface Temperature Difference at Different Elevations in the Qinling–Daba Mountains Using MODIS and the Random Forest Model. International Journal of Environmental Research and Public Health, 19(18), 11442. https://doi.org/10.3390/ijerph191811442

Tobler, W. R. (1970). A computer movie simulating urban growth in the Detroit region. Economic geography, 46(sup1), 234-240.

Tomlinson, C. J., Chapman, L., Thornes, J. E., & Baker, C. J. (2012). Derivation of Birmingham's summer surface urban heat island from MODIS satellite images. International Journal of Climatology, 32(2), 214-224. https://doi.org/10.1002/joc.2261

Tran, D. X., Pla, F., Latorre-Carmona, P., Myint, S. W., Caetano, M., & Kieu, H. V. (2017). Characterizing the relationship between land use land cover change and land surface temperature. ISPRS Journal of Photogrammetry and Remote Sensing, 124, 119-132. https://doi.org/10.1016/j.isprsjprs.2017.01.001

United Nations. (2018). World Urbanization Prospects The 2018 Revision. Retrieved April 14, 2023, from https://esa.un.org/unpd/wup/

Vancouver, C. O. (n.d.). Geography. Geography | City of Vancouver. https://vancouver.ca/news-calendar/geo.aspx

Voogt, J. A., & Oke, T. R. (2003). Thermal remote sensing of urban climates. Remote sensing of environment, 86(3), 370-384. https://doi.org/10.1016/S0034-4257(03)00079-8

Wan, Z. (2014). New refinements and validation of the collection-6 MODIS land-surface temperature/emissivity product. Remote sensing of Environment, 140, 36-45. https://doi.org/10.1016/j.rse.2013.08.027

Wang, Y. (2018). Temporal and Spatial Evolution Patterns and Influencing Factors of Urban Heat Island and Air Quality in China (Doctoral Dissertation, East China Normal University).https://kns.cnki.net/KCMS/detail/detail.aspx?dbname=CDFDLAST2019&filename=1019811076.nh

Wang, Y., Berardi, U., & Akbari, H. (2016). Comparing the effects of urban heat island mitigation strategies for Toronto, Canada. Energy and buildings, 114, 2-19. https://doi.org/10.1016/j.enbuild.2015.06.046

Welegedara, N. P., Agrawal, S. K., Gajjar, S., & Joshi, N. (2021). Variations in direct greenhouse gas emissions across neighbourhoods: A case of Edmonton in Canada. Environmental Challenges, 5, 100312. https://doi.org/10.1016/j.envc.2021.100312

Wheeler, D., & Tiefelsdorf, M. (2005). Multicollinearity and correlation among local regression coefficients in geographically weighted regression. Journal of Geographical Systems, 7(2), 161-187. https://doi.org/10.1007/s10109-005-0155-6

Wienert, U., & Kuttler, W. (2005). The dependence of the urban heat island intensity on latitude-A statistical approach. Meteorologische Zeitschrift, 14(5), 677-686. DOI: 10.1127/0941-2948/2005/0069

Yin, C., Yuan, M., Lu, Y., Huang, Y., & Liu, Y. (2018). Effects of urban form on the urban heat island effect based on spatial regression model. Science of the Total Environment, 634, 696-704. https://doi.org/10.1016/j.scitotenv.2018.03.350

Young, R. R., Burns, J. A., Smith, D. G., Arnold, L. D., & Rains, R. B. (1994). A single, late Wisconsin, Laurentide glaciation, Edmonton area and southwestern Alberta. Geology, 22(8), 683-686.

Zhang, H., Qi, Z. F., Ye, X. Y., Cai, Y. B., Ma, W. C., & Chen, M. N. (2013). Analysis of land use/land cover change, population shift, and their effects on spatiotemporal patterns of urban heat islands in metropolitan Shanghai, China. Applied Geography, 44, 121-133. https://doi.org/10.1016/j.apgeog.2013.07.021

Zhang, Y., Hu, D., Cao, S., Chen, S., & Yu, C. (2018). Remote Sensing Monitoring of Heat Island Intensity in Beijing-Tianjin-Hebei Urban Agglomeration and Analysis of Urban

Scale Effect. Journal of Capital Normal University (Natural Science Edition), 39(5), 72-80. DOI:10.19789/j.1004-9398.2018.05.015

Zhao, C., Jensen, J., Weng, Q., & Weaver, R. (2018). A geographically weighted regression analysis of the underlying factors related to the surface urban heat island phenomenon. Remote Sensing, 10(9), 1428. https://doi.org/10.3390/rs10091428

Zhao, L., Lee, X., Smith, R. B., & Oleson, K. (2014). Strong contributions of local background climate to urban heat islands. Nature, 511(7508), 216-219. https://doi.org/10.1038/nature13462

Zhao, M., Cai, H., Qiao, Z., & Xu, X. (2016). Influence of urban expansion on the urban heat island effect in Shanghai. International Journal of Geographical Information Science, 30(12), 2421-2441. https://doi.org/10.1080/13658816.2016.1178389

Zhao, M., Zhou, Y., Li, X., Cao, W., He, C., Yu, B., ... & Zhou, C. (2019). Applications of satellite remote sensing of nighttime light observations: Advances, challenges, and perspectives. Remote Sensing, 11(17), 1971. https://doi.org/10.3390/rs11171971

Zhou, D., Zhao, S., Liu, S., Zhang, L., & Zhu, C. (2014). Surface urban heat island in China's 32 major cities: Spatial patterns and drivers. Remote sensing of environment, 152, 51-61. https://doi.org/10.1016/j.rse.2014.05.017

Zhou, X., & Chen, H. (2018). Impact of urbanization-related land use land cover changes and urban morphology changes on the urban heat island phenomenon. Science of the Total Environment, 635, 1467-1476. https://doi.org/10.1016/j.scitotenv.2018.04.091

Zhu, W., Lű, A., & Jia, S. (2013). Estimation of daily maximum and minimum air temperature using MODIS land surface temperature products. Remote Sensing of Environment, 130, 62-73. https://doi.org/10.1016/j.rse.2012.10.034

Zhu, X. (2016). GIS for environmental applications: a practical approach. Routledge.